Title
Site-Specific Irrigation Management Strategies for Almond Orchards

Author
Drechsler, Kelley

Publication Date
2021

Peer reviewed|Thesis/dissertation

Site-Specific Irrigation Management Strategies for Almond Orchards

By

KELLEY DRECHSLER
DISSERTATION

Submitted in partial satisfaction of the requirements for the degree of

DOCTOR OF PHILOSOPHY

in

Biological Systems Engineering

in the

OFFICE OF GRADUATE STUDIES

of the

UNIVERSITY OF CALIFORNIA

DAVIS

Approved:

_____
Isaya Kisekka, Chair

_____
Andre Daccache

_____
Mallika Nocco

Committee in Charge

2021

Acknowledgments

Thank you to the Almond Board of California for funding most of my graduate tuition, stipend, and research expenses. I hope that the results of my graduate research will in some way help almond farmers work towards greater irrigation sustainability. I am also very grateful to the Biological Systems Engineering Graduate Group, the US Department of Education, Santa Barbara High School Alumni Association, and the Irrigation Foundation for helping to fund my tuition and stipend. I am also thankful to the California Institute for Water Resources and the Grant A. Harris Fellowship from METER Group for helping to fund the expenses of my graduate research.

There are many people to thank in helping me through my journey through graduate school. I am very thankful to the undergraduate research assistants, Jazmin Melendez, Aya Suzuki, Kyle Johnson, Mackenzie Guilliams, Carson Fogg, Nitya Raisinghani, and Marcoluis Garcia for their help with data collection and field work. Thanks to the postdocs, visiting scholars, and fellow graduate students, Prudentia Gugulethu Zikalala, Jingyuan Xue, Iael Raij Hoffman, Yangyang Li, Jae Sung Kim, Tibin Zhang, Srinivasa Rao Peddinti, Fatemeh Mehrabi, Jesús Domínguez, Usama Al-Dughaishi, Floyid Nicolas, Omar Samara, and Julie Meyers who helped me with field work and data collection. I am very thankful to Matt Read, Kameron Chun, Jed Roach and Tom Bell for always being willing to help with odds and ends, drilling a hole, finding a shovel, etc. I am thankful for the Nickels Soil Lab crew, Franz Niederholzer. Stan Cutter, Ubaldo Salud and the rest of the farm crew there for maintaining an almond orchard to conduct my research in Arbuckle. Thanks to Allan Fulton and Cayle Little for helping me with the research in Corning. I am very thankful to Steve Gruenwald for allowing us to conduct research on his private almond orchard in Corning.

I am especially thankful to Professor Shrinivasa Upadhyaya who offered me a Junior Specialist position in his research group in 2016 and inspired my curiosity of plant-water relations and data analysis, and ultimately led me to pursue graduate school. I am very grateful of my MS and PhD major advisor, Professor Isaya Kisekka, who offered me all the resources I needed for successful graduate research. I am thankful to Andre Daccache and Mallika Nocco for serving on my dissertation committee. I am grateful to Mark Grismer, Alireza Pourezza, Sam Sandovol, Andre Daccache, and Shrinivasa Upadhyaya for serving on my qualifying exam committee and for their insightful feedback on my dissertation proposal. I am also very thankful to the professors of all the courses I took while I was a student.

Most of all, I am thankful to my family for nurturing me into a strong, analytically minded person. My parents taught me to think for myself, to question everything, and to take nothing for granted, all of which has been crucial to my success in school and beyond. My dissertation is in memory of my grandparents, Albert and Dorothea Drechsler, who loved tending to their vegetable garden and fruit orchard. My sister and I spent many summer days as kids in their fruit orchard, which I still believe produced the best fruit I have ever eaten. I am very thankful to my fiancée, David Moyers, who is always willing to have intellectual conversations about my research and continuously inspires me to pursue my scientific and engineering curiosities.

Abstract

In response to water uncertainties, the almond community has set a goal to reduce the amount of water used to grow a pound of almonds by 20% by the year 2025. The research presented in this paper addresses this goal by developing site-specific irrigation management strategies in different ages and varieties of almond trees using field experiments and data-driven modeling.

Crop water use and crop coefficients for young almond trees (1-5 years old) were determined at three adjacent Nonpareil/Monterey almond orchards in the northern Sacramento Valley. Crop water use was determined through a land surface energy balance using eddy covariance. Crop coefficients were determined using the evapotranspiration estimates from each orchard and a short grass reference evapotranspiration from the nearest California Irrigation Management Information System (CIMIS) station. Results showed that crop water use and crop coefficients increased until the 4th year, suggesting that farmers should closely monitor tree development and orchard age and adjust irrigation scheduling as young trees grow. The results led to the conclusion that farmers should use age-specific crop coefficients until the 4th year and then they can start using mature almond crop coefficients.

In mature almonds orchards, regulated deficit irrigation (RDI) during hull-split can reduce water use, but limited research has been done on strategies for imposing RDI in almond orchards with multiple varieties with different hull-split schedules. A 2-year study evaluated the impacts of two different regulated deficit irrigation schedules under two levels of crop evapotranspiration irrigation replacement rates in an almond orchard with Butte, Aldrich, and Nonpareil varieties in the Sacramento Valley of California, USA. The two irrigation schedules were (1) regulated deficit irrigation in Butte, Aldrich, and Nonpareil varieties during Nonpareil hull-split timing and (2) regulated deficit irrigation in each variety according to variety-specific

hull-split timing. The two levels of irrigation were 50% and 75% of crop evapotranspiration (ET_c) replacement during the hull-split period. Results show that the kernel thickness of Aldrich almonds significantly increased under 75% ET_c irrigation replacement during Aldrich hull-split period compared to 75% ET_c and 50% ET_c irrigation replacement during Nonpareil hull-split period. In the Butte almonds, 75% ET_c and 50% ET_c irrigation replacement during variety-specific hull-split significantly reduced the fraction of sealed shells of the Butte variety compared to 75% ET_c and 50% ET_c irrigation replacement during Nonpareil hull-split period. This study demonstrated that almond physical quality could change in the Butte and Aldrich varieties when RDI is imposed according to variety-specific hull-split schedules. No marketable kernel yield improvements were achieved by implementing RDI according to variety-specific hull-split after two years. The least labor-intensive strategy of RDI during Nonpareil hull-split in all three varieties is recommended.

Advanced RDI regimes should use a sensitive indicator of plant water status to avoid excessive accumulation of plant water stress. In this research, a low-cost site-specific data-driven modeling scheme was developed for estimating midday stem water potential in different varieties of almond trees under various RDI regimes. The available explanatory data for the data-driven model of MSWP included soil water content at 30 cm, 60 cm, 90 cm, 120 cm, and 150 cm, solar radiation, air temperature, relative humidity, soil texture and gravel content at four layers, and fraction of photosynthetically active radiation intercepted by the canopy. Soil water content at 30 cm was the most significant explanatory variable of MSWP and showed a nonlinear relationship with MSWP. The square of soil water content at 30 cm was included in the model to approximate the nonlinear relationship between MSWP and soil water content at 30 cm. When all varieties were combined, the best regression model included the following explanatory variables of MSWP that were significant to enter and exit the model at the 0.001

significance level: soil water content at 30 cm, the square of soil water content at 30 cm, daily minimum air temperature, daily maximum relative humidity, daily minimum relative humidity, fraction of photosynthetically active radiation, and soil texture class between 10 to 86 cm (adjusted R^2=0.66, RMSE=0.31). Separate regression models for each variety improved the correlations in the Aldrich and Butte varieties with explanatory inputs selected at the 0.05 significance level to enter and exit the model (adjusted R^2=0.74, RMSE=0.27 and adjusted R^2=0.73, RMSE=0.28, respectively), but slightly worsened in the Nonpareil variety (R^2=0.64, RMSE=0.30). The results from this work indicate that the explanatory variables can vary across almond varieties and that site-specific characteristics, such as soil texture and the fraction of photosynthetically active radiation, are significant in determining MSWP in addition to the meteorological conditions and soil water content.

Key results of this research include (1) baseline data on crop water requirements in young almond trees, (2) new data and refined methods on regulated deficit irrigation in multi-variety almond orchards, and (3) a site-specific data-driven model for estimating stem water potential. This research directly addresses pressing issues affecting almond production, including uncertainties in water supplies and labor shortages in agriculture, that merit advanced research on precision irrigation.

Table of Contents

List of Figures

List of Tables

Chapter 1
Introduction

1.1 Problem statement

Farmers face mounting pressure to use water wisely due to limitations in water resources and increasing demands for food and biomass production. Recent policy changes such as the Sustainable Groundwater Management Act (SGMA) in California, water scarcity, and climate change challenge the way farmers have traditionally irrigated their crops and require advanced studies to improve irrigation management. California is the top producer of almonds in the world with almost 1.4 million acres (567,000 hectares) of almond orchards with an increase of 7% between 2016 and 2017 (California Department of Food and Agriculture, 2018a, 2018b). Almonds were California's third most valuable agricultural commodity, worth $5.47 billion in 2018 (California Department of Food and Agriculture, 2018b). The combination of high value, increasing crop acreage, and reliance on irrigation under limited water supplies requires improved techniques for sustainable irrigation management of almond orchards. In January 2019, the Almond Board of California set a bold goal of reducing the amount of water used to produce a pound of almonds by 20% by the year 2025 (Almond Board of California, 2019).

The goal of this research was to develop site-specific irrigation management strategies to help almond farmers conserve water while continuing profitable production levels. The word site-specific refers to specific characteristics or local conditions about the orchard that may merit adjustments to irrigation management. Every orchard has unique characteristics such as soil texture, tree age, tree varieties, canopy cover, topography, irrigation system design, climate, and so on. There is limited research on irrigation management strategies for almond orchards with young trees (<5 years) and multiple varieties (most of California's almond orchards). Also, there is a gap in research on developing site-specific models of plant water status.

1.2. Background and rationale

Almond orchards are perennial crops with a profitable production lifespan of approximately 25-30 years (Holtermann, 2016). Farmers must carefully manage their irrigation to achieve long-term productivity without under- or over-using water. Some important considerations in knowing the proper location, amount, and timing of irrigation include tree age, soil type, tree variety, and the plant water status response to irrigation scheduling. Young trees are smaller and require less water than older trees. Different varieties may be different sizes or have different tolerances to soil water supplies and atmospheric evaporative demands. Different soil types have different storage and infiltration properties. Stem water potential and evapotranspiration can serve as metrics of the plant water status response to irrigation scheduling, but these responses may vary by age, variety, and soil type. It is important to understand the implications of these site-specific factors on achieving sustainable irrigation management.

Satisfactory irrigation in young almond orchards is essential for canopy and root establishment during the non-bearing years and is the topic of Chapter 3. Young almond trees have small root systems, so there is a greater possibility of irrigating outside of the root zone than in mature trees. Too much irrigation can result in additional pruning and weed control requirements (Jarvis-Shean et al., 2018). Under- or over-irrigation can influence tree health, orchard uniformity, years to full production potential, and the total cost to establish an orchard (Jarvis-Shean et al., 2018). With a 7% increase in new almond orchards in California between 2016 and 2017, knowing how much to irrigate young almond orchards is critical to the future of the state's almond production (California Department of Food and Agriculture, 2018a). Limited research has been done in California to quantify actual evapotranspiration and crop coefficients

in young almond trees during the non-bearing years (Jarvis-Shean et al., 2018). As a result, farmers have little information to consider when irrigating their young almond trees.

Evapotranspiration is a measure of crop water use and can serve as the basis for scheduling irrigation in young almond trees. A farmer can irrigate in the amount that replaces the water lost due to evaporation and transpiration (i.e. evapotranspiration). Eddy covariance is a method for measuring turbulent fluxes such as sensible heat flux density. When sensible heat flux density is measured in conjunction with net radiation and ground heat flux density, the latent heat flux density can be calculated as the residual of the surface energy balance. The latent heat flux density can be converted into half-hourly and daily evapotranspiration measurements in mm/day using a turnkey data logger program and commercial sensors (Shapland et al., 2013). If evapotranspiration of a well-watered crop of interest and reference evapotranspiration from a standard well-watered grass surface are known, a crop coefficient can be calculated following Equation 1.1 (R.G. Allen et al., 1998).

$$K_c = \frac{ET_c}{ET_o} \qquad \textit{Equation 1.1}$$

where ET_c is the crop evapotranspiration, ET_o is the reference evapotranspiration, and K_c is the crop coefficient. The crop coefficient method is a convenient and often cost-free way for farmers to approximate the crop water requirements for their orchard by calculating ET_c=K_c*ET_o using tabulated K_c values specific to their crop and ET_o from a local weather station, such as the California Irrigation Management Information System (CIMIS). A farmer could reasonably guess that their orchard needs approximately 100% ET_c replacement in irrigation, with some error due to canopy and soil characteristics that differ from the orchard from which K_c was developed and discrepancies in the atmospheric evaporative demand due to the difference in location between the weather station and the orchard. Not many farmers use CIMIS data to aid

in irrigation scheduling. Twenty-six percent of registered CIMIS users identified themselves as farmers in a survey in 2013 (1,220 out of 45,000 registered users) (Eching et al., 2013). An estimated 15,000 farmers receive CIMIS related irrigation advisory services from agricultural consultants (Eching et al., 2013).

When water resources are limited, farmers may have to irrigate less than 100% ET replacement. Strategically applying less than 100% ET replacement during specific phenological stages when the trees can tolerate less water is known as regulated deficit irrigation (RDI) and is the topic of Chapter 4 (Zhang and Theib, 1999). A farmer may limit irrigation during growth stages that are minimally sensitive to drought, but not during critical development stages when drought could compromise crop yield or quality, such as during kernel development and during the non-bearing years (<5 years) in almonds. The relationship between applied water and yield has been shown to be nonlinear (Goldhamer and Fereres, 2017), so regulated deficit irrigation has the potential to reduce the amount of water used to produce a pound of almonds. RDI in mature almond trees has been studied under different severities and growth stages (Goldhamer et al., 2006; Kizer et al., 2017). Moderate RDI during the hull-split period has been shown to be successful in Nonpareil almond trees without significantly reducing crop yield or quality (Kizer et al., 2017). On the other hand, severe RDI during hull-split in Nonpareil almond trees, especially over multiple years, can significantly reduce kernel weight at harvest (Goldhamer et al., 2006). While RDI generally reduces kernel yields, the overall effect on yield is modest. For example, an irrigation treatment of 45% full ET replacement reduced yield by only 13% (Goldhamer et al., 2006). This shows that major reductions in water use through RDI may result in moderate losses in yield and profits for almond orchards. RDI can also improve orchard health and crop quality. Moderate RDI at hull-split can reduce hull rot, which is a disease caused by pathogens that colonize the hull tissue in the natural wounds that develop as

the hulls split (Gordon, 2019). Research has shown that short and severe pre-harvest RDI can reduce leaf and shoot death (Teviotdale et al., 2001). RDI during hull split can also reduce 'sticktights' (i.e., hulls that don't split) (Goldhamer et al., 2006).

Although regulated deficit during hull-split may seem straightforward, the strategy becomes more complicated when factoring in the different hull-split schedules of multiple varieties in the same orchard. Since most almond varieties are self-incompatible, farmers typically plant almond orchards in rows alternating between two or three different varieties for effective cross-pollination. Hull-split initiates at different times in each variety, as shown in Table 1.1. Farmers who cut back irrigation during hull-split usually do so according to the hull-split schedule of the Nonpareil variety in California because it is easier to irrigate the entire orchard the same way. The Nonpareil variety is highly valued for its soft thin outer shell, smooth attractive kernel, and consistently high yields, so farmers typically favor the irrigation toward optimizing this variety's output (Almond Board of California, 2015). No research has been published on RDI according to variety-specific hull-split schedules.

Table 1.1. 2019 Hull-Split and Harvest Dates in a Nonpareil-Butte-Aldrich Almond Orchard in Arbuckle, CA

2019 Dates	Nonpareil	Aldrich	Butte
1% hull-split initiation	7/9	7/27	8/7
Harvest date	8/22	9/11	9/11
Pickup date	9/4	9/25	9/25

Regulated deficit irrigation can lead to increased plant water stress. If not controlled, the plant water stress can become challenging to control later in the growing season. Effective indicators of the plant response to irrigation scheduling are important to avoid an accumulation of water stress during regulated deficit irrigation. Midday stem water potential (MSWP) has been showed to be a sensitive indicator of plant water status in tree crops and has been widely

recommended by crop advisors as a guide for irrigation scheduling (A. Fulton et al., 2017; Harold McCutchan and Shackel, 1992). The pressure chamber is the standard instrument for measuring MSWP, but it has the disadvantage of being labor-intensive and time-consuming. Multiple efforts have attempted to automate the pressure chamber with some success by commercial companies. However, these sensors have not been widely validated against the pressure chamber, they are expensive, and they are usually installed on a single tree for the entire season, limiting the flexibility to measure MSWP anywhere in the orchard. The labor-intensive nature of measuring MSWP has led to several efforts to model MSWP. Limited research has been published on site-specific data-driven modeling of midday stem water potential, which is the topic of Chapter 5.

1.3. Statement of research objectives

The primary goal of this research was to develop new strategies for site-specific irrigation management in almond orchards by assessing the implications of tree age and variety on irrigation scheduling and developing a site-specific data-driven modeling approach for estimating midday stem water potential. The overarching hypothesis is that tree age and variety have considerable implications on improving water use efficiency in almond orchards. The main objectives of this dissertation include:

1. Determine crop coefficients and crop water use of young almond orchards (Chapter 3).
2. Develop and evaluate a strategy for implementing regulated deficit irrigation based on variety-specific hull-split schedule in almond orchards (Chapter 4).
3. Develop a site-specific data-driven modeling approach for estimating midday stem water potential for different varieties of almond trees (Chapter 5).

1.4. Hypotheses

This research addresses the following hypotheses:

1. Crop water use and crop coefficients changes as the trees mature, and farmers should adjust the applied water depths as the trees grow.
2. Regulated deficit irrigation during variety-specific hull-split schedules can improve yield and nut quality and reduce the amount of water used to produce a pound of almonds.
3. Almond varieties have different stem water potential responses to regulated deficit irrigation, suggesting the need for irrigation by variety.
4. Multiple linear regression and nonlinear regression models can satisfactorily predict midday stem water potential from local plant, soil, and weather data.

Chapter 2
Literature Review

Abstract

The intersection of limited water resources and increasing water demand for agriculture has presented an urgency to develop strategies for improving water use efficiency. Regulated deficit irrigation (RDI) is a potential method for optimizing crop yield and quality while conserving water under limited water supplies. Effective implementation of RDI requires understanding water consumption—or evapotranspiration (ET)—of the plant and other site-specific characteristics, such as the soil, species, cultivar, and climate. Many methods exist to measure ET, each with advantages and disadvantages. RDI has been tested in a variety of crops, including peach, almond, walnut, apple, lemon, and mandarin, resulting in improved—or worse—crop production, depending on the crop, the phenological stage during which RDI was implemented, and the severity of deficit irrigation. Monitoring the plant water status is also crucial to successfully implementing RDI. Midday stem water potential is a sensitive indicator of plant water status than can be used as a guide for implementing regulated deficit irrigation. Together, regulated deficit irrigation, evapotranspiration, and plant water status measurements can be valuable tools for improving water use efficiency in agricultural regions with limited water supplies.

2.1. Introduction

With limited water resources and increasing food demands for a growing population, farmers face increasing pressure to improve water use efficiency. In 2010, irrigation in California used an average of 60.7% of total water withdrawals, averaging 87,000 m^3 of water, per day (United States Geological Survey, 2017). In drought, many farmers must cut back irrigation. Regulated deficit irrigation (RDI) may help improve water use efficiency while minimizing detrimental effects to crop production in drought.

RDI is an optimization approach to irrigation scheduling in which the farmer restricts water application during strategic phenological stages (Zhang and Theib, 1999). RDI is a type of precision irrigation—applying the right amount of water at the right place and at the right time. The purpose of RDI is to reduce water use and sometimes to improve crop quality. The farmer may limit irrigation during growth stages that are minimally sensitive to soil water deficit, but not during critical development stages when soil water deficit could compromise crop yield or quality.

RDI should optimize the water productivity of the crop, balancing competing goals of conserving water and optimizing crop yield and quality. The water productivity, colloquially referred to as the 'crop per drop,' is a measure of the water required to produce a unit of profitable yield. Measuring water productivity requires knowing the water consumption of the plant, also known as the evapotranspiration (ET), and the effective precipitation. ET is defined as the combination of water loss due to free-water evaporation, plant transpiration, and soil moisture evaporation (Fetter, 2001). Most ET in California occurs during the hot and dry summer, when precipitation is usually zero (Fetter, 2001). Intuitively, farmers should irrigate an amount equal the ET minus any effective precipitation. However, the water holding capacity of

soil enables farmers to strategically irrigate less than the ET minus the effective precipitation (i.e. RDI) by forcing plants to use more of the water already in the soil. Ideally, RDI would be implemented to avoid depleting the soil water storage beyond the management allowable depletion (MAD) set by the farmer, at which point the yield and/or quality of the crop begins to decline. Figure 2.1 shows the nonlinearity of a typical water production curve, where a small reduction of irrigation does not significantly reduce crop yield while reducing water use.

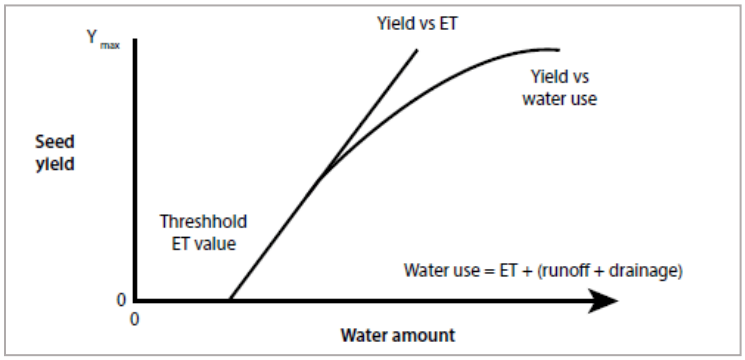

Figure 2.1. Generalized relationship between corn seed yield and water applied or water use (*Crop water use and yield*, 2015).

Small reductions in irrigation could be particularly important, especially for perennial crops (e.g. fruit and nut trees). Perennial crops are a large part of California's agricultural economy with walnuts, almonds, and grapes worth $1.24 billion, $5.16 billion, and $5.58 billion in 2016 (California Department of Food and Agriculture, 2019). Perennial crops such as fruit and nut trees cover large swaths of California's agricultural land and consume much of California's available freshwater. The acreage of land in California for producing fruit and nut crops continues to increase (e.g. almond acreage in California increased 7% between the years 2016 and 2017 according to the CDFA). This expanse of fruit and nut tree production coupled with growing criticism from the media toward tree farmers for using too much water partly explains the Almond Board of California's recent motivation to improve water use efficiency in almond trees. RDI in tree crops merits special research consideration because these crops experience

prolonged effects in irrigation management from year to year, unlike annual crops. Irrigation management decisions made this year affects the number of buds formed for next year's yield. Optimal RDI regimes require knowledge of the phenological stages where water stress would significantly compromise the crop yield or quality (González-Altozano and Castel, 1999).

This paper discusses the relevance and uses of RDI in perennial crops, starting with the origins of RDI and moving onto examples of RDI research in various tree crops. This paper presents a literature review of existing methods for measuring or estimating evapotranspiration and their applications to regulated deficit irrigation. Then this paper discusses stem water potential as a sensitive indicator of plant water status, which could be used as the basis of irrigation scheduling.

2.2. Regulated deficit irrigation

Regulated deficit irrigation (RDI) was introduced in the 1980s in peach and pear orchards to reduce excessive vegetative growth by increasing water stress (Chalmers et al., 1981; Mitchell et al., 1984). Excessive watering could increase production of vegetative growth rather than more fruit or nut, so RDI could prevent 'wasting' water on producing non-profitable parts of the crop. Further studies on RDI in the 1990s concluded that RDI also could improve fruit shelf life, taste, and quality in some fruit tree species but not others (Fereres and Goldhamer, 1990). Research in the 2000s expanded on the idea that reducing applied water during certain phenological stages of the year could improve water use efficiency and conservation, perhaps at the expense of decreased fruit production (Girona et al., 2003).

Early research on RDI resulted in questionable results on the effects of RDI on fruit growth partly due to different experimental conditions such as the cultivar, soil type, plant spacing, and meteorological conditions (Chalmers et al., 1981; Mitchell et al., 1984). Soil depth

and soil water holding capacity appear to be critical factors in determining the success of RDI regimes (Girona et al., 2003). RDI in tree orchards with shallow soils where the root system is more restricted can be more successful because it is easier to control excessive shoot growth. However, orchards with expansive root systems can seek water in far reaches of the soil even when the grower restricts water, making it harder to control excessive vegetative growth using RDI (Girona et al., 2003). Furthermore, cultivar, plant spacing, and climatic conditions could affect the sensitivity of an orchard to an RDI regime. Different cultivars may have different plant sizes, which would affect plant water consumption (i.e. larger plants need more water). Orchards with dense plant spacing and/or arid climate would also require more water (partly due to increases in evaporative water loss), increasing the sensitivity of the orchard to RDI. The tree species is one of the most important variables to consider in implementing RDI, partly because different tree species have unique physiological development stages that affect water needs. The rest of this section describes RDI experiences in different fruit and nut trees and is summarized in Table 1.

Moderate RDI during the hull-split period has been shown to be successful in nonpareil almond trees without significantly affecting crop yield or quality (Kizer et al., 2017). In a 2016 experiment in Arbuckle, CA, two management zones were created based on soil and plant characteristics and were managed via RDI. Of the two treatment zones, 69% ET and 80% ET were applied in irrigation (Kizer et al., 2017). Differences in yield and quality compared to the grower treatment (94% ET treatment) were not statistically significant. Severe pre-harvest RDI in nonpareil almond trees, especially over multiple years, reduces kernel weight at harvest (Goldhamer et al., 2006). While RDI generally reduces kernel yields, the overall effect on yield is modest (i.e., an irrigation treatment of 45% full ET replacement reduced yield by only 13%). Hull splitting can be delayed by severe pre-harvest stress but accelerated by milder stress. RDI

during hull split can also reduce 'sticktights' (i.e., hulls that don't split) and hull rot. Severe water stress induced by RDI can reduce canopy size without reducing fruit load (number of nuts/tree), although kernel sizes will be reduced. Processors tend to pay less for smaller kernels, where each of approximately five kernel size categories is worth about 5% less than the next biggest size (Goldhamer et al., 2006). In conclusion, major reductions in water use through RDI may result in moderate losses in yield for almond orchards.

Although RDI can improve quality for some crops, it can worsen the quality of others, including apple and peach, especially during some growth stages. At harvest, 'Delicious' apples (*Malus domestica Borkh.*) under RDI during cell-elongation phase of fruit growth were smaller, had higher soluble solids concentration (SSC), and lower titratable acidity than apples under full irrigation (Ebel et al., 1993). RDI could reduce fruit size but advance fruit maturity in apples while reducing water use. In peaches, RDI during the lag phase of the fruit growth curve can increase fruit yield but reduce fruit size (Girona et al., 2003). However, post-harvest RDI can lower peach yield but increase fruit size (Girona et al., 2003). A combination of RDI during the lag phase of the fruit growth curve and post-harvest periods could leave fruit yield and size relatively unchanged with water savings of 22% of the control applied water (Girona et al., 2003).

Previous research on RDI in citrus fruits in Spain's Mediterranean region may be relevant for evaluating potential RDI use in citrus orchards in California because of the similar climate. In mandarin oranges, summer RDI treatments could allow water savings between 7 and 14% without significantly affecting the yield or fruit quality, as long as the pre-dawn stem water potential does not surpass -1.3 MPa (González-Altozano and Castel, 1999). However, even small drops in pre-dawn stem water potential (0.1 to 0.2 MPa) due to spring RDI reduced yield by 62% and 28%, respectively, in the 25% ET and 50% ET treatments as a result of

increased "June drop," or early falling of fruit. Fall RDI resulted in 25 to 11% reduction in fruit size for the 25% ET and 50% ET treatments and increased external peel disorders, degrading fruit quality. In conclusion, summer RDI in mandarin oranges may result in water savings with little to no effects in yield or quality, but growers should be careful about doing spring and fall RDI.

An RDI study in Fino lemon trees subjected trees to three different irrigation levels: 100% ET_c all year (T0), 25% ET_c all year except during the rapid fruit development period during which 100% ET_C was applied (T1), and 100% ET_c all year except during the rapid fruit growth period during which 70% ET_c was applied (T2) (Domingo et al., 1996). Water savings of 30% and 20% were achieved in the T1 and T2 treatments, respectively. The T1 and T2 treatments did not result in significant yield reduction, but the T2 treatment did cause delay in reaching the marketable fruit size. Chemical characteristics related to the quality of the lemons were not significantly affected by any of the irrigation treatments. In conclusion, RDI in lemon trees may be promising for reducing water use.

Several studies have investigated the potential for RDI in walnut orchards. An RDI study in 'Chandler' walnut subjected trees to mild, moderate, and well-watered treatments (Buchner, R.P, 2008). The well-watered trees were irrigated to achieve midday stem water potential between -0.3 MPa and -0.6 MPa. The mild and moderate treatments were irrigated to achieve -0.3 MPa and -0.6 MPa early in the season and -0.7 to -0.9 MPa or -0.9 to -1.1 MPa, respectively, until harvest. Both RDI treatments reduced nut load and kernel quality. Similar results were found in 'Chico' walnuts (Goldhamer, 1988). In a study on 'Serr' walnuts, well-watered trees resulted in 43% higher returns than non-irrigated trees (Ramos, 1978). Another study found that water stress due to RDI decreased the number of dormant buds that flowered,

reducing nut load in English walnuts (Little, 2006). In conclusion, walnut trees do not appear to be good candidates for RDI regimes.

Table 2.1: Summary of RDI Experiences with Positive/Neutral Effects on Crop Yield and Quality

Crop	General RDI Regime with Positive/Neutral Effects	Effects on Quality	Effects on Yield
Almond	Moderate RDI during hull-split.	- Pros: Can reduce 'sticktights' and hull rots and speed up hull-split. - Cons: May reduce kernel size.	Modest reductions in yield, which could be offset by improvements in quality and water savings
Apple	None	-Pros: May advance fruit maturity -Cons: RDI could reduce fruit size and alter chemical characteristics	Would reduce yield due to smaller fruit sizes.
Peach	A combination of RDI during the lag phase of the fruit growth curve and post-harvest periods	Relatively unchanged	Relatively unchanged
Mandarin	Summer RDI with pre-dawn stem water potential not surpassing -1.3 MPa	Relatively unchanged	Relatively unchanged
Lemon	RDI all year except during rapid fruit development stage	Relatively unchanged	Relatively unchanged
Walnut	None	RDI would have major negative effects on quality.	RDI would have major negative effects on yield.

2.3. Evapotranspiration and crop coefficients

Farmers must know the water consumption or ET of their orchard to intelligently implement RDI. Several techniques exist to measure or model ET, each with pros and cons. Major methods include mass balance using a lysimeter, crop coefficient methods, surface energy balance algorithms using remote sensing, statistical methods of eddy covariance, and basic water balance methods. In this paper, each method will be considered in terms of spatial and

temporal resolution, accuracy, convenience, cost, and other relevant criteria and whether it can be used for implementing RDI. Although most methods for estimating ET are not currently employed by farmers, future water limitations and water budgets may make formal ET estimates more important in irrigation management and water rights administration.

2.3.1. Weighing Lysimeter

A direct measurement of actual evapotranspiration, or ET_a, can be obtained from a lysimeter. A lysimeter is a large container holding soil and plants suspended on a weighing system to measure changes in soil moisture storage (Jensen and Allen, 2016). The initial soil water content is recorded. Any irrigation water or precipitation into the container is measured, so changes in soil moisture storage can be calculated (Fetter, 2001). The amount of water lost through evaporation and transpiration is determined by the change in weight in the lysimeter. ET_a measurements from a lysimeter can be combined with meteorologically derived grass ET estimations (ET_o) to estimate crop coefficients (Ayars et al., 2003; Wright, 1991). A problem with lysimeters is that the container holds only one or a small number of plants, so it must accurately represent the soil type and profile, moisture content, and type and size of vegetation of the entire surrounding field (Jensen and Allen, 2016). In addition, lysimeters are time-consuming to validate, expensive, and are typically only used by researchers (Fetter, 2001). Lysimeters have been used to measure crop water requirements and determine crop coefficients of a variety of crops, including pomegranate and vegetables (Bryla et al., 2010; Zhang et al., 2017).

2.3.2. Soil Water Balance Method

The ET_a can be estimated from the following soil water balance equation:

$$ET_a = I + P - (SW_2 - SW_1) - D \qquad \textit{Equation 2.1}$$

where I is the applied irrigation water (mm) and P is the precipitation (mm) during the sampling duration, SW_1 is the soil water content at the beginning of the sampling period (mm), SW_2 is the soil water content at the end of the sampling period (mm), and D is the drainage during the sampling period (mm) (Jensen and Allen, 2016). Soil water content measurements derived from neutron probe counts can be used to measure the change in soil water content at the beginning and end of the sampling period. Electromagnetic devices based on capacitive and dielectric properties can also be used for determining the soil water content, but the volume of influence of these devices is much smaller than the neutron probe (size of a volleyball) and may not be appropriate for sampling large and representative area for estimating evapotranspiration.

2.3.3. Crop Coefficient Methods

Reference evapotranspiration (ET_0) is the evapotranspiration that would occur for a standard crop under unlimited soil moisture given the climatic conditions (Jensen and Allen, 2016). The ET_0 is usually measured from a well-watered field of grass with an assumed crop height of 0.12 m, a fixed surface resistance of 70 s m^{-1}, and an albedo of 0.23 (R.G. Allen et al., 1998). To compute ET for a different crop, the ET_0 should be multiplied by a crop coefficient, K_c, to obtain the crop evapotranspiration, or the ET_c (R.G. Allen et al., 1998). The crop coefficient corrects for differences in the vegetative density and maturity, the climatic conditions, and the water-storage capacity of the actual crop of interest compared to the reference crop (R.G. Allen et al., 1998).

Since 1982, the California Irrigation Management Information System (CIMIS) has provided hourly and daily ET_0 data. The ET_0 from the CIMIS stations is measured as the evapotranspiration of a well-watered 0.08 to 0.15 m grass surface using either the Penman-

Monteith equation or the CIMIS Penman equation ("California Irrigation Management Information System," 2018). There are several limitations to using CIMIS stations for irrigation management. ET_0 from CIMIS weather stations could poorly represent the water consumption of a farmer's orchard because the weather stations may be far away from the field and not in the same climatic conditions. Also, the required crop coefficients to estimate the ET_c are tabulated values that may not represent the climatic or vegetative conditions of a specific field (A. E. Fulton et al., 2017). Furthermore, any increase in water stress through RDI would cause the ET_a to be less than the ET_c because transpiration—the T component in ET—would decline due to stomatal closure induced by water stress (Jensen and Allen, 2016). The difference between ET_a and ET_c under deficit irrigation highlights the importance of measuring ET_a when implementing RDI.

Crop coefficient values have been tabulated for a variety of crops (R.G. Allen et al., 1998; Jensen and Allen, 2016). The crop coefficient does not account for variations in region or climate between the reference crop and the actual crop. Therefore, it is usually assumed that the ET_0 contains all information regarding variation in weather and climate. A problem with tabulated crop coefficients is that they do not consider the variation in vegetation height, amount, and density throughout the growing season or from year to year. Typically, crop coefficient values are tabulated by the month for a specific crop and these values may not be updated frequently—the same crop coefficients may be used for a decade or more.

The simplest crop coefficient method for estimating the ET_c is known as the single crop coefficient method, where $ET_c = K_c * ET_0$. This method assumes the plant is under well-watered conditions. If the plant is not under well-watered conditions, a stress coefficient can be factored in through the 'dual crop coefficient' method, where the total crop coefficient is computed as follows (Allen et al., 2005):

$$K_c = K_{cb} * K_s + K_e$$ *Equation 2.2*

where K_c is the total crop coefficient, K_s is the dimensionless 'stress' coefficient ranging from 0 to 1, K_e is a coefficient that adjusts for changes in evaporation due to wet soil from an irrigation or precipitation, and K_{cb} is a basal crop coefficient representing the transpiration component of ET and a small amount of evaporation from soil that is dry at the surface. The ET_a can be estimated from the 'dual crop coefficient' approach using the following equation (Richard G. Allen et al., 1998)

$$ET_a = (K_{cb} * K_s + K_e) * ET_0$$ *Equation 2.3*

The derivation of K_e comes from daily soil water balance curves and depends on the shape function of K_s versus soil water content or soil water potential (R.G. Allen et al., 1998). The K_{cb} is a function of the fractional canopy cover, which can be determined using the Normalized Difference Vegetation Index (NDVI).

$$K_{cb} = f(f_c)$$ *Equation 2.4*

$$f_c = f(NDVI)$$ *Equation 2.5*

The NDVI quantifies vegetation from multispectral remote sensing data by measuring the difference between near-infrared—strongly reflected by plants—and red light—absorbed by plants. Sensors that detect near infrared (NIR) light are used on satellites, unmanned aerial vehicles (UAVs), planes, and/or static sensors for quantifying NDVI. Healthy vegetation reflects considerable amounts of NIR, whereas unhealthy vegetation does not. Additionally, soil does not reflect much NIR, so NDVI can be used for vegetation and land change detection (Glenn, E., 2011). NDVI can be calculated from the following equation:

$$NDVI = \frac{(NIR-Red)}{(NIR+Red)}$$ *Equation 2.6*

where Red and NIR are the spectral reflectance measurements obtained in the red (visible) and near-infrared regions, respectively. The individual reflectances are ratios of reflected over

incoming radiation in each spectral band. Therefore, reflectances range from 0.0 to 1.0. NDVI ranges in value from -1.0 to +1.0.

Typically, the total crop coefficient increases during the growing season due to plant development, wet soil surface, and limitations in available water. Under well-watered conditions, K_s is 1, but less than 1 under water limited conditions (Richard G. Allen et al., 1998). The computation of K_{cb} has been widely studied in recent years with the increasing availability of data from multispectral remote sensing at varying temporal and spatial resolutions (Allen and Pereira, 2009; Anderson et al., 2017).

2.3.4. Modeling evapotranspiration using energy balance theory

Energy balance methods for estimating ET are based on a key requirement for the process of evapotranspiration to occur—the existence of available energy for water to change phase from liquid to vapor (Jensen and Allen, 2016). To use energy balance methods, the following parameters typically must be known: net solar radiation input, energy output through conduction to the ground, net output of sensible heat to the atmosphere, change in heat energy stored in the ground per unit of surface area, and the latent heat of vaporization at the given temperature. Heat transfer models over canopy cover typically involve solving for *ET* as a residual of the one-dimensional surface energy transfer equation (Kustas, 1990).

$$\lambda E = R_n - G - H \qquad \textit{Equation 2.7}$$

where R_n is the energy flux of net radiation (W/m^2), H is the sensible heat flux into the air (W/m^2), λE is the latent heat flux into the air (W/m^2), and G is the ground heat flux (W/m^2) (Bastiaanssen et al., 1998). Other energy components such as the heat storage in the vegetation or canopy air space and the energy associated with photosynthesis are considered negligible and are typically not included in these modeling schemes.

2.3.5. Eddy Covariance Method

The eddy covariance method is based on turbulent transport theory in the atmospheric surface layer (Jensen and Allen, 2016). Eddy covariance is based on the concept of the covariance (or the correlation) between the vertical fluxes of vapor (H_2O or CO_2) or the sensible heat in the vertical portion of the movement of the eddies. Eddies are defined as turbulent airflow due to the Earth's undulating surface, wind, and the convective heat flow between the Earth's surface and the surrounding atmosphere. Evapotranspiration occurs when more water vapor occurs in upward moving eddies than downward moving eddies. The eddy covariance method directly measures components in the eddies such as water vapor, carbon dioxide, or heat. The eddy covariance method measures evapotranspiration using eddy covariance sampling of the boundary layer using the relationship between the vapor flux (E) and a specific form of the covariance of the H_2O concentration and the vertical wind speed as shown in equation 2.8.

$$\lambda E = \rho\overline{w'q'} = \frac{0.622}{P}\rho\overline{w'e'} \qquad \textit{Equation 2.8}$$

where E is the vapor flux [kg m^{-2} s^{-1}], q' is the instantaneous deviation of specific humidity from the mean specific humidity (q) [kg kg^{-1}], e' is the instantaneous deviation of vapor pressure from the mean vapor pressure (e) [kPa], w' is the instantaneous deviation of vertical wind velocity from the mean vertical wind velocity (w) [m s^{-1}], P is the atmospheric pressure, ρ is the air density [kg m^{-3}], and the overbar representing the means of the products of the instantaneous deviations, typically over 15 to 30 minute periods (Jensen and Allen, 2016; Swinbank, 1951).

The sensible heat flux density (H) can also be measured using the eddy covariance method, as shown in equation 2.9.

$$H = \rho C_p\overline{w'T'} \qquad \textit{Equation 2.9}$$

where T' is the instantaneous deviation of air temperature from the mean air temperature [K] and H is in W m^{-2}.

The eddy covariance method can provide ET estimates with high temporal resolution through the use of high-speed, high-precision instruments (Wilson et al., 2001). Covariances between high-frequency (10 or 20 Hz) vertical wind speed and H_2O concentration can be used to estimate the latent heat flux density using co-located sonic anemometer and infrared gas analyzer (Jensen and Allen, 2016). Measuring small changes in upward and downward moving air is critical to accurately determine ET using the eddy covariance method because turbulent flow is continually changing. The eddy covariance method has the challenge of lack of closure of the energy balance, where the sum of the measured latent heat flux density and the sensible heat flux density ($\lambda E + H$) does not equal the measured $R_n - G$ (Jensen and Allen, 2016; Twine et al., 2000; Wilson et al., 2001). Lack of closure could be due to unaccounted contributors to the energy balance such as storage of heat in canopies, horizontal advection, and change in storage of heat in the boundary layer underneath the instrumentation, as well as frequency responses of the eddies that are not detected by the sensors (Jensen and Allen, 2016). Covariances between high-frequency (10 or 20 Hz) vertical wind speed and the air temperature can be used to estimate the sensible heat flux density using a sonic anemometer and calculating the latent heat flux density through the residual λE from the energy balance equation: $\lambda E = R_n - G - H$ (Shapland et al., 2013).

2.3.6. Surface Renewal Method

Like eddy covariance, surface renewal method is based on turbulent transport theory in the atmospheric surface layer (McElrone, 2013). With the surface renewal method, the ET is determined by calculating the latent heat flux density as the residual of the energy balance

equation, as shown in Equation 2.7. While measurements of R_n and G are simple and inexpensive, direct measurements of H can be more difficult because high-frequency measurements are needed due to the ephemeral nature of air parcels above the canopy. The surface renewal method uses fine thermocouples to measure high frequency air temperatures at the surface-atmosphere interface, reducing the cost and complexity of the method (French et al., 2012; Snyder et al., 1996).

2.3.7. Bowen Ratio Method

The Bowen Ratio is the ratio of the sensible heat flux and the latent heat flux. Flux densities of sensible and latent heat are expressed as:

$$H_{BR} = (R_n - G)/(1 + \beta^{-1}) \quad \textit{Equation 2.10}$$

$$\lambda E_{BR} = (R_n - G)/(1 + \beta) \quad \textit{Equation 2.11}$$

where β is the Bowen Ratio ($H/\lambda E$) (Bowen, 1926). It is assumed that the principle of similarity holds and atmospheric resistances to heat and water vapor are equivalent, so β can be obtained from the following:

$$\beta = \gamma(\partial T/\partial e) \quad \textit{Equation 2.12}$$

where e is the vapor pressure of the air and γ is the psychrometric constant with a value of 0.066 MPa K^{-1} at 20 °C and a pressure of 101.3 MPa.

A minimum of two sets of measurements at two heights are required, but systematic measurement errors can be reduced by calculating values of H_{BR} and λE_{BR} from plots of temperature against vapor pressure (Huband and Monteith, 1985). The Bowen ratio method can accurately estimate λE when $-1.5 < \beta < -0.5$.

The Bowen Ratio method has the advantage of canceling the aerodynamic transport terms from the energy balance equation. Also, only simple measurements of air temperature

and vapor pressure at two different elevations as well as net radiation and ground heat flux (Wang, 2015). The Bowen Ratio method has the advantage of being able to estimate λE for potential and nonpotential surfaces. On the other hand, the Bowen ratio method has the disadvantages of numerical instability of β near -1 and requires large fetch (Jensen and Allen, 2016).

2.3.8. Spatial evapotranspiration using remote sensing

Remote sensing data, such as from satellites or unmanned aerial vehicles (UAV), are useful for deriving maps of ET using energy balance methods (Allen et al., 2007; Bastiaanssen et al., 1998; Norman et al., 1995). ET is generally determined from aerial imagery by calculating the latent heat energy consumed by ET, which is equal to the residual of the surface energy balance equation. One surface energy balance algorithm is the Surface Energy Balance Algorithm for Land (SEBAL) (Bastiaanssen, W, 2005; Bastiaanssen et al., 1998). A distinct feature of the SEBAL algorithm is the calculation of a near-surface temperature gradient, dT, using two points to represent 'hot' pixels and 'cold' pixels to denote hydrologic contrast (i.e., dry and wet land surfaces). The dT is indexed to the radiometric surface temperature, eliminating the problematic need for absolute surface temperature calibration. SEBAL uses land surface characteristics such as surface albedo, vegetation index (or leaf area index), and surface temperature derived from satellite imagery. Meteorological data such as wind speed, relative humidity, solar radiation, and air temperature must also be measured. R_n is calculated from satellite-measured narrow-band reflectance and surface temperature. G is estimated from R_n, surface temperature, and leaf area index. H is calculated from surface temperature ranges, surface roughness, and wind speed.

The Mapping Evapotranspiration at High-Resolution with Internalized Calibration (METRIC) method is another satellite-based method for estimating ET as a residual of the surface energy balance equation and is based on the SEBAL method (Allen et al., 2007). METRIC differs from SEBAL in that it uses ET_o from weather stations to define the energy balance condition of the 'cold' pixel, or well-watered condition. The energy balance is internally calibrated at the dry and wet extreme conditions usually local weather data, such as from CIMIS weather stations. Factoring in weather station data is a way to ground-truth satellite-based ET estimations.

While SEBAL and METRIC treat soil and vegetation as one lumped component, the Two-Source Energy Balance Model (TSEB) treats them separately. TSEB uses directional radiometric surface temperature for partitioning soil and vegetation heat fluxes (William P Kustas and Norman, 2000; Norman et al., 1995). Remote sensing-based ET estimations for sparse canopies, such as tree orchards, can be more accurate by considering the effects of soil and vegetation temperatures (Burchard-Levine et al., 2019; William P. Kustas and Norman, 2000; Semmens et al., 2016). TSEB estimates of ET tend to agree better with ET flux tower observations for bare soil and sparsely vegetated areas (William P Kustas and Norman, 2000). Large discrepancies in sensible heat flux (H) estimates can arise due to inadequacies in accurately representing land cover scenarios. For energy balance residual methods, inaccuracies in H estimates will ultimately lead to inaccuracies in ET estimates, emphasizing the importance of knowing the land cover type for which ET will be estimated. Although TSEB may be more accurate for estimating ET in sparse canopies, this method requires additional information on the fractional canopy cover and high spatial resolution for distinguishing between canopy and soil surfaces.

2.3.9. Comparison of Methods for Measuring ET

ET has been studied for decades, but challenges remain in accurately, continuously, and remotely quantifying it. Not all methods for estimating ET are practical for farmers to use in irrigation management. Table 2.2 compares major methods for estimating ET in terms of spatial and temporal resolution, challenges, and advantages.

Weighing lysimeter and soil water balance methods have the advantage of being simple to understand, but neither method is practical for farmers, each for unique reasons. ET measurements from lysimeters can have high accuracy if set up correctly but are very expensive and cannot provide high-resolution spatial measurements of ET. Lysimeters also must be installed upon planting a new tree because it is difficult to transplant a tree into a lysimeter once it is mature. Lysimeters are labor-intensive to use because they must be continuously maintained to represent the conditions of the rest of the orchard (e.g., weeds cannot grow in the lysimeter when they are not in the rest of the orchard). The soil water balance also can be labor-intensive to implement. The soil moisture must be measured at multiple locations and depths to obtain a spatial representation of the soil moisture in the orchard. Also, not all soil moisture sensors have the same accuracies, and labor-intensive manual methods (e.g., neutron probe, volumetric method) for measuring soil moisture still surpass most remotely and continuously sensing soil moisture measurements in terms of accuracy. Furthermore, it can be difficult to close the soil water balance due to poor estimates of drainage, which is sometimes assumed to be zero. ET estimates from the soil water balance method do not include evaporation from canopy interception (Wilson et al., 2001). Simplicity is a huge advantage of the lysimeter and soil water balance methods, but maintenance and data collection issues make them unattractive for use by most farmers.

Unlike the lysimeter and soil water balance methods, the crop coefficient methods provide farmer-friendly methods for estimating ET where the data is open-source and has high temporal resolution (i.e., hourly, daily, and monthly estimates are available through CIMIS). Crop coefficient methods may be easy to use for irrigation scheduling, but crop coefficients are developed from experimental studies and are limited in how well they represent a farmer's orchard characteristics, such as the soil type, vegetative cover, and species. Despite inadequacies in the crop coefficient method, it is probably the most popular choice among tree farmers for estimating ET because the data are free to California almond farmers, the calculations are simple, and the data are available daily.

Satellite-based residual energy balance methods attempt to fill in some gaps from crop coefficient methods, including the need to accurately represent the vegetative cover conditions, the climatic region, and plant water stress level of the vegetation. Satellite-based approaches have the advantage of estimating ET_a instead of ET_c, so dry conditions can be more accurately measured. Furthermore, satellite imagery can be obtained above specific sites, making it possible to factor in the climate of a specific agricultural site. Some satellite-based algorithms for estimating ET such as TSEB can separate vegetation and soil in the same image, offering more detailed analysis of ET in regions where crop coefficients may not be accurate due to differences in tree spacing, cover crop, and weeds between the orchard where the crop coefficients were derived and a farmer's orchard (Norman et al., 1995).

A disadvantage of residual energy balance approaches is that the ET estimate is only as accurate as the R_n, G, and H components. METRIC attempts to overcome this disadvantage by applying internalized calibration on H instead of λE to absorb estimation errors and biases introduced during the data processing. There is also a strong need to evaluate uncertainties in

satellite-based ET_a algorithms across a range of hydrometeorological and surface cover scenarios to improve the operationality of the algorithms (Paul et al., 2012).

Another problem with remote sensing methods for estimating ET is that satellites typically have an inverse relationship between spatial resolution and temporal resolution. Satellite imagery with high temporal resolution tend to have low spatial resolution and vice versa. Landsat 8 attempts to balance the tradeoff between spatial and temporal resolution by offering imagery once every 16 days (if no clouds interfere with image quality) and 30 m spatial resolution, so it is a popular satellite for ET estimations. The temporal resolution could be further improved by also using satellite imagery from Sentinel, which has similar temporal and spatial resolution but flies over California on a different schedule than Landsat 8. Landsat 8 and Sentinel imagery are open-source, so they essentially free sources of data for estimating ET. Although the imagery is open-source, the labor and expertise required to process satellite imagery into meaningful ET estimates is beyond what a typical farmer would be willing to do. Therefore, the applicability of satellite-based ET estimates partly relies on successfully transforming the complex algorithms into a farmer-friendly platform displaying ET estimates.

Eddy covariance methods are complex due their foundation in turbulent transport theory. Independent measurements of the flux components used in eddy covariance methods can lead to lack of closure of the surface energy balance (Jensen and Allen, 2016). As a result, the sensible and latent heat fluxes can be underestimated (Twine et al., 2000). Data processing can be very complex and not something a typical farmer would have the expertise to do. Eddy covariance methods also has the disadvantage of being very expensive ($30,000+) and requiring a large fetch to accurately represent the turbulent transport of the vegetation of interest (Jensen and Allen, 2016). It requires the following sensors: net radiometer, soil temperature sensors, air temperature sensor, relative humidity sensor, wind vane to measure wind direction,

anemometer to measure wind speed, soil heat flux plates to measure ground heat flux, soil temperature sensors, a rain gauge to measure precipitation, and an infrared gas analyzer to measure the densities of water vapor, CO_2, and CH_4 (Jensen and Allen, 2016; Lee et al., 2005). Despite these disadvantages, the eddy covariance method is still one of the most accurate methods for estimating ET_a as long as there is enough fetch

The eddy covariance method can be simplified into the surface renewal method for estimating ET_a by eliminating the sonic anemometer (McElrone, 2013; Shapland et al., 2013). However, eddy covariance is still needed to calibrate the sensible heat flux density in the surface renewal method, so the sonic anemometer is still for calibration. Also, ET flux towers for eddy covariance and surface renewal methods require adequate fetch for incoming atmospheric gases to flow to accomplish an accurate ET_a estimate of the orchard. An expert is essentially required to correctly install an ET flux tower and specialized software would be needed to analyze the data. The complexity and the cost of eddy covariance and surface renewal systems make it less attractive to farmers.

Variations in the uncertainty among ET estimation methods complicates accurately accounting for ET in water management and planning. Medellin-Azuara et al. (2018) attempted to reveal the uncertainty in ET estimates in several field crops in the Sacramento-San Joaquin Delta (Medellin-Azuara, J., 2018). Future research should do a similar study focusing on ET estimation uncertainty in perennial crops in other regions, especially where canopies are sparse and varying in age. ET is one of the largest and most important components not only in agriculture, but also in regional water budgets.

Table 2.2: Comparison of methods for estimating evapotranspiration

Method	General Operation	Resolution	Challenges	Advantages
Lysimeter	A large container measures changes in soil water storage	- Measures Et_a at one location - Can have frequent temporal resolution	- Labor-intensive to validate - Expensive - Only used by researchers	- Direct measurement of Et_a - Highly accurate if set up correctly - Simple
Soil Water Balance	Estimates the ET_a as the residual of the soil water balance equation, which considers the irrigation, precipitation, drainage, and change in soil water content at the site.	- Manual measurements can lead to infrequent spatial and temporal resolution.	- Labor-intensive - Only used by researchers - Difficulty factoring in drainage.	- Simple
Crop Coefficient	The ET of a reference crop is multiplied by a crop coefficient to estimate ET_c	- One ET estimate is assumed to represent the entire orchard - Can be hourly, daily, or monthly	- Not site-specific - The single-crop coefficient method measures the ET_c, not Et_a. - The dual crop-coefficient method is complex to implement.	- Open-source data - Easy calculations - High temporal resolution
Satellite-Based Energy Balance	ET is calculated from satellite imagery as the latent heat flux consumed by ET, which is equal to the residual of the surface energy balance equation.	- Inverse relationship between spatial and temporal resolution	- ET_a estimate is only as good as the net radiation, ground heat flux, and sensible heat flux estimates. - Must be ground-truthed. - Complex calculations.	- Estimates ET_a, - Can factor in the climate, vegetative cover, and plant water stress level - Open-source data
Eddy Covariance	Covariances between the wind speed and gas concentration are used to estimate scalar and energy fluxes, such as water vapor, carbon dioxide, and heat.	- High temporal resolution, but usually one tower per orchard	-Complex turbulent transport theory -Issues with lack of closure in the surface energy balance -Expensive -Need expert installation	-Highly accurate - Frequent ET_a estimates
Surface Renewal	ET is computed as the residual of the energy balance of the crop canopy using complex turbulent transport theory.	- High temporal resolution, but usually one tower per orchard	-Complex turbulent transport theory -Sensible heat flux estimates require eddy covariance calibration -Moderately expensive -Need expert installation	-Can be highly accurate if properly calibrated - Frequent ET_a estimates

2.4. Leaf and stem water potential

Plant water status measurements can serve as a useful guide for optimizing water use. Water potential is a measurement that combines the effects of the soil, plant, and atmospheric conditions on water availability within the plant (Harold McCutchan and Shackel, 1992). Sunlit leaf water potential has been used to measure the plant water stress, but it is known to have rapid temporal fluctuations as a function of the environmental conditions (such as passing clouds) (Jones, 2004). Pre-dawn leaf water potential can reduce the variability associated with changing environmental conditions, but it measures the overnight recovery of water potential rather than the maximum water demand during the day (Meyers and Green, 1980). Leaf water potential has also been shown to have little or no statistically significant differences between wet and moderate irrigation treatments, so it may not be a good indicator of plant water status under moderate soil water depletion (Harold McCutchan and Shackel, 1992).

Stem water potential, also known as the xylem water potential, is another measurement of the plant water status. Stem water potential is more stable to environmental conditions than leaf water potential (Jones, 2004). Stem water potential can be measured using a pressure chamber on shaded leaves. Since there can be a within-leaf water potential gradient, the leaves should be enclosed inside mylar bags for about 10-20 minutes before measurement to allow for the equilibrium between the leaf and the adjacent branches and trunk (Fulton et al., 2014). Midday stem water potential is measured between 12:00 and 4:00 p.m., which is when the plant is experiencing relatively constant and maximum water demand. Placing the leaf inside a mylar bag limits photosynthesis, reducing the measurement variability associated with using sunlit leaves with varying exposures to light and heat (Fulton et al., 2014).

Stem water potential has been shown to be a sensitive indicator of water stress in tree crops, including almonds, walnuts, and prunes (A. Fulton et al., 2017; Harold McCutchan and Shackel, 1992). Furthermore, stem water potential has relative predictability with respect to the environmental vapor pressure deficit and is closely related to the crop water use and stomatal conductance. Irrigated and unirrigated trees have shown clear differences in stem water potential in prunes.

2.5. Conclusions

The review of literature shows that the tools for developing site-specific irrigation management exist but need to be refined into information that a farmer can use towards building strategies for improving water use efficiency. Various studies have been done on regulated deficit irrigation in various crops, but strategies need to be developed for implementing regulated deficit irrigation at specific sites, such as almond orchards with multiple varieties. Furthermore, the methodology for developing crop coefficients and water use of various crops exist, but research needs to employ that methodology towards determining site-specific crop coefficients and water use estimates, such as almond orchards with young trees. Lastly, stem water potential has clearly been shown to be a good indicator of plant water status, but further research needs to examine how site-specific characteristics, such as climate, canopy size, and soil texture, affect the midday stem water potential, which can be investigated through site-specific data-driven modeling.

Chapter 3
Crop coefficients and water use of young almond orchards

Abstract

An observational study was conducted in the northern Sacramento Valley to determine crop water use and crop coefficients of three adjacent young Nonpareil/Monterey almond orchards. Methods used to quantify evapotranspiration estimates of crop water use include (1) soil water balance and (2) land surface energy balance using eddy covariance. Three adjacent almond orchards that were planted in 2016, 2017, and 2018 were monitored from 2018 to 2020. Crop coefficients were determined using actual evapotranspiration estimates from each orchard and short grass reference evapotranspiration from the Gerber South California Irrigation Management Information System (CIMIS) station (ID #222) and refined to adjust for water stress using a dual crop coefficient approach. Results showed that crop water use and crop coefficients increased until the 4th leaf, indicating the need to closely consider tree development and orchard age as factors in irrigation scheduling of young almond trees. The results led to the conclusion that farmers should use development or age-specific crop coefficients in developing orchards for irrigation-scheduling until the 4th leaf when they can start using mature almond K_c values. This study has generated baseline data on crop water requirements of young almond orchards that could prove useful for (1) developing irrigation scheduling tools for young almond orchards, and for (2) determining water budgets for areas with new almond orchards.

3.1. Introduction

California almond acreage continues to rise as more farmers are converting from annual to permanent crops such as almonds. Total almond acreage in California, including non-bearing trees, increased by 10% between 2018 and 2019 (CDFA, 2019). Of the total almond area of 619,000 hectares in California, 142,000 hectares were non-bearing almond trees (22.9%). The necessity for irrigation to achieve profitable production of almond trees, especially in developing trees, coupled with increasing uncertainty in California water supplies, requires the adoption of management practices that optimize irrigation water use.

Optimal irrigation scheduling requires information about the crop water use, also known as the evapotranspiration (ET). The ratio between the evapotranspiration of a well-watered crop (ET_c) and the evapotranspiration of a well-watered reference crop such as grass (ET_0), known as a crop coefficient (K_c), can serve as a tool for irrigation scheduling of a variety of crops (Jensen and Allen, 2016). Crop coefficients are primarily a function of the vegetative cover and are expected to increase as young trees grow in size (Jensen and Allen, 2016). The maximum daily transpiration of young almond trees near Córboda, Spain has been shown to increase from 1 mm to 4 mm as canopy ground cover increases from 3 to 50%, confirming the need to adjust irrigation amounts as the young trees increase in size (Espadafor et al., 2015). Under- or over-irrigation can influence tree health, orchard uniformity, years to full production potential, and the total cost to establish an orchard (Jarvis-Shean et al., 2018). Prevention of under-irrigation throughout the growing season in young almond trees is essential for accelerating canopy and root establishment during the non-bearing years (Fereres et al., 1981). Over-irrigation outside the small root zones of young almond trees can result in additional pruning and weed control requirements (Jarvis-Shean et al., 2018).

Estimates of ET and K_c in almonds have primarily focused on mature trees. In recent years, the

recommended maximum (mid-stage) K_c for mature almonds has ranged between 0.90 and 1.15 (Richard G. Allen et al., 1998; Goldhamer, 2012; Sanden et al., 2012). Developing almond trees, which have smaller canopies and root systems, are expected to have lower K_c values than mature trees. Efforts have been made to scale K_c values of mature almond trees to young almond trees using either the percent ground cover (GC) or the midday fraction of photosynthetically active radiation intercepted by the canopy (fPAR). Doorenbos and Pruitt (1977) recommended a reduction in maximum K_c values by 25-35% and by 10-15% for canopies with 20 and 50% ground cover, respectively (Doorenbos and Pruitt, 1977). Espadafor et al. (2015) measured the ratio between K_T, which is equivalent to the ratio between the transpiration (T) and ET_0, and fPAR in 3rd and 4th year 'Guara' almond trees and found that the ratio oscillated around a value of 1.2 during the entire irrigation season from mid-May to early September.

Fereres et al. (1982) measured the ET of drip-irrigated young almond trees (ages 1-6 years) using a soil water balance procedure. They obtained a relationship between the percentage ground cover (GC) and the ET of young trees as a percentage of calculated ET of mature trees. Their empirical relationship has been extensively used to estimate ET of young trees (Ayars et al., 2003). In contrast to the Fereres et al. (1982) study which involved an orchard with 7.3 x 7.3 meter tree spacing, modern almond orchards tend to have tighter tree spacing (commonly, 4.3 x 6.7 meter), and thus, crop water use is expected to be significantly higher in modern orchards. Updated research is needed on crop water requirements of young almond orchards to better reflect current orchard management practices.

Evapotranspiration and crop coefficients are typically determined using weighing lysimeters, but lysimeter data may not be representative of field conditions with potential errors of up to 200% (Allen et al., 1991). Evapotranspiration estimates determined through energy balance principles using modern meteorological instrumentation can measure field-scale

evapotranspiration. Although evapotranspiration can be estimated using measurements of latent heat flux density, λE, using the eddy covariance method, the requirement of an expensive quick-response infrared gas analyzer limits the practical use of that method. Computing λE as the residual of the soil-vegetation surface energy balance removes the need for an infrared gas analyzer but requires estimation or assumption of all other components in the energy balance of the soil-vegetation surface.

The objectives of this study were to: (1) estimate evapotranspiration in 1st through 5th leaf almond trees using energy balance and soil water balance methods, and (2) determine crop coefficients that farmers could use for irrigation scheduling of young almond trees.

3.2. Materials and Methods

3.2.1. Study Area

The study was conducted at a commercial almond orchard [*Prunus dulcis*, cultivars 75% Nonpareil and 25% Monterey], located in Corning, California (39.95° N, 122.13° W) with rows North-South oriented. The study area consisted of three adjacent orchards that were planted in 2016, 2017, and 2018 as shown in Figure 3.1. Row spacing was 6.7 meters and tree spacing was 4.3 meters, resulting in 348 trees per hectare. The plots were irrigated with one Olsen microspinkler per tree at 9.7 gph. Each plot had a Tule station that estimated ET_a using a propriety version of the surface renewal method, which the farmer used as the primary (but not the only) basis for irrigation scheduling (www.tuletechnologies.com). The farmer also considered midday stem water potential measurements from a pressure bomb for the irrigation scheduling. The farmer implemented deficit irrigation for approximately a week before shaking the almond trees during harvest in the 4th and 5th year trees to minimize the risk of bark splitting and improve the ease of access of the harvesting machine. The plots were monitored from 2018 to 2020 to determine crop

water use and crop coefficients in 1st through 5th leaf almond orchards. The study area has a warm-summer Mediterranean climate with mean monthly minimum and maximum temperatures of 7.5 °C (January) and 26.5 °C (July), respectively. Average annual rainfall in this region of California is 548 mm, which mainly occurs between the months of October and May. Little to no rainfall occurs in the months leading up to almond maturity (June to September), requiring irrigation to maintain plant health and productivity. The primary soil series was Kimball loam with some sections of Perkins gravelly loam and Tehama loam (USDA NRCS National Cooperative Soil Survey). Cover crop was grown in each orchard during the fall/winter and terminated in the spring prior to the peak irrigation season.

3.2.2. Estimation of ET_a Using an Energy Balance

Field-scale energy flux densities were measured to evaluate the actual evapotranspiration (ET_a) to determine the crop water use in each orchard. Estimations of sensible heat flux density, ground heat flux density, and net radiation were used to calculate latent heat flux density as the residual of soil-vegetation surface energy balance, as shown in equation 3.1.

$$\lambda E = R_n - G - H \qquad \textit{Equation 3.1}$$

where R_n is net radiation [W m^{-2}], G is ground heat flux density [W m^{-2}], H is the sensible heat flux density [W m^{-2}], and λ is the latent heat of vaporization of water [MJ kg^{-1}]. The change in energy stored in the canopy or surface boundary layer between the ground surface and the height where H was measured, and the energy consumed by photosynthesis are usually less than a few percent of the energy balance and can be assumed to be negligible (Jensen and Allen, 2016). The energy balance was forced closed by assuming that H was accurately measured and solving for λE as the residual of the energy balance equation shown by equation 3.1. This method obeys conservation of energy and does not require measurements of λE (Twine et al., 2000).

The latent heat flux density was converted into half-hourly and daily evapotranspiration, ET_a, measurements in mm/day using a turnkey data logger program and commercial sensors (Shapland et al., 2013). A two-dimensional coordinate rotation correction was applied to the sonic anemometer wind speed data in the datalogger program to force the mean crosswind and vertical wind velocities to zero (Shapland et al., 2013). ET_a instead of ET_c was measured because the orchard was commercial with occasional water stress and heterogeneity of vegetation within the orchard.

Between 2018 and 2019, three flux stations were installed in each of the three adjacent young almond orchards to estimate R_n, G, and H, as shown in Figure 3.1. Each flux station consisted of a three-dimensional, sonic anemometer (Model 81000 VRE, R.M. Young Company, Traverse City, MI, USA) oriented in the prevailing wind direction (North to South) and installed approximately 1 m above the top of the canopy, two Type E fine-wire thermocouples with 0.0762 mm diameter (FW3, Campbell Scientific, Logan, UT, USA) at the same height as the sonic anemometer, a net radiometer (NR-LITE2, Campbell Scientific, Logan, UT, USA), and soil heat flux plates at 5 cm depth (HFT3.1, REBS, Bellevue, WA, USA), as shown in Figure3.2. Auxiliary data included air temperature and relative humidity (HMP45C, Campbell Scientific, Logan, UT, USA), soil water content at 5 cm depth (EC5, METER Group, Pullman, WA, USA), and soil temperature from thermocouples at 5 cm depth (TCAV-L, Campbell Scientific, Logan, UT, USA), and a tipping rain gauge with a 20 cm orifice (TE525WS, Campbell Scientific, Logan, UT, USA). Each orchard had enough fetch to accurately estimate ET using each flux station. P18 was 13 hectares, P17 was 8 hectares, and P16 was 14 hectares. The flux stations had the capability of estimating H using both eddy covariance and surface renewal methods (Shapland et al., 2013).

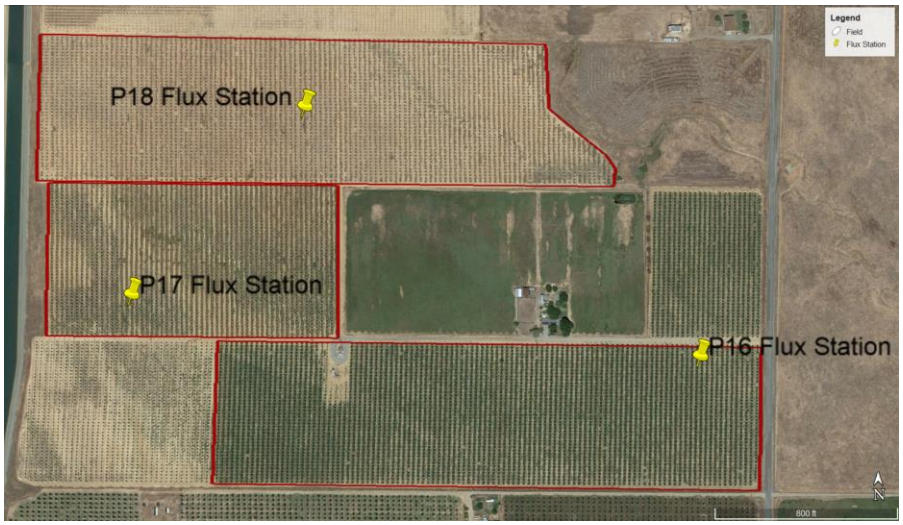

Figure 3.1. Locations of the three flux stations near Corning, CA to estimate evapotranspiration in young almond orchards.

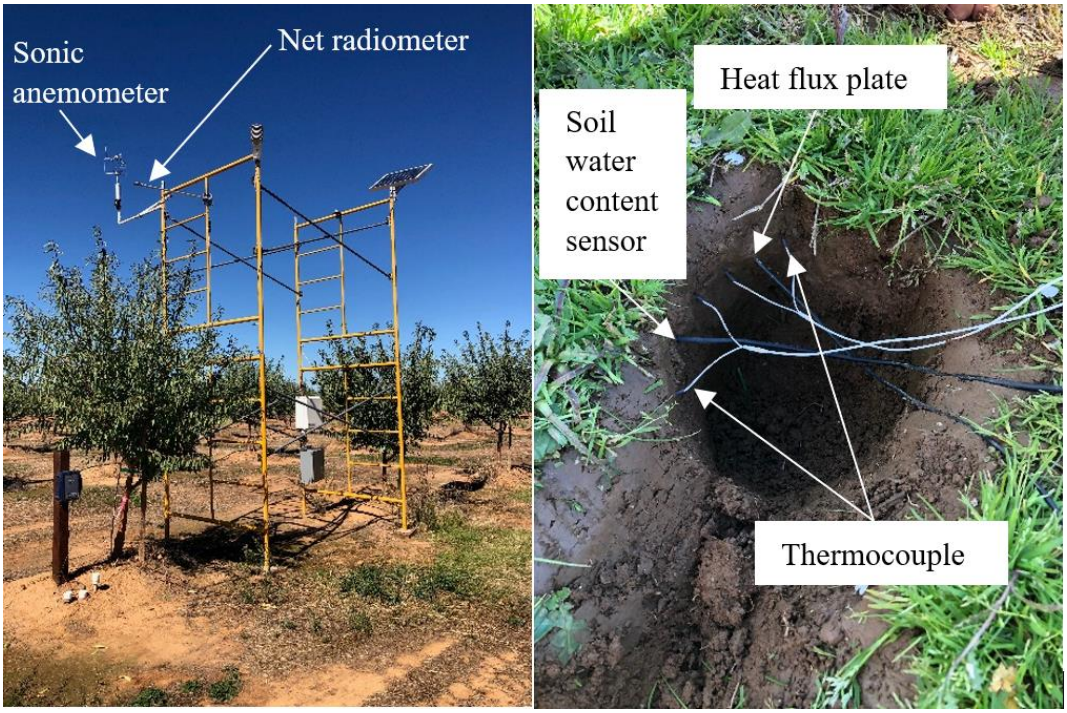

Figure 3.2. Left: A picture of the flux station in the 2nd leaf orchard in 2019, showing the sonic anemometer and the net radiometer. Right: A picture of the soil water content sensor, heat flux plate, and thermocouples installed at 5 cm depth to measure the ground heat flux.

3.2.3. Estimation of ET_a Using a Soil Water Balance

Neutron probe access tubes were installed in the orchards planted in 2017 and 2018 using a Geoprobe (Salina, KS, USA). Four transects of six tubes centered around a tree trunk were installed in each of the two orchards. In each transect, two access tubes were installed 90 and 180 cm from the tree trunk into the row to the east, two access tubes were installed at 90 and 180 cm from the tree trunk along the tree row to the north, and two access tubes were installed at 90 and 180 cm from the tree trunk along the tree row to the south. The soil texture was analyzed using the pipette method at 0-30, 30-60, 60-90, 90-120, 120-240 cm sections at the same locations that the soil was excavated for installing the access tubes (Soil Survey Laboratory Methods Manual, Soil Survey Investigations Report No. 42, 1992). Neutron counts were measured before the irrigation season began and immediately prior to harvest in 2019 and 2020. Seasonal ET_a was estimated using a soil water balance, as shown in equation 3.2.

$$ET_a = P + I - D - R - \Delta S \qquad \textit{Equation 3.2}$$

where P is precipitation, I is irrigation, D is drainage, R is runoff, and ΔS is the change in soil water storage during the period used for assessing the water balance. Runoff was observed to be negligible. Minimal or no rainfall occurred during the major periods of the study and neutron probe data showed that drainage was negligible. Most of the change in soil water content was driven by root water uptake in response to irrigation events.

3.2.4. Estimation of Crop Coefficients

Actual crop coefficients, K_a, were calculated as the ratio between ET_a and the reference evapotranspiration from a standard well-watered grass surface (ET_o) as shown in equation 3.3.

$$K_a = \frac{ET_a}{ET_o} \qquad \textit{Equation 3.3}$$

where ET_a is the actual evapotranspiration, ET_o is the reference evapotranspiration, and K_a is the actual crop coefficient. ET_o was obtained from the CIMIS (California Irrigation Management Information System) Gerber South Station ID 222 (40.028778° N, 122.15575° W), located approximately 9.6 kilometers from the flux stations used in this study. The FAO Penman-Monteith method was used to estimate hourly ET_o (Richard G. Allen et al., 1998).

K_a estimates were converted into standardized crop coefficients, K_c, through the dual crop coefficient approach shown in equation 3.4.

$$K_a = K_s K_{cb} + K_e \; where \; 0 \leq K_s \leq 1 \qquad Equation\ 3.4$$

where K_{cb} is a basal crop coefficient, K_s is a water stress coefficient, and K_e is an evaporation coefficient.

K_{cb} during the mid-season ($K_{cb\ mid}$)was estimated from leaf area index (LAI) using equation 3.5 with K_{cmin}=0.15 and $K_{cb,full}$ assumed to be 0.85 for almonds (Richard G. Allen et al., 1998).

$$K_{cb\ mid} = K_{c\ min} + \left(K_{cb\ full} - K_{c\ min}\right)(1 - \exp[-0.7\ LAI\ ]) \qquad Equation\ 3.5$$

where $K_{cb\ mid}$ is the estimated basal K_{cb} during the mid-season when the plant density are lower than the full cover condition, $K_{cb\ full}$ is the estimated basal K_{cb} during the mid-season when the vegetation is at full cover condition (0.85), $K_{c\ min}$ is the minimum K_c for bare soil (0.15), and LAI is the leaf area index, or the area of leaves per area of underlying ground surface averaged over a large area [$m^2\ m^{-2}$] (R.G. Allen et al., 1998). LAI for each plot was estimated using the fractional photosynthetically active radiation (PAR) intercepted by the canopy (fPAR) derived from a mule lightbar that consisted of 18 ceptometers (Lampinen et al., 2012; Zarate-Valdez et al., 2012). The fPAR is the ratio of the PAR measurements below the canopy and outside the canopy. The LAI was calculated using the inverted formula for predicting scattered and transmitted PAR under a canopy shown in equation 3.6 (Campbell and Norman, 1998).

$$LAI = \frac{\left[\left(1-\frac{1}{2K}\right)*f_b-1\right]*\ln(\tau)}{A*(1-0.47*f_b)} \qquad Equation\ 3.6$$

where K is the canopy extinction coefficient calculated using an assumed spherical leaf angle distribution (LAD) and the zenith angle of the sun, f_b is the sun beam fraction (0.98 measured in an almond orchard from a different study, Zarate-Valdez et al. (2012)), A is the leaf absorptivity in the PAR band and assumed to by 0.86071 for green plants (Ross, 1975), and τ is the transmittance of the canopy in the PAR range (calculated as 1-fPAR).

K_s was estimated using a weekly soil water balance as shown in equation 3.7 (Richard G. Allen et al., 1998).

$$D_{r,i} = D_{r,i-1} - (P - RO)_i - I_i - CR_i + ET_{c,i} + DP_i \qquad Equation\ 3.7$$

where $D_{r,i}$ is the root zone depletion at the end of the week [mm], $D_{r,i-1}$is the water content in the root zone on the previous week [mm], P_i is the precipitation on week i [mm], RO_i is the runoff from the soil surface on week i which was observed to be negligible [mm], I_i was the net irrigation on week i [mm], CR_i was the capillary rise from the groundwater table on week i which was assumed to be negligible according to knowledge about the site [mm], $ET_{c,i}$ was the crop evapotranspiration on week i estimated using the eddy covariance energy budget method from the onsite flux stations [mm], and DP_i was the water loss out of the root zone due to deep percolation [mm] which was observed to be negligible based on the neutron probe observations (Richard G. Allen et al., 1998). The maximum rooting depth was estimated to be roughly 106 cm (42 in) for the almond trees (2nd through 5th year) by observing that most of the changes in the soil water content estimates derived from the neutron probe data occurred in the top 106 cm (42 in) of the soil and observing that root water uptake was responsible for most of the changes in soil water content throughout the study. The initial depletion within the maximum rooting depth (106 cm) was assumed to be equal to the readily available water (RAW) of 26.7 cm (10.5 in) which was

determined for the site's Kimball loam soil based on the NRCS Soil Survey which approximately corresponded with the soil texture determined from the pipette method. The total available water (TAW) in the root zone was determined to be 66.7 cm (26.25 in) from the NRCS Soil Survey for Kimball loam soil. The K_s was calculated using equation 3.8.

$$K_s = \frac{TAW - D_{r,i}}{TAW - RAW} \qquad \textit{Equation 3.8}$$

Once K_a, K_{cb}, and K_s were determined, K_e was calculated as the residual of equation 3.4. Not enough data was determined to conduct a weekly soil water balance of the topsoil, so the K_e was not estimated using the methods described in FAO no. 56 (Richard G. Allen et al., 1998).

$$K_e = K_a - K_s K_{cb} \; where \; 0 \leq K_s \leq 1 \qquad \textit{Equation 3.9}$$

Once K_e, K_s, and K_{cb} have been estimated, K_c can be calculated using equation 3.5.

$$K_c = K_s K_{cb} + K_e \; where \; K_s = 1 \qquad \textit{Equation 3.10}$$

Equation 3.10 assumes that K_e is the same when the almond trees are under well-watered conditions (K_c) and under water stressed conditions (K_a). Under well-watered conditions, there might be increased evaporation of the topsoil compared to under-watered conditions, so K_e might be underestimated and, as a result, K_c would be underestimated in equation 3.10.

3.2.5. Auxiliary Plant and Soil Measurements

The fraction of photosynthetically active radiation intercepted by the canopy (fPAR) was determined using a mule lightbar to gain insight on differences in canopy size between the three orchards (Lampinen et al., 2012; Zarate-Valdez et al., 2012). The fPAR of 7 to 14 rows in each orchard were averaged to determine a single fPAR estimate in each orchard in 2019 and 2020, as shown in Table 3.1. Leaf area index was estimated from fPAR measurements using equation 3.6 as described in section 3.2.4 (Campbell and Norman, 1998).

Table 3.1. Fraction of photosynthetically active radiation intercepted by the canopy in relation to orchard age

Orchard	Age	Date	Average fPAR
P18	second leaf	6/5/2019	0.09
P17	third leaf	6/5/2019	0.23
P16	fourth leaf	6/5/2019	0.47
P18	third leaf	6/19/2020	0.25
P17	fourth leaf	6/19/2020	0.22
P16	fifth leaf	6/19/2020	0.55

Midday stem water potential (MSWP) was measured using a pressure chamber once a week during the irrigation season in all three orchards in all years of the study. Neutron probe counts were measured at depths 20, 46, 76, 107, 137, 168, and 198 cm and converted into soil water content measurements through a local calibration equation.

3.2.6. Multiple Linear Regression Model of Crop Coefficients

A stepwise selection procedure was used to select significant predictor variables in a multiple linear regression model to predict ET_a/ET_o. The significance levels to enter and exit the model were set at 0.2. Variables that were tested for significance in the model included MSWP, fPAR, and soil water content at 20, 46, and 76 cm. Soil water content at 107, 137, 168, and 198 cm had severe multicollinearity (i.e. variance inflation factor > 10 and Pearson correlation coefficient > 0.95) and were not included in the multiple linear regression model. The C_p statistic was computed and used to determine the model with the least bias. The Proc Reg procedure in SAS was used to conduct stepwise selection and multiple linear regression. Data from the months of June through August of 2019 and 2020 were included in the model from all three orchards.

3.3. Results

3.3.1. Daily evapotranspiration

Daily reference evapotranspiration (ET_o) from the Gerber South CIMIS station from 2018-2020 are shown in Figure 3.3. The Penman-Monteith equation was used to calculate ET_o. The data shows that the climate was relatively consistent in all years of the study.

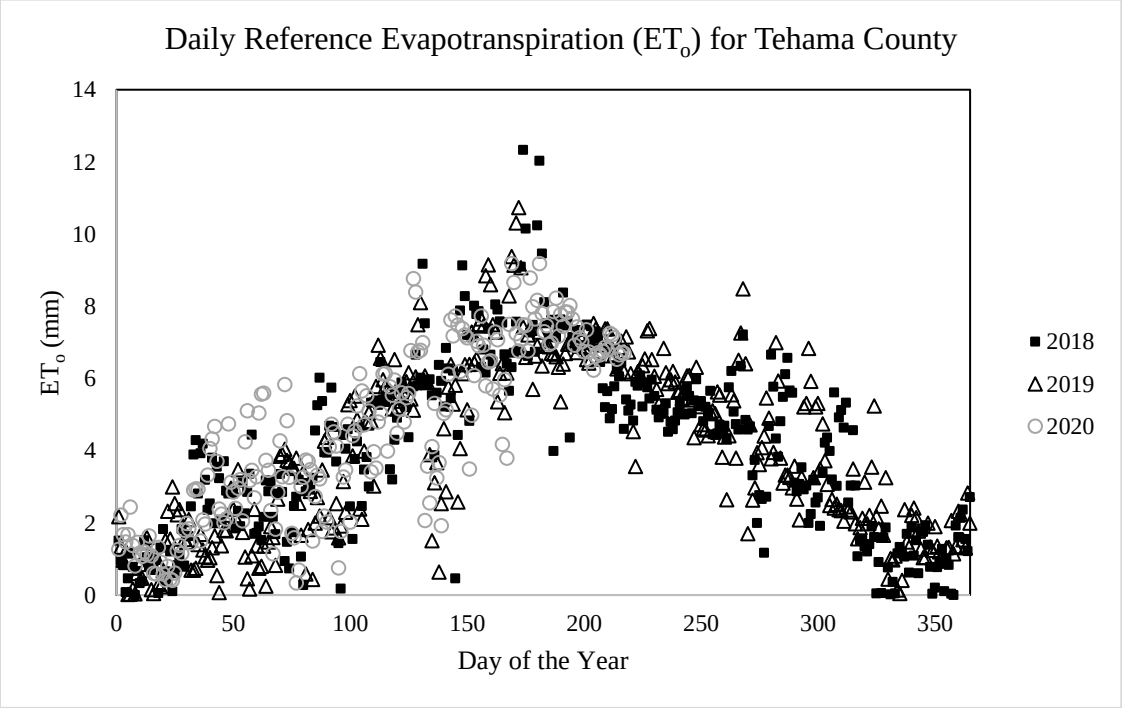

Figure 3.3: Daily reference evapotranspiration (ET_o) for 2018-2020 near Corning, CA obtained from the Gerber South CIMIS (California Irrigation Management Information System) station #222.

Monthly crop water use (ET_a) of each orchard from 2018-2020 is shown in Table 3.2. ET_a was calculated using an eddy covariance energy balance method. In every year of the study, monthly ET_a was higher in the older orchards except in 2020 when the 4th leaf orchard had higher monthly ET_a than the 5th leaf orchard.

Table 3.2. Monthly crop water use (ET_a) of young almond trees measured using an eddy covariance energy balance in the 2016 (P16), 2017 (P17), and 2018 (P18) plantings in 2018-2020.

Month	*2018 1st leaf P18*	*2018 2nd leaf P17*	*2019 2nd leaf P18*	*2019 3rd leaf P17*	*2019 4th leaf P16*	*2020 3rd leaf P18*	*2020 4th leaf P17*	*2020 5th leaf P16*
February						42	57	39
March						66	78	73
April						114	135	128
May						151	186	172
June			98	198		175	212	202
July	61		97	193	219	197	245	229
August	67	105	84	129	130	137	164	151
September	47	92	50	95	99			
October	28	48	25	86	67			

Note on missing data: The flux stations were installed in June and July in 2018 and were taken down in the winter of 2018 and re-installed in June and July of 2019.

Figure 3.4 shows the daily ET_a [mm/day] of 1st and 2nd leaf almond orchards in 2018 measured using eddy covariance energy balance method. The 2nd leaf trees had higher daily ET_a than the 1st leaf trees in June through September. Normally, almond farmers reduce irrigation during the week leading up to the harvests of each variety in August and September to reduce damage to tree trunks and to improve orchard access of harvest machinery, which would reduce ET_a and increase water stress. The farmer normally continues to withhold irrigation for a couple of weeks after harvest while the almonds are drying on the ground, which also contributes to water stress and a reduction in ET_a. However, neither the 1st nor 2nd leaf trees were harvested using a mechanical shaker to avoid damaging the tree trunks of the developing trees. The 1st and 2nd leaf orchards approached similar daily ET_a at the end of September and early October as the leaves progressed into senescence and atmospheric evaporative demand decreased. By mid-October, the daily ET_a was again higher in the 2nd leaf orchard than in the 1st leaf orchard.

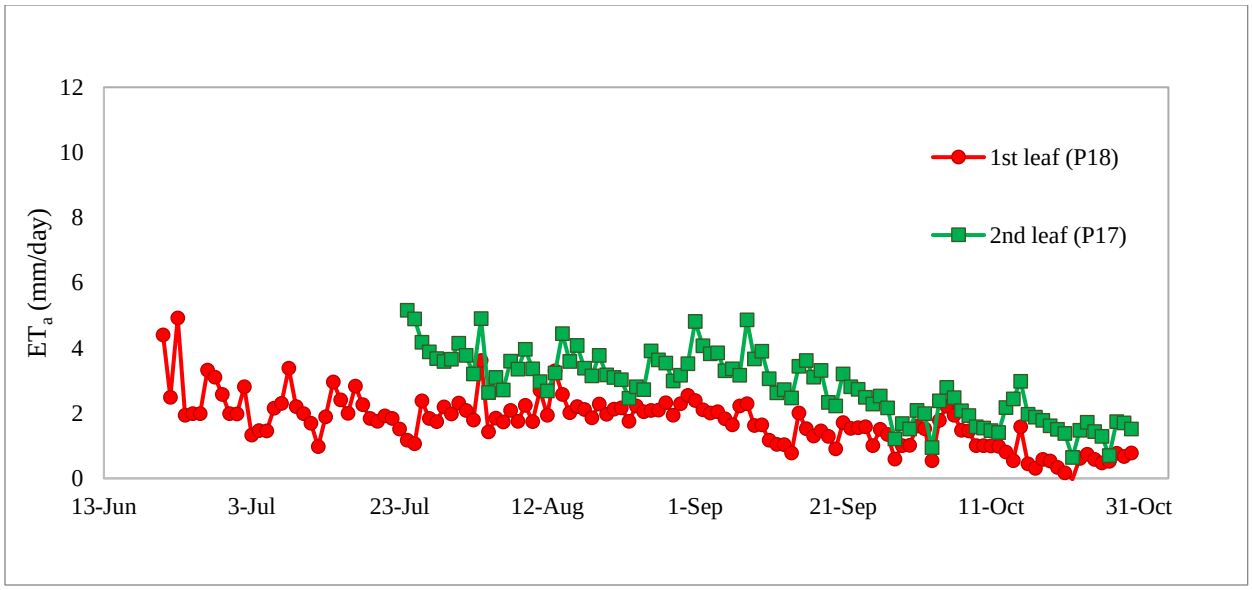

Figure 3.4. Daily crop water use (ET_a) of 1st and 2nd leaf almond orchards in 2018 near Corning, CA measured using an eddy covariance energy balance.

Figure 3.5 shows the daily ET_a [mm/day] of 2nd, 3rd, and 4th leaf almond orchards in 2019 measured using eddy covariance energy balance method. The 2nd leaf almond orchard had the lowest daily ET_a. The 3rd and 4th leaf orchards had similar daily ET_a except in July when the 4th leaf orchard had higher daily ET_a than the 3rd leaf orchard. Both the 3rd and 4th leaf orchards were harvested using a mechanical shaker in August for the Nonpareil trees and September for the Monterey trees. The farmer reduced irrigation in August during the harvest activities, so the ET_a declined in the 3rd and 4th leaf orchards. The 2nd leaf orchard was not mechanically shaken to avoid damaging the tree trunks, so there was no decrease in ET_a during August.

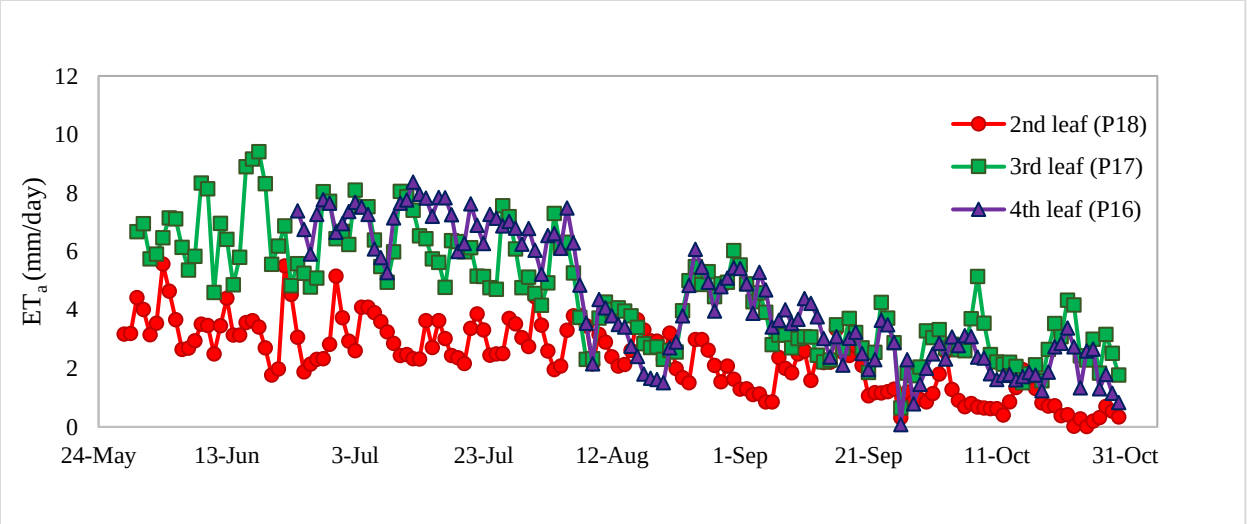

Figure 3.5. Daily crop water use (ET_a) of 2nd, 3rd, and 4th leaf almond orchards in 2019 near Corning, CA measured using an eddy covariance energy balance.

Figure 3.6 shows the daily ET_a [mm/day] of 3rd, 4th, and 5th leaf almond orchards in 2020 measured using eddy covariance energy balance method. Both the 4th and 5th leaf orchards had similar daily ET_a, with the 4th leaf orchard typically slightly above the 5th leaf orchard. The 3rd leaf orchard had the lowest daily ET_a. Daily ET_a increased beginning in January and peaked in all three orchards in July before decreasing as the atmospheric evaporative demand lowered in August through October and leaves began to fall due to harvest activities and senescence. All three orchards were harvested with a mechanical shaker in August for the Nonpareil trees and September for the Monterey trees. The farmer reduced irrigation during August and September to prepare for the harvest activities, resulting in a reduction in ET_a. Also, smoke from the LNU Lightning Complex Fires between August 17th and the end of September reduced net radiation, which also contributed to a decline in ET_a.

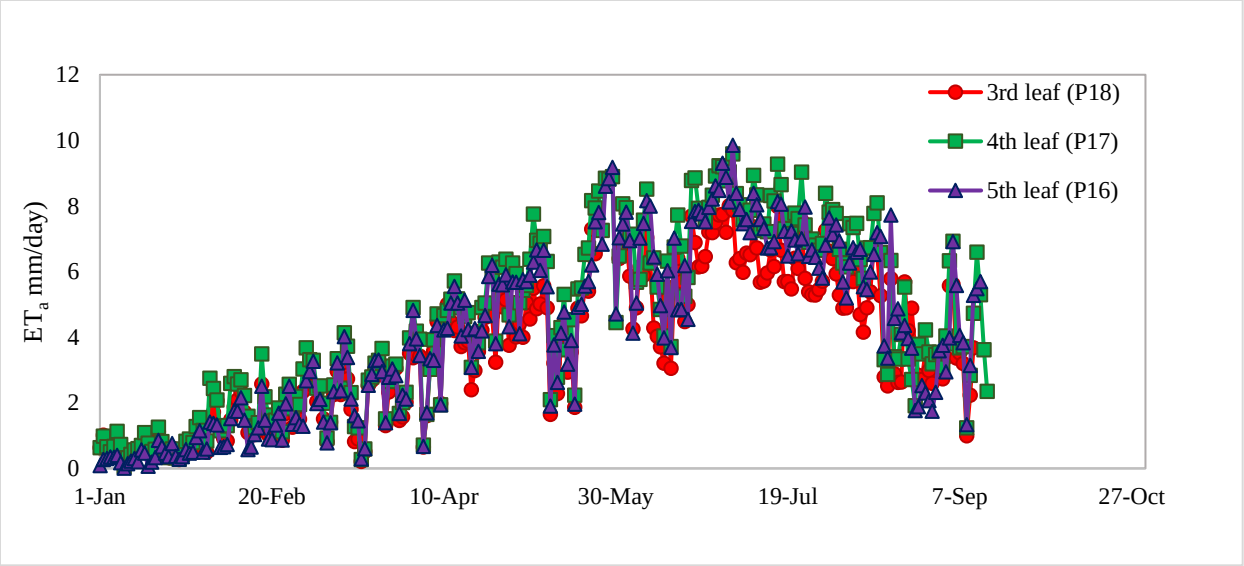

Figure 3.6. Daily crop water use (ET_a) of 3rd, 4th, and 5th leaf almond orchards in 2020 near Corning, CA measured using an eddy covariance energy balance.

3.3.2. *Daily actual crop coefficients (ET_a/ET_o)*

Figure 3.7 shows the daily actual crop coefficients (ET_a/ET_o) for 1st and 2nd leaf orchards in 2018. Daily ET_a/ET_o was consistently higher in the 2nd leaf orchard than in the 1st leaf orchard, indicating the need to use crop coefficients according to age to schedule irrigation through crop water use replacement. Spikes in the ET_a/ET_o throughout the season aligned with irrigation events. Daily ET_a/ET_o considerably increased around 229 to 233 days after bloom because there was low ET_o on those days. Daily ET_a/ET_o was smoother when the ET_o was also smoother. When ET_o decreases, ET_a theoretically should decrease accordingly because the environmental conditions that drive ET_o also drive ET_a. However, low ET_o due to clouds at the CIMIS station may not always be present at the flux station at the orchard where ET_a was measured. Therefore, ET_o and ET_a may not always increase or decrease accordingly.

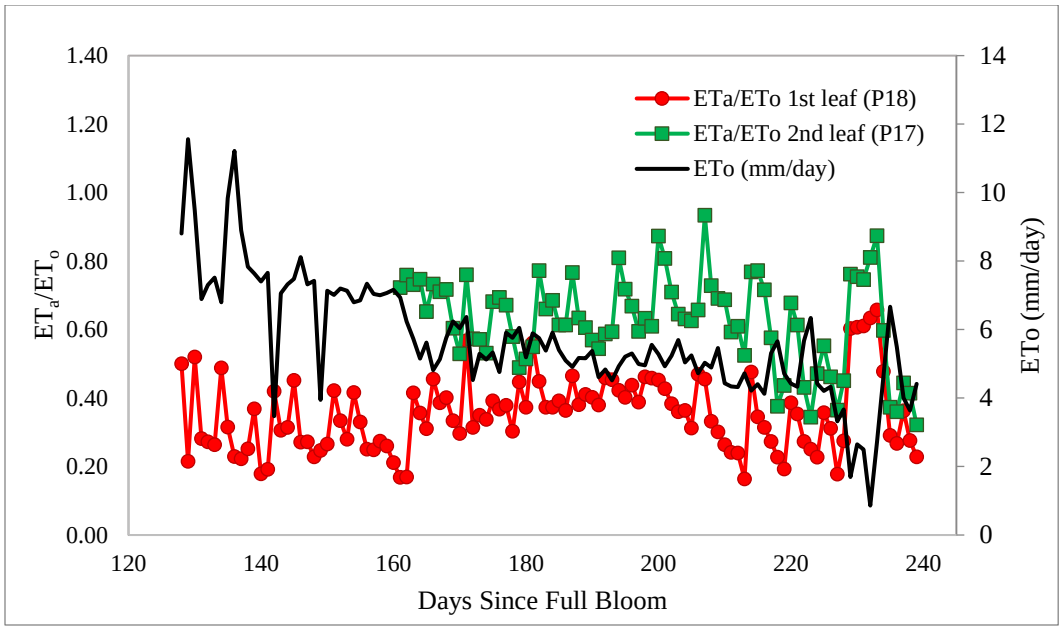

Figure 3.7. Daily actual crop coefficients (ET_a/ET_o) for young almond orchards in 2018.

Figure 3.8 shows the daily actual crop coefficients (ET_a/ET_o) for 2nd, 3rd, and 4th leaf orchards in 2019. Daily ET_a/ET_o was consistently higher in the 3rd and 4th leaf orchards than in the 2nd leaf orchard. The ET_a/ET_o declined between 150 and 170 days since full bloom due to the farmer's reduction in irrigation during the harvest activities.

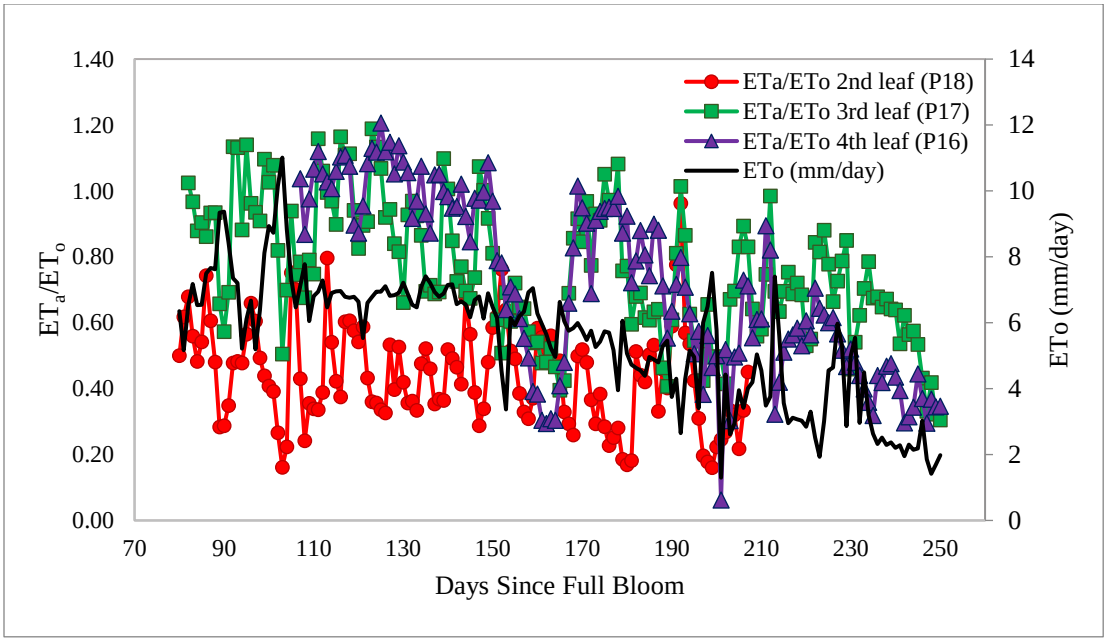

Figure 3.8 Daily actual crop coefficients (ET_a/ET_o) for young almond orchards in 2019.

Figure 3.9 shows the daily actual crop coefficients (ET_a/ET_o) for 3rd, 4th, and 5th leaf orchards in 2020. Daily ET_a/ET_o was the lowest in the 3rd leaf orchard. In 2020, the 4th leaf orchard sometimes had a higher daily ET_a/ET_o than the 5th leaf orchard, indicating that age is not the only development factor that affects the crop coefficient. Like in 2019, daily ET_a/ET_o decrease between 150 and 170 days since full bloom due to a reduction in irrigation during harvest activities. The reduction in daily ET_a/ET_o during this period was lower in 2020 than in 2019 because the farmer irrigated more in 2020 prior to harvest to avoid the severe water stress that he experienced in 2019 during the harvest period.

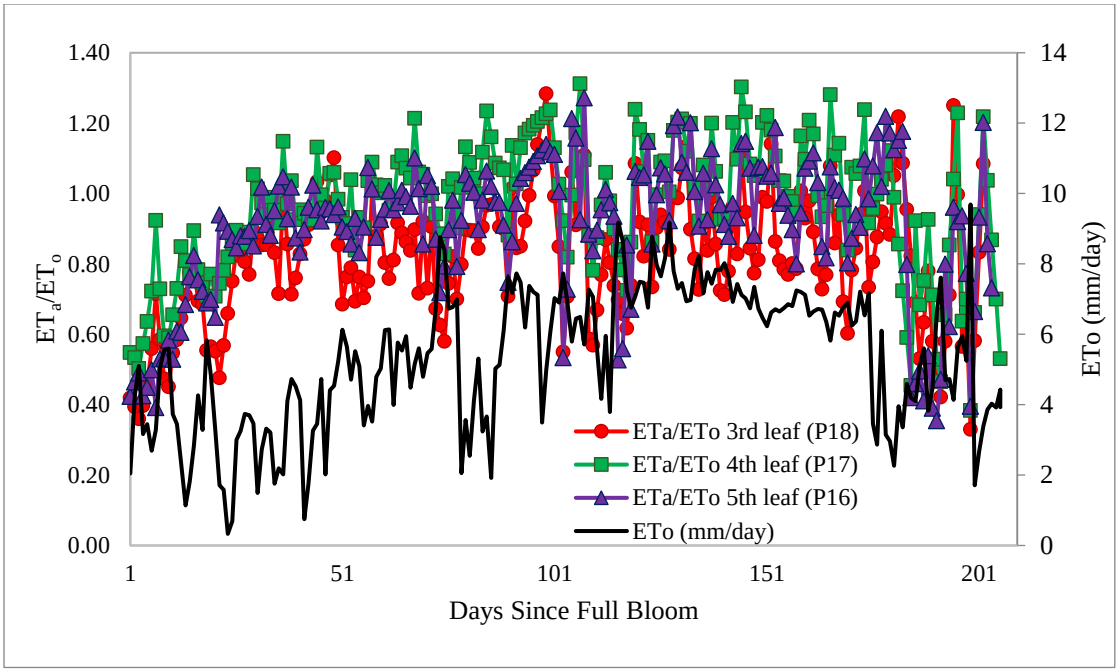

Figure 3.9. Daily actual crop coefficients (ET_a/ET_o) for young almond orchards in 2020.

3.3.3. Seasonal crop water use estimated from a soil water balance

Table 3.3 shows results of the soil water balance for the period April 12, 2019 to July 12, 2019 in the 2nd and 3rd leaf orchards, representing the crop water use of the spring to mid-summer period. The grower applied 149 mm of irrigation to the 2nd leaf orchard and 234 mm of irrigation to the 3rd leaf orchard, indicating that he intended to irrigate the older trees with more water. The soil water content decreased by 81 mm and 164 mm in the 2nd and 3rd leaf orchards, respectively, during the period. The crop water use was 315 mm in the 2nd leaf orchard and 484 mm in the 3rd leaf orchard.

Table 3.3 Soil water balance for the period April 12, 2019 to July 12, 2019

	2018 Planting (2nd leaf)	2017 Planting (3rd leaf)
Irrigation (mm)	149	234
Rainfall (mm)	85	85
Δ Soil water (mm)	-81	-164
Evapotranspiration (mm)	315	484

Figures 3.10 and 3.11 show the soil texture at the locations of the neutron probe measurements used in the soil water balance calculations. The soil texture was primarily sandy loam, loam, and loamy sand in P18 and sandy loam, clay loam, silt loam, and loam in P17. The predominance of loam in P17 may explain the increased root water uptake of that orchard that may have contributed to greater ET_a in the 4th leaf orchard in 2020 (P17) than the 5th leaf orchard in 2020 (P16). Not enough access tubes were installed for neutron probe measurements in the orchard planted in 2016 (P16), so no soil water balance was computed and soil texture was not analyzed.

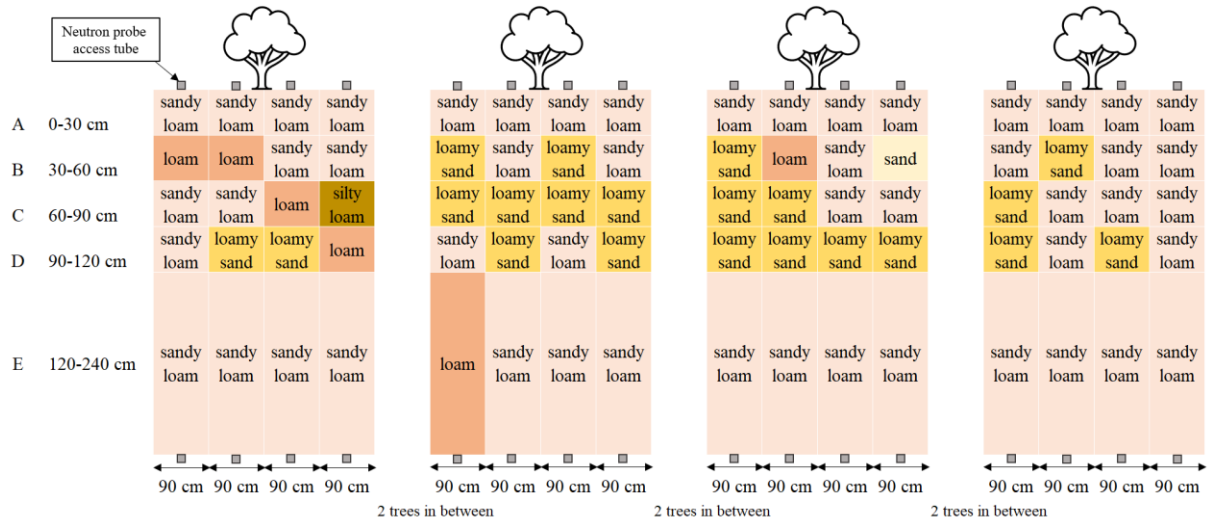

Figure 3.10. A diagram of the soil texture of P18 (orchard planted in 2018) measured using the pipette method at the locations of the neutron probe measurements.

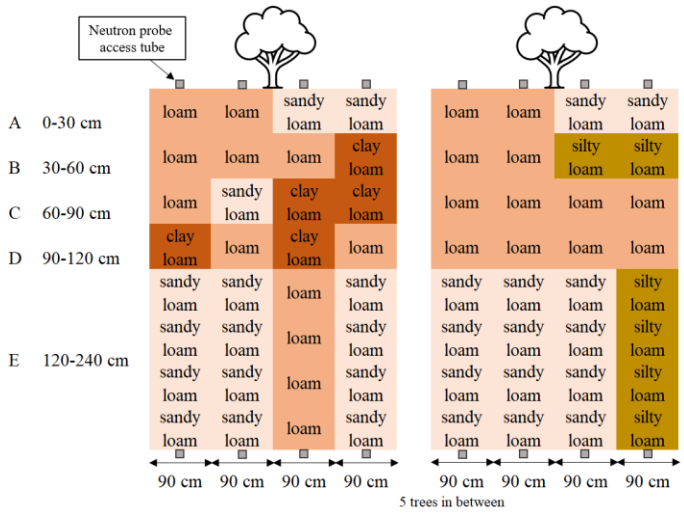

Figure 3.11. A diagram of the soil texture of P17 (orchard planted in 2017) measured using the pipette method at selected locations of the neutron probe measurements.

Table 3.4. shows results of the soil water balance for the period of July 12, 2019 to September 10, 2019 (in the 3rd leaf orchard) and September 18, 2019 (in the 4th leaf orchard), representing the late summer period. During this period, the grower applied approximately the same amount of water to both ages of orchards, 147 mm in the 2nd leaf orchard and 142 mm in the 3rd leaf orchard. Despite approximately the same amount of irrigation water applied, the soil water content decreased more in the 3rd leaf orchard than in the 2nd leaf orchard—81 mm versus 29 mm—likely due to larger canopy sizes and root systems in the 3rd leaf orchard. The crop water use was higher in the 3rd leaf orchard than in the 2nd leaf orchard—223 mm versus 184 mm.

Table 3.4. Soil water balance between July 12, 2019 and mid-September of 2019

	2018 Planting (2^{nd} leaf)	2017 Planting (3^{rd} leaf)
Irrigation (mm)	147	142
Rainfall (mm)	8	0
Δ Soil water (mm)	-29	-81
Evapotranspiration (mm)	184	223

Note: The soil water balance was computed for the period of July 12, 2019 to September 10, 2019 in P17 and for the period July 12, 2019 to September 18, 2019 for P18.

Table 3.5 shows the soil water balance for the period February 26, 2020 to September 16, 2020 in the 3^{rd} and 4^{th} leaf orchards. The grower applied 672 mm of irrigation to the 3^{rd} leaf orchard and 725 mm of irrigation to the 4^{th} leaf orchard, indicating that he irrigated the older trees more than the younger trees and increased the irrigation amount compared to 2019 in both orchards. The soil water content decreased by 19 mm in the 3^{rd} leaf orchard whereas the soil water content decreased by 175 mm in the 4^{th} leaf orchard. The net result was 817 mm of crop water use in the 3^{rd} orchard and 1026 mm of crop water use in the 4^{th} leaf orchard.

Table 3.5. Soil water balance between February 26, 2020 and September 16, 2020

	2018 Planting (3^{rd} leaf)	2017 Planting (4^{th} leaf)
Irrigation (mm)	672	725
Rainfall (mm)	125	125
Δ Soil water (mm)	-19	-175
Evapotranspiration (mm)	817	1026

Table 3.6 compares the seasonal ET_a estimates using a soil water balance method versus an eddy covariance energy balance method. Seasonal ET_a estimates were in close agreement between the two methods with percent errors ranging between 3% and 20% for the different periods analyzed. A shorter sample interval may have contributed to an increased percent error in the

soil water balance derived ET_a estimate of the 3rd leaf orchard during the July 15, 2019 to September 10, 2019 period.

Table 3.6. Comparison of seasonal evapotranspiration estimates

Field	Age	Period	ET_a (mm) Soil Water Balance	ET_a (mm) Energy Balance	Percent Error
P18	2nd leaf	July 12, 2019 to September 18, 2019	180	175	3%
	3rd leaf	February 26, 2020 to September 16, 2020	817	899	10%
P17	3rd leaf	July 15, 2019 to September 10, 2019	223	268	20%
	4th leaf	February 26, 2020 to September 16, 2020	1026	1090	6%

3.3.4. Seasonal crop water use estimated from eddy covariance energy balance

Figure 3.12 shows the cumulative crop water use as measured through eddy covariance energy budget method in 3rd, 4th, and 5th leaf almond trees in 2020 starting from peak bloom. The cumulative ET_a from full bloom until September 11th (around the end of harvest activities) was 888, 1075, and 995 mm in the 3rd, 4th, and 5th leaf orchards, respectively, in 2020. The cumulative ET_a was 21% higher in the 4th leaf orchard than in the 3rd leaf orchard, 12% higher in the 5th leaf orchard than in the 3rd leaf orchard, and 8% lower in the 5th leaf orchard than in the 4th leaf orchard. Differences in canopy size and root system may have resulted in lower cumulative ET_a in the 5th leaf orchard than in the 4th leaf orchard, indicating that age is not the only factor to consider in deciding what crop coefficients to use for irrigation scheduling.

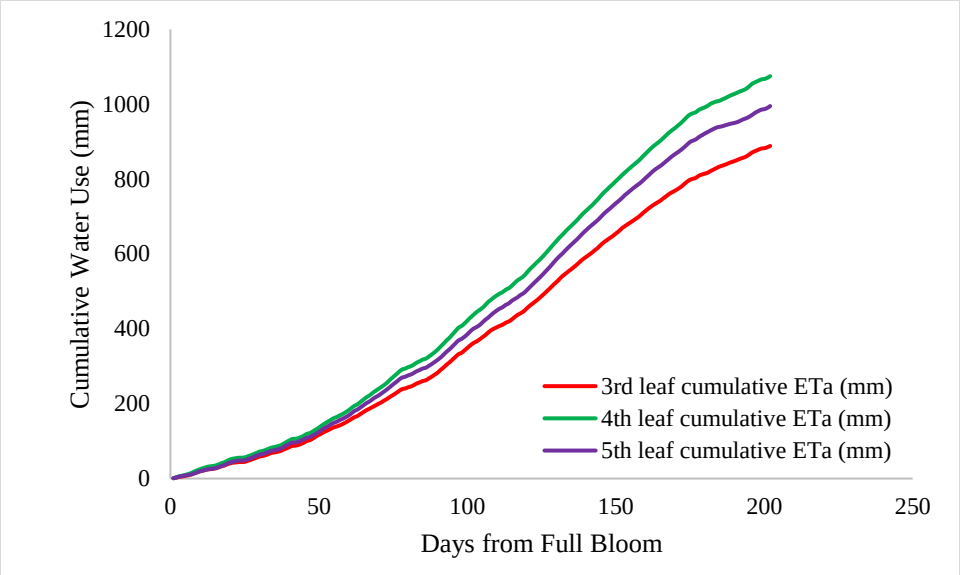

Figure 3.12 Cumulative crop water use in 3rd, 4th, and 5th leaf almond trees in 2020 near Corning, CA.

3.3.5. Dual crop coefficient approach

Tables 3.7 to 3.13 show the results of the dual crop coefficient approach in the 2nd leaf orchard in 2018, the 2nd through 4th leaf orchards in 2019, and the 3rd through 5th leaf orchards in 2020. The K_s estimates show that water stress was not a major issue except in the 2nd and 3rd leaf orchards in 2019 (average K_s of 0.42 and 0.6, respectively) when the farmer struggled to maintain adequate soil water content levels leading up to and during harvest activities when reduced irrigation was necessary to allow farm vehicles to enter the orchard and the farmer was concerned about overirrigation. The K_s estimates had good correlations with measurements of midday stem water potential. Average K_e ranged from 0.27 to 0.63. Typically, the K_c was similar to the K_a value except in the 2nd and 3rd leaf orchards in 2019 when the low K_s values resulted in higher calculated K_c than the measured K_a. When K_s decreases, the calculated K_c will be higher than the measured K_a, which is evident from equations 4 and 5. The farmer's irrigation scheduling resulted in sub-optimal, underirrigated conditions during the Nonpareil and Monterey harvest activities (mid-August and mid-September).

Table 3.7. Dual crop coefficient results in the 2nd leaf orchard in 2018

Period	Start Date	End Date	Ks	Ke	Kcb	Kc	Ka
1	25-Jul	31-Jul	0.93	0.46	0.28	0.74	0.72
2	1-Aug	7-Aug	0.95	0.34	0.28	0.63	0.61
3	8-Aug	14-Aug	0.99	0.32	0.28	0.60	0.60
4	15-Aug	21-Aug	0.97	0.41	0.28	0.69	0.68
5	22-Aug	27-Aug	0.97	0.35	0.28	0.63	0.62
6	28-Aug	6-Sep	0.93	0.43	0.28	0.71	0.69
7	7-Sep	13-Sep	0.91	0.45	0.28	0.73	0.70
8	14-Sep	20-Sep	0.92	0.36	0.28	0.64	0.62
9	21-Sep	4-Oct	0.89	0.31	0.28	0.59	0.56
10	5-Oct	17-Oct	0.94	0.25	0.28	0.53	0.51
11	18-Oct	26-Oct	0.95	0.26	0.28	0.54	0.53
		Average	0.94	0.36	0.28	0.64	0.62

Table 3.8. Dual crop coefficient results in the 2nd leaf orchard in 2019

Period	Start Date	End Date	Ks	Ke	Kcb	Kc	Ka
1	29-May	4-Jun	0.49	0.44	0.30	0.74	0.59
2	5-Jun	11-Jun	0.42	0.30	0.30	0.60	0.43
3	12-Jun	18-Jun	0.40	0.39	0.30	0.69	0.51
4	19-Jun	25-Jun	0.43	0.27	0.30	0.57	0.40
5	26-Jun	2-Jul	0.44	0.32	0.30	0.62	0.45
6	3-Jul	9-Jul	0.45	0.40	0.30	0.70	0.53
7	10-Jul	14-Jul	0.42	0.26	0.30	0.56	0.38
8	15-Jul	21-Jul	0.43	0.28	0.30	0.58	0.41
9	22-Jul	30-Jul	0.41	0.32	0.30	0.62	0.44
10	31-Jul	6-Aug	0.45	0.34	0.30	0.64	0.47
11	7-Aug	12-Aug	0.45	0.43	0.30	0.73	0.57
12	13-Aug	20-Aug	0.42	0.34	0.30	0.63	0.46
13	21-Aug	27-Aug	0.39	0.29	0.30	0.59	0.41
14	28-Aug	3-Sep	0.41	0.18	0.30	0.47	0.30
15	4-Sep	10-Sep	0.38	0.23	0.30	0.53	0.34
16	11-Sep	17-Sep	0.39	0.46	0.30	0.76	0.58
17	18-Sep	27-Sep	0.40	0.20	0.30	0.50	0.32
		Average	0.42	0.32	0.30	0.62	0.45

Table 3.9. Dual crop coefficient results in the 3rd leaf orchard in 2019

Period	Start Date	End Date	Ks	Ke	Kcb	Kc	Ka
1	29-May	4-Jun	0.95	0.53	0.43	0.97	0.94
2	4-Jun	12-Jun	0.94	0.46	0.43	0.89	0.86
3	12-Jun	19-Jun	0.91	0.60	0.43	1.03	0.99
4	19-Jun	26-Jun	0.80	0.45	0.43	0.88	0.80
5	26-Jun	3-Jul	0.75	0.59	0.43	1.02	0.91
6	3-Jul	10-Jul	0.71	0.69	0.43	1.12	0.99
7	10-Jul	15-Jul	0.67	0.75	0.43	1.19	1.04
8	15-Jul	22-Jul	0.63	0.60	0.43	1.03	0.87
9	22-Jul	31-Jul	0.57	0.57	0.43	1.00	0.81
10	31-Jul	7-Aug	0.51	0.62	0.43	1.05	0.84
11	7-Aug	13-Aug	0.46	0.46	0.43	0.89	0.66
12	13-Aug	21-Aug	0.39	0.38	0.43	0.82	0.55
13	21-Aug	4-Sep	0.42	0.62	0.43	1.05	0.80
14	4-Sep	11-Sep	0.36	0.59	0.43	1.02	0.74
15	11-Sep	18-Sep	0.33	0.45	0.43	0.89	0.60
16	18-Sep	27-Sep	0.27	0.50	0.43	0.93	0.62
		Average	0.60	0.55	0.43	0.99	0.81

Table 3.10. Dual crop coefficient results in the 4th leaf orchard in 2019

Period	Start Date	End Date	Ks	Ke	Kcb	Kc	Ka
1	19-Jun	26-Jun	1.00	0.40	0.64	1.04	1.04
2	26-Jun	3-Jul	1.00	0.38	0.64	1.02	1.02
3	3-Jul	10-Jul	1.00	0.37	0.64	1.01	1.01
4	10-Jul	15-Jul	1.00	0.49	0.64	1.13	1.13
5	15-Jul	22-Jul	1.00	0.41	0.64	1.05	1.05
6	22-Jul	31-Jul	0.97	0.37	0.64	1.00	0.98
7	31-Jul	7-Aug	0.98	0.35	0.64	0.99	0.97
8	7-Aug	13-Aug	0.91	0.18	0.64	0.82	0.76
9	13-Aug	21-Aug	0.86	0.00	0.64	0.64	0.42
10	21-Aug	28-Aug	0.95	0.05	0.64	0.69	0.66
11	28-Aug	4-Sep	0.95	0.29	0.64	0.93	0.90
12	4-Sep	11-Sep	0.93	0.26	0.64	0.90	0.85
13	11-Sep	18-Sep	0.89	0.17	0.64	0.81	0.73
14	18-Sep	27-Sep	0.84	0.00	0.64	0.64	0.52
		Average	0.95	0.27	0.64	0.90	0.86

Table 3.11. Dual crop coefficient results in the 3rd leaf orchard in 2020

Period	Start Date	End Date	Ks	Ke	Kcb	Kc	Ka
1	30-Apr	7-May	0.92	0.37	0.44	0.82	0.78
2	7-May	23-May	1.00	0.40	0.44	0.84	0.84
3	23-May	2-Jun	0.91	0.64	0.44	1.08	1.05
4	2-Jun	9-Jun	0.91	0.48	0.44	0.92	0.88
5	9-Jun	16-Jun	1.00	0.33	0.44	0.77	0.77
6	16-Jun	23-Jun	1.00	0.34	0.44	0.78	0.78
7	23-Jun	30-Jun	1.00	0.42	0.44	0.87	0.87
8	30-Jun	7-Jul	0.96	0.52	0.44	0.96	0.95
9	7-Jul	14-Jul	0.98	0.40	0.44	0.84	0.83
10	14-Jul	21-Jul	0.98	0.46	0.44	0.91	0.90
11	21-Jul	28-Jul	0.96	0.48	0.44	0.92	0.91
12	28-Jul	4-Aug	1.00	0.44	0.44	0.88	0.88
13	4-Aug	12-Aug	1.00	0.36	0.44	0.81	0.81
14	12-Aug	17-Aug	0.98	0.43	0.44	0.87	0.87
15	17-Aug	26-Aug	0.90	0.57	0.44	1.02	0.97
16	26-Aug	2-Sep	0.98	0.16	0.44	0.60	0.59
17	2-Sep	9-Sep	0.96	0.31	0.44	0.75	0.73
		Average	0.97	0.42	0.44	0.86	0.85

Table 3.12. Dual crop coefficient results in the 4th leaf orchard in 2020

Period	Start Date	End Date	Ks	Ke	Kcb	Kc	Ka
1	30-Apr	7-May	0.89	0.65	0.41	1.07	1.02
2	7-May	23-May	1.00	0.63	0.41	1.04	1.04
3	23-May	2-Jun	0.89	0.80	0.41	1.22	1.17
4	2-Jun	9-Jun	0.88	0.69	0.41	1.10	1.05
5	9-Jun	16-Jun	0.97	0.55	0.41	0.96	0.95
6	16-Jun	23-Jun	0.98	0.53	0.41	0.94	0.93
7	23-Jun	30-Jun	0.98	0.63	0.41	1.05	1.04
8	30-Jun	7-Jul	0.92	0.74	0.41	1.15	1.12
9	7-Jul	14-Jul	0.93	0.64	0.41	1.05	1.02
10	14-Jul	21-Jul	0.92	0.77	0.41	1.18	1.15
11	21-Jul	28-Jul	0.88	0.75	0.41	1.16	1.11
12	28-Jul	4-Aug	0.89	0.71	0.41	1.12	1.08
13	4-Aug	12-Aug	0.89	0.67	0.41	1.08	1.04
14	12-Aug	17-Aug	0.86	0.69	0.41	1.11	1.05
15	17-Aug	26-Aug	0.78	0.55	0.41	0.97	0.87
16	26-Aug	2-Sep	0.87	0.35	0.41	0.77	0.71
17	2-Sep	9-Sep	0.84	0.44	0.41	0.85	0.79
		Average	0.90	0.63	0.41	1.05	1.01

Table 3.13. Dual crop coefficient results in the 5th leaf orchard in 2020

Period	Start Date	End Date	Ks	Ke	Kcb	Kc	Ka
1	30-Apr	7-May	0.90	0.33	0.68	1.01	0.95
2	7-May	23-May	0.98	0.28	0.68	0.96	0.94
3	23-May	2-Jun	0.97	0.40	0.68	1.08	1.06
4	2-Jun	9-Jun	1.00	0.27	0.68	0.95	0.95
5	9-Jun	16-Jun	1.00	0.29	0.68	0.98	0.98
6	16-Jun	23-Jun	1.00	0.13	0.68	0.81	0.81
7	23-Jun	30-Jun	1.00	0.33	0.68	1.02	1.02
8	30-Jun	7-Jul	0.95	0.45	0.68	1.13	1.10
9	7-Jul	14-Jul	0.93	0.35	0.68	1.04	0.99
10	14-Jul	21-Jul	0.99	0.36	0.68	1.04	1.03
11	21-Jul	28-Jul	1.00	0.36	0.68	1.04	1.04
12	28-Jul	4-Aug	1.00	0.31	0.68	0.99	0.99
13	4-Aug	12-Aug	1.00	0.25	0.68	0.93	0.93
14	12-Aug	17-Aug	0.93	0.37	0.68	1.05	1.00
15	17-Aug	26-Aug	0.84	0.46	0.68	1.14	1.03
16	26-Aug	2-Sep	1.00	0.00	0.68	0.68	0.45
17	2-Sep	9-Sep	1.00	0.09	0.68	0.77	0.77
18	9-Sep	16-Sep	0.92	0.25	0.68	0.93	0.88
		Average	0.97	0.30	0.68	0.97	0.94

3.3.6. Seasonal average crop coefficients as a function of orchard age

Figure 3.13 shows the seasonal average K_c in each age orchard from 1st leaf to 5th leaf. The correlation between orchards of different age and canopy size and K_c is excellent (R^2=0.94) and the curve flattened when the age reached 4th and 5th leaf.

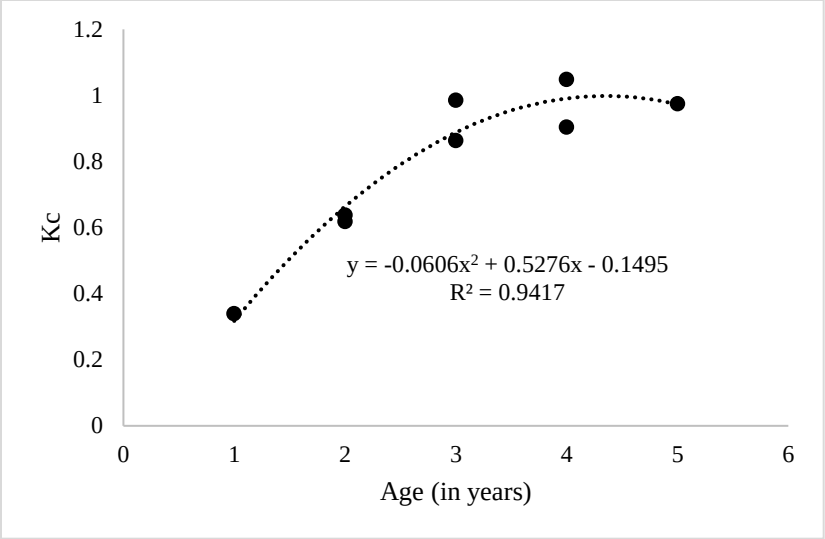

Figure 3.13. Seasonal average K_c in young almond orchards of age 1 to 5 years.

Table 3.14 shows the seasonal average crop coefficients in 1st through 5th leaf almond orchards estimated in 2018 to 2020. Generally, the crop coefficient increased as each orchard increased in age.

Table 3.14. Seasonal average K_c in 1st through 5th leaf almond orchards in 2018 to 2020

Age (Years)	2018	2019	2020
1	0.34		
2	0.64	0.62	
3		0.99	0.86
4		0.90	1.05
5			0.97

3.3.7. Crop coefficients as a function of radiation interception

Figure 3.14 shows actual crop coefficients (ET_a/ET_o) as a function of fraction of photosynthetically active radiation intercepted by the canopy (fPAR) estimated through lightbar measurements. As fPAR increased, ET_a/ET_o increased nonlinearly and plateaued at approximately fPAR of 0.55.

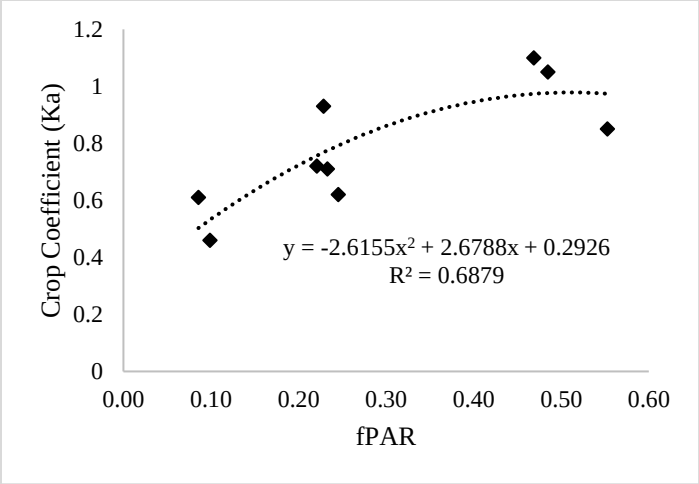

Figure 3.14. K_a as a function of fraction of PAR intercepted by the canopy.

Table 3.15 shows the crop coefficient as a function of percent PAR intercepted by the canopy in relation to the percentage of ET_c of a mature almond orchard using K_c estimates from the average of Sanden (2007) June and July estimates.

Table 3.15. Crop coefficient as a function of percent PAR intercepted by the canopy in relation to % ET_c of a mature almond orchard

Percent PAR Intercepted by the Canopy	ET_a/ET_o	Mature K_c (June/July Average from Sanden, 2007)	% ET_c of a Mature Almond Orchard
10	0.53	1.05	51
20	0.72	1.05	69
30	0.86	1.05	82
40	0.95	1.05	90
50	0.98	1.05	94

3.3.8. Multiple linear regression model of ET_a/ET_o

The stepwise selection procedure chose the following independent variables: MSWP, fPAR, and soil water content measured at 46 and 76 cm. Other parameters were tried in the model, but

were found insignificant such as soil water content shallower than 46 cm and deeper than 76 cm. Table 3.16 shows the parameter estimates and p-value for each independent variable in the model.

Table 3.16. Multiple linear regression model of the ratio of actual evapotranspiration to reference evapotranspiration

Variable	Parameter Estimate	P-Value
Intercept	1.05	<0.0001
MSWP [MPa]	0.32	<0.0001
fPAR	1.71	<0.0001
Soil Water Content at 46 cm [cm/cm]	−0.13	0.0004
Soil Water Content at 76 cm [cm/cm]	0.05	0.0019

The adjusted R-square value was 0.68 and the RMSE was 0.15. The model had a C(p) of 4.6. All the data available was used to develop the model, so no data was left over for validation.

$$\frac{ET_a}{ET_0} = 1.05 + 0.32\ [MPa^{-1}] * MSWP\ [MPa] + 1.71 * fPAR - 0.13 * SWC_{46\ cm} + 0.05 * SWC_{76\ cm}$$

Equation 3.11

3.4. Discussion

Within each year of the study and for each age of almond orchard, daily ET_a peaked in June through August, as shown in Figures 3.4 through 3.6. Daily ET_a was relatively consistent in June through August due to little or no precipitation and clear sky conditions. Precipitation and ephemeral clouds in the spring and fall months resulted in some sporadic ET_a estimates. The grower's irrigation scheduling resulted in a peak in ET_a after each irrigation event followed by a period of decreasing ET_a for several days. The grower's reduction in irrigation during harvest activities in August and September reduced ET_a in the 3rd through 5th leaf orchards. Wildfire smoke from the LNU Lightning Complex Fires resulted in low net radiation in mid-August and

September of 2020, resulting in reduced ET_a measurements.

The ET_a data from this study were similar to crop water use estimates of young almond orchards from Jarvis-Shean et al. (2018). This study's 1st leaf ET_a estimates of 61 mm and 67 mm in June and July were close to the Jarvis-Shean et al. (2018) estimates of 64 mm and 68 mm, respectively. This study's August and September 1st leaf ET_a estimates of 47 mm and 28 mm were considerably lower than the Jarvis-Shean et al. (2018) 1st leaf estimates of 61 mm and 45 mm, respectively. This study's 2nd leaf ET_a estimates from P17 (orchard planted in 2017) were 105 mm, 92 mm, and 48 mm in August, September, and October, compared to the Jarvis-Shean et al. (2018) estimates of 112 mm, 82 mm, and 49 mm, respectively. Tables 3.17 through 3.19 show comparisons of 1st, 2nd, and 3rd leaf crop water use between this study and Jarvis-Shean et al. (2018).

Table 3.17. Comparison of 1st leaf crop water use in P18 versus Jarvis-Shean et al. (2018)

Month	ET_a of 1st leaf P18 [mm/month]	ET_c of 1st leaf Jarvis-Shean et al. (2018) [mm/month]
June	61	64
July	67	68
August	47	61
September	28	45

Note: P18 refers to the orchard planted in 2018

Table 3.18. Comparison of 2nd leaf crop water use in P17 and P18 versus Jarvis-Shean et al. (2018)

Month	ET_a of 2nd leaf P18 [mm/month]	ET_a of 2nd leaf P17 [mm/month]	ET_c of 2nd leaf Jarvis-Shean et al. (2018) [mm/month]
August	84	105	112
September	50	92	82
October	25	48	49

Note: P18 refers to the orchard planted in 2018 and P17 refers to the orchard planted in 2017

Table 3.19. Comparison of 3rd leaf crop water use in P17 and P18 versus Jarvis-Shean et al. (2018)

Month	ET_a of 3rd leaf P18 [mm/month]	ET_a of 3rd leaf P17 [mm/month]	ET_c of 3rd leaf Jarvis-Shean et al. (2018) [mm/month]
June	175	198	159
July	197	193	171
August	137	129	152
September		95	112
October		86	67

Note: P18 refers to the orchard planted in 2018 and P17 refers to the orchard planted in 2017

The ET_a/ET_o shown in Figure 3.7 to 3.9 increased with increasing age, indicating the need for different crop coefficients for each age of young almond orchards. Like the crop water use estimates, ET_a/ET_o also tended to be more consistent in the summer months June-August when ET_o was more consistent from day to day. ET_a/ET_o became erratic in the spring and fall months, primarily because the ET_o and ET_a were so small that any changes in one or the other resulted in considerable changes in ET_a/ET_o.

Table 3.20 compares the average ET_a/ET_o of each age almond orchard to the mature almond K_c estimates from Sanden (2007) that were obtained from eddy covariance heat flux estimates of ET_c divided by the modified Penman ET_o data. By the 4th leaf, ET_a/ET_o in June and July (1.02 and 1.09, respectively) had approached mature almond K_c in June and July (1.01 and 1.08, respectively). 5th leaf orchard (P16 planted in 2016) had lower ET_a/ET_o values in May through July than the average ET_a/ET_o of the 4th leaf orchard, which may have been due to extreme water stress during August of 2019 during harvest activities (midday stem water potential as low as -3.11 MPa on August 21, 2019) which may have reduced shoot growth and tree development, carrying over to lower ET_a levels in 2020. Another explanation would be that the 5th leaf trees in 2020 were not irrigated enough to compensate for the year older trees than the 4th leaf trees and, as a result, the ET_a was lower in the 5th leaf trees than in the 4th leaf trees. ET_a/ET_o was higher in the 4th and 5th leaf orchards in May, but lower in August and September than the Sanden (2007)

mature K_c estimates. Lower ET_a/ET_o during August and September may be due to the commercial grower's difficulty in controlling water stress during the harvest season. The Sanden (2007) study attempted to control water stress through neutron probe and stem water potential readings, which was not done in the present study since it was a purely grower-managed commercial orchard. The Sanden (2007) ET_c data was highly variable from year to year during the 4-year study in the months of May, August, and especially September, which indicated increased uncertainty in the K_c estimates during those months. Table 3.21 shows the percentage of mature almond Kc in 1st through 5th leaf almond orchards. By the 4th leaf, the ET_a/ET_o reached 101% of mature almond K_c in June and July.

Table 3.20. Comparison of young and mature almond orchard Kc estimates

Month	1st leaf P18	2nd leaf P17 & P18 Average	3rd leaf P17 & P18 Average	4th leaf P17 & P18 Average	5th leaf P16	Mature Almond (Sanden, 2007)
May			0.92	1.11	1.02	0.92
June		0.65	0.89	1.02	0.94	1.01
July	0.30	0.61	0.99	1.09	1.06	1.08
August	0.40	0.62	0.92	0.90	0.96	1.08
September	0.32	0.63	0.81	0.84	0.85	1.02

Table 3.21. Percentage of mature almond Kc in 1st through 5th leaf almond orchards

Month	1st leaf P18	2nd leaf P17 & P18 Average	3rd leaf P17 & P18 Average	4th leaf P17 & P18 Average	5th leaf P16	Mature Almond Sanden (2007)
May			99	121	111	100
June		64	88	101	93	100
July	28	57	92	101	98	100
August	37	58	85	83	89	100
September	32	62	79	82	84	100

Evapotranspiration was the largest component in each of the soil water balances shown in Tables 3.3 through 3.5. The close estimates of ET_a determined by eddy covariance energy balance method and soil water balance methods (less than 20% error and often less than 10% error) validate the ET_a estimates determined in this study for determining crop water use and crop coefficients.

The correlation between age and K_c shown in Figure 3.13 was excellent (R^2=0.94) and showed that the K_c increased until approximately the 4th leaf before becoming flat. This relationship indicates that almond farmers need to adjust the K_c values as the almond orchards develop until at least the 4th leaf before using the mature almond orchard K_c values.

Fraction of photosynthetically active radiation intercepted by the canopy (fPAR) had a good correlation with ET_a/ET_o (R^2=0.69), which possibly could have been improved if water stress were controlled. By 50% fPAR, the ET_a/ET_o of the developing almond orchard reached 94% of the mature almond K_c. When fPAR was regressed against the K_c estimates obtained through the dual crop coefficient method shown in Tables 3.7 through 3.13, the resulting curve was non-monotonic.

The multiple linear regression model of ET_a/ET_o resulted in a good prediction of ET_a/ET_o using fPAR, MSWP, and soil water content measured at 46 and 76 cm. The adjusted R-square value of 0.68 and RMSE of 0.15 were promising considering that two years of data from all three orchards were combined to develop this model.

The crop coefficients were not determined in a controlled environment that prevented water stress from occurring in the orchards. The crop coefficients in this study were the ratio of the ET_a and ET_o of a commercial almond orchard and were affected by the grower's management practices. Further research should investigate the crop water use of young almond orchards in an environment where water stress is controlled and prevented. This study provides insight on crop water use of one commercial almond farmer in the Sacramento Valley of California.

3.5. Conclusions

Actual evapotranspiration was measured using eddy covariance energy balance method to estimate crop water use in young almond orchards aged 1st leaf through 5th leaf. Crop water use increased as the orchards increased in age, indicating the need to adjust irrigation applied as orchards grow. Crop coefficients (K_c) were determined by calculating the ratio between actual evapotranspiration and reference evapotranspiration (ET_a/ET_o) and corrected for water stress using the dual crop coefficient approach, resulting in an excellent correlation between K_c and orchard development and age (R^2=0.94). The results show that almond farmers should use age and development-specific K_c values for irrigation scheduling until the 4th leaf when mature almond K_c could be used. Fraction of photosynthetically active radiation (fPAR) intercepted by the canopy, midday stem water potential, and soil water content at 46 and 76 cm were found to be good predictors of ET_a/ET_o and could be used for determining site-specific crop coefficients. Further research should focus on determining crop water use by young almond orchards with different irrigation systems, varieties, soils, and management practices.

Acknowledgements

Thanks to the Almond Board of California for funding this research. Thanks to Steve Gruenwald (farmer) for allowing us to conduct this research on his private orchard. We are very grateful for Cayle Little for contributing his technical expertise in installing the flux stations. Thanks to Richard Snyder for contributing his expertise on data processing. Thanks to Bob Mahoney and Carol Haynes for auxiliary data collection. Thanks to Matt Read, Aya Suzuki, David Moyers, Marcoluis Garcia, Fatemeh Mehrabi, Kyle Johnson, Prudentia Gugulethu Zikalala, Jingyuan Xue, Iael Raij Hoffman, Omar Samara, and Srinivasa Rao Peddinti for assistance with

field work and equipment installation. Thanks to Jazmin Melendez for analyzing the soil texture. Thanks to Sam Metcalf for collecting lightbar measurements and Tran Nguyen for processing the lightbar data.

Chapter 4

Regulated deficit irrigation in almonds by variety during hull-split

Abstract

Regulated deficit irrigation (RDI) during hull-split can reduce water use in almond orchards, but strategies for imposing RDI in almond orchards with multiple varieties with different hull-split schedules have not been extensively developed. Commonly, irrigation system design restricts all varieties in the same orchard to be on the same irrigation schedule. A 2-year study evaluated the impacts of two different regulated deficit irrigation schedules under two levels of crop evapotranspiration irrigation replacement rates in an almond orchard with Butte, Aldrich, and Nonpareil varieties in the Sacramento Valley of California, USA. The two irrigation schedules were (1) regulated deficit irrigation in Butte, Aldrich, and Nonpareil varieties during Nonpareil hull-split timing and (2) regulated deficit irrigation in each variety according to variety-specific hull-split timing. The two levels of irrigation were 50% and 75% of crop evapotranspiration (ET_c) replacement during the hull-split period. Results show that the kernel thickness of Aldrich almonds increased under 75% ET_c irrigation replacement during Aldrich hull-split period compared to 75% ET_c and 50% ET_c irrigation replacement during Nonpareil hull-split period. In the Butte almonds, 75% ET_c and 50% ET_c irrigation replacement during variety-specific hull-split reduced the fraction of sealed shells of the Butte variety compared to 75% ET_c and 50% ET_c irrigation replacement during Nonpareil hull-split period. This study demonstrated that almond physical quality can be changed in the Butte and Aldrich varieties when RDI is imposed according to variety-specific hull-split schedules, revealing previously unknown opportunities from irrigation system designs that permit independent irrigation scheduling of each variety. No marketable kernel yield improvements were achieved

by implementing RDI according to variety-specific hull-split after two years. Under conditions similar to those in this study, the least labor-intensive strategy of RDI during Nonpareil hull-split in all three varieties is recommended. More research should be conducted for different orchard designs, varieties, and climates.

4.1. Introduction

Uncertainty of water availability is a significant concern for almond farmers. California, USA, is the world leader in almond production with a $6.09 billion (USD) almond industry, covering almost 619,000 hectares in 2019 (California Department of Food and Agriculture, 2020, 2019). Increasing acreage of almonds and uncertainty about water deliveries from the Sacramento-San Joaquin Delta has contributed to a greater demand for groundwater by farmers (Harter, 2015). The increased pressure on groundwater as a water resource for agriculture effectively led to the passage of the Sustainable Groundwater Management Act (SGMA) in 2014, which will ultimately limit the amount of groundwater that farmers can pump to halt groundwater overdraft (Pavley and Dickinson, 2014). Furthermore, climate change has resulted in increased uncertainty of water availability for agriculture and increased crop water demands, a trend that is expected to continue in the future (Pathak et al., 2018). Improvements in water use efficiency must be developed to address uncertainties in water availability due to climate change, water policies, and water scarcity.

In January 2019, the Almond Board of California set a goal of reducing the amount of water used to produce a pound of almonds by 20% by the year 2025 (Almond Board of California, 2019). Meeting this goal could involve irrigating less than 100% crop evapotranspiration (ET_c) through regulated deficit irrigation (RDI). RDI is a strategy that involves applying less than 100% ET_c during specific phenological stages when a crop is less

sensitive to water deficit with the goal of reducing water use while minimizing losses in crop productivity (Zhang and Theib, 1999). Hull-split is one phenological stage when almond yield is less sensitive to deficit irrigation (Stewart et al., 2011). Mild to moderate RDI at hull-split in almonds can decrease water consumption and reduce hull rot, which is a disease caused by pathogens that colonize the hull tissue in the natural wounds that develop as the hulls split (Teviotdale et al., 2001).

A complication of RDI during hull-split is that orchards with multiple varieties have different hull-split schedules, with hull-split initiating between late June to mid-August, depending on the variety, in the Sacramento Valley of California (Connell et al., 2010). Most commercial almond varieties are self-incompatible, so almond orchards usually have two or three different varieties for effective cross-pollination (Hamby and Zalom, 2013). Farmers who cut back irrigation during hull-split usually do so according to the hull-split schedule of the Nonpareil variety in California because irrigation systems are usually designed for irrigating the entire orchard on the same irrigation schedule. Farmers typically favor the irrigation toward optimizing yield and quality of the Nonpareil variety, which is the most valuable almond variety in California (Almond Board of California, 2015). However, other varieties in the same orchard as the Nonpareil variety may not be optimally irrigated according to the variety-specific phenological stages.

Despite the large number of studies on RDI in almond orchards, there is a lack of research on the RDI strategies for multi-variety almond orchards, which make up approximately 97% of California's almond orchards (California Department of Food and Agriculture, 2020). No research has been published on implementing RDI in almond orchards with multiple varieties in California, USA, but some research has been done in Spain. In a study in Spain, three almond varieties received various deficit irrigation amounts and the Marta variety was more sensitive to

drought conditions than the other varieties according to stem water potential and stomatal conductance measurements, indicating the need to consider variety as a factor in irrigation scheduling (Gutiérrez-Gordillo et al., 2019).

The relationship between applied water and yield in almond orchards has been shown to be nonlinear, so RDI has the potential to improve the amount of water used to produce a pound of almonds (Goldhamer and Fereres, 2017). Deficit irrigation during the pre-harvest period has been shown to less damaging to sustained productivity than deficit irrigation during the post-harvest period (Goldhamer and Viveros, 2000). While RDI generally reduces kernel yields in almond orchards, the overall effect on yield is modest. For example, an irrigation treatment of 45% ET_c reduced yield by only 13%, showing that major reductions in water use through RDI may result in moderate losses in yield and profits for almond orchards (Goldhamer et al., 2006). On the other hand, severe RDI during hull-split in Nonpareil almond trees, especially over multiple years, can significantly reduce kernel weight at harvest (Goldhamer et al., 2006). Furthermore, RDI has been shown to improve almond quality. Short and severe pre-harvest RDI can reduce leaf and shoot death (Teviotdale et al., 2001). RDI during hull-split can also reduce 'sticktights' (i.e., hulls that don't split) (Goldhamer et al., 2006). The research shows that almonds are a suitable crop for RDI as a strategy for reducing water use while minimizing crop losses.

This paper aims to compare regulated deficit irrigation during Nonpareil hull-split timing and regulated deficit irrigation during variety-specific hull-split timing in Nonpareil, Aldrich, and Butte almond varieties at 50% ET_c and 75% ET_c irrigation replacement rates in terms of marketable nut yield, total water applied, water use efficiency, nut physical quality, light interception, soil water content, and midday stem water potential.

4.2. Materials and Methods

4.2.1. Study area

This study was conducted at a 1.6-hectare almond [*Prunus dulcis*] orchard of mature cv. 'Nonpareil,' 'Aldrich,' and 'Butte' trees planted on peach rootstock (4.3 m tree spacing x 6 m row spacing) located near Arbuckle, California, United States (38.97 °N, 122.07° W). The climate of the region is semi-arid Mediterranean with warm dry summers and cool wet winters. The soil was sandy loam with a gravel layer at approximately 1 m below the soil surface. Figure 4.1 shows the digital elevation, shallow electrical conductivity, leaf temperature, canopy cover, and silt and sand content in the top 30 cm. Figure 2 shows the soil texture of the orchard. The root zone depth was about 1 m, typical for mature almond orchards. Each row of the orchard was irrigated with two lines of polyethylene drip tubing (18 mm diameter) with 38 cm emitter spacing and average emitter flow rate of 1.9 L/h. There were approximately 22 emitters per tree. The runtimes of each subplot within the orchard were adjusted to implement the irrigation treatments.

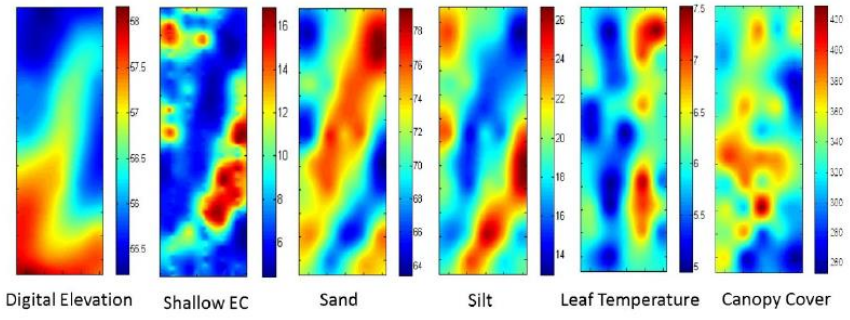

Figure 4.1. Digital elevation, shallow electrical conductivity, leaf temperature, canopy cover, and silt and sand content in the top 30 cm. Reproduced from Kizer et al. (2017).

4.2.2. Experimental design

Figure 4.2 shows the study experimental design of this study. The almond orchard was designed in rows that alternate between three varieties, where each row contains all the same

variety. Since the rows of almond trees cannot be moved, randomization of the variety factor was not possible using the land available for the experiment. The orchard was divided into five main blocks or replications, each block divided vertically into three rows (i.e., one Nonpareil row, one Butte row, and one Aldrich row). Each block was split horizontally into four sections in a strip plot experimental design, resulting in 12 subplots in each block. Since there were concerns of lateral movement of water in the soil between adjacent subplots, it made sense to strip the rows in a strip-plot design and randomize the irrigation among the strips. The Nonpareil, Butte, and Aldrich rows of each block had treatments S1 (75% ET_c during Nonpareil hull-split) and S3 (50% ET_c during Nonpareil hull-split). In addition, the Aldrich and Butte rows of each block had treatments S2 (75% ET_c during variety-specific hull-split) and S4 (50% ET_c during variety-specific hull-split). In Nonpareil, S1 and S2 would be identical and S3 and S4 would be identical, so only this paper will only mention S1 and S3 in Nonpareil in this paper. The Nonpareil row in each block also had a control treatment S5 (100% ET_c during Nonpareil hull-split), which took two subplots in each block to double the number of replicates of this control treatment. In total there were 15 rows and each row contained approximately 50 trees. Each of the four subplots within each row contained approximately 10 trees, allowing approximately five trees to serve as border trees at the ends of each row.

	Irrigation Schedule	Varieties
	S1: 75% ET_c during Nonpareil hull-split period	Nonpareil, Butte, Aldrich
	S2: 75% ET_c during variety-specific hull-split period	Butte, Aldrich
	S3: 50% ET_c during Nonpareil hull-split period	Nonpareil, Butte, Aldrich
	S4: 50% ET_c during variety-specific hull-split period	Butte, Aldrich
	S5: 100% ET_c during Nonpareil hull-split period	Nonpareil

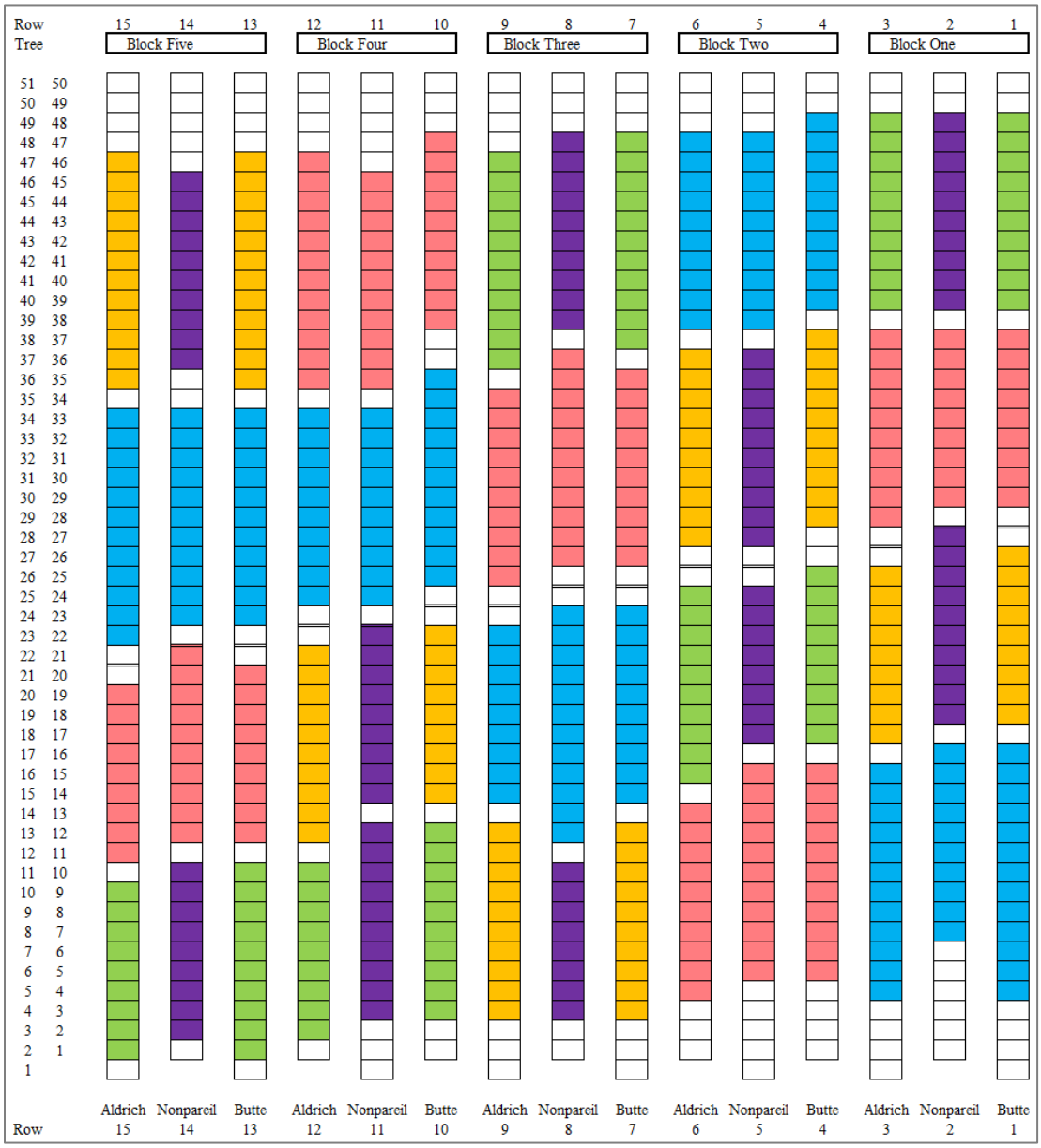

Figure 4.2. The experimental layout for the almond irrigation by variety study at Nickels Soil Lab near Arbuckle, CA.

4.2.3. Irrigation scheduling

A wireless network of solenoid valves controlled the irrigation in all 60 subplots. One solenoid valve actuator circuit board controlled all four irrigation treatments in each row. In 2019, the solenoid valve actuator circuit boards used were developed by Metronome Systems (Berkeley, CA). In 2020, the solenoid valve actuator circuit boards used were developed at University of California, Davis (Coates et al., 2013). The remote valve actuator system required manually inputting the irrigation runtimes for all 60 subplots into a website every irrigation.

Irrigation runtimes were determined based on ET_c, which was calculated using the single crop coefficient method using the reference evapotranspiration, ET_o, from the Williams California Irrigation Management Information System (CIMIS) station (obtained from the CIMIS Penman equation, which uses a wind function developed at University of California, Davis and unique cloud factor values for each CIMIS station location (https://cimis.water.ca.gov/Resources.aspx) and crop coefficients (K_c) for mature almonds, as shown in equation 1. K_c values of 1.15, 1.17, and 1.12 were used in the months of July, August, and September, respectively (Goldhamer, 2012). Cumulative ET_c since the previous irrigation was computed in terms of water depth, which was then converted into a runtime using the representative area of the subplot (approximately 10 trees), the irrigation system specifications, and either 50% or 75% ET_c adjustment depending on the RDI regime. The emitter spacing was 38 cm and the average emitter flow rate was 1.89 L/h. There was dripline on both sides of the tree rows and the diameter of the dripline was 18 mm. There were about 22 emitters per plant. A plant spacing of 4.3 m, row spacing of 6 m, and a distribution uniformity of 0.9 were used to calculate a net application rate of 0.147 cm per hour. Before hull-split initiation, the orchard was irrigated by the farmer, guided by a watermark sensor at one location in the orchard.

$ET_c = ET_o * K_c$ *Equation 4.1*

Careful observation of the orchard leading up to when hull-split was expected to begin based on historical hull-split initiation data led to the decision of when to begin RDI treatments. Although the trees at the ends of the rows began hull-split first, RDI treatments were postponed until most of the trees in the inner parts of the orchard showed approximately 1% hull-split initiation, typically starting at the top of the trees. The hulls with blanks (no kernel inside the shell) usually begin splitting about a week before the hulls with kernels begin splitting, so careful observations were made to wait until hulls not containing blanks began splitting. The 1% hull-split initiation, harvest, pickup dates, and days between 1% hull-split initiation and harvest in 2019 and 2020 are shown in Table 4.1. The number of days between 1% hull-split initiation and harvest (i.e., shaking of the nuts to the ground) influenced the total amount of water applied in each RDI treatment in this study.

Table 4.1. Number of days between 1% hull-split and harvest in Nonpareil, Butte, and Aldrich varieties at Nickels Soil Lab near Arbuckle, CA

2019	Nonpareil	Aldrich	Butte
1% hull-split initiation	July 9th	July 27th	August 7th
Harvest	August 22nd	September 11th	September 11th
Pickup	September 4th	September 25th	September 25th

2020	Nonpareil	Aldrich	Butte
1% hull-split initiation	July 7th	July 23rd	August 3rd
Harvest	August 13th	September 4th	September 4th
Pickup	August 26th	September 15th	September 15th

Days between 1% hull-split initiation and harvest	Nonpareil	Aldrich	Butte
2019	44	46	35
2020	37	43	32

4.2.4. Tree and soil water status

Neutron probe counts were measured at 30 cm, 60 cm, 90 cm, 120 cm, and 150 cm depths using a neutron probe (CPN 503 ELITE Hydroprobe, InstroTek, Raleigh, North Carolina, USA) in all subplots twice a week between April and September of both years of the experiment and usually immediately before irrigation. A local calibration equation was developed using the gravimetric method based on soil samples collected at 30 cm and 60 cm depths from the study field in 2020 using a Madera probe with a soil volume of 66 cc (N=11, R^2=0.86). The bulk density was measured using the same soil samples and was between 1.28 to 1.72 g/cc. The neutron probe counts were converted into volumetric soil water content with the calibration equation. For each subplot, average soil water content was calculated for the top 150 cm of the soil.

Midday stem water potential (MSWP) was also measured using a pressure chamber (Model 615D, PMS Instruments, Albany, Oregon, USA) in all subplots on most occasions that neutron probe counts were measured, which was usually immediately before irrigation. The MSWP measurements were used as feedback for irrigation adequacy. The expectation was that the 50% ET_c treatments would be water stressed, but irrigation was scheduled frequently enough to keep the MSWP above -20 bars, although this became challenging later in the season as soil water deficit progressed. Typically, all treatments were irrigated once every three or four days.

4.2.5. Almond yield, quality, and water use efficiency

The almonds were harvested from the trees with a mechanical shaker on the dates listed in Table 4.1 using a Shockwave Sprint model made by Orchard Machinery Corporation (OMC) in Yuba City, CA, USA. The almonds dried on the orchard ground for 12-15 days after the trees were shaken before being picked up by a tree shaker when total yield and almond samples were collected.

All almonds in each subplot were picked up with a harvesting machine and total yield was measured with a load cell-based scale retrofitted onto a tractor that picks up the almonds off the ground at harvest of each variety. The total yield was multiplied by the fraction of kernel weight to total weight (hulls, shells, and kernels) to determine the kernel yield of each subplot. The marketable kernel yield measurements have been reduced by 10% to account for rocks, leaves, and other debris collected with the almonds based on expert consultation with the farm advisor of the almond orchard. The orchard ground was thoroughly conditioned with a blower to remove most of the pre-existing debris before the harvest, so only a 10% correction was needed to account for leaves from the harvest and any rocks not moved by the blower, unlike at larger commercial orchards which may have less thorough conditioning and may require a larger correction than 10%.

Almond samples were collected at harvest in all subplots of each variety for a physical nut quality analysis. The quality analysis included quantifying (1) the number of sealed shells out of 50 shells, (2) weights of 50 hulls, 50 inshell kernels, and 50 shelled kernels, (3) counts of double, twin, blank, gum, severe shrivel, and insect damage detected in 50 almonds, and (4) measurements of kernel length, width, and thickness of 10 kernels lined up end to end in a row, side by side, and flipped each possible way (length, width, and height).

Nonpareil is a soft-shelled almond whereas Aldrich and Butte are hard-shelled almonds, so it is expected that Nonpareil would have fewer sealed shells per 50 than Aldrich and Butte almonds (Almond Board of California, 2015). Double is when two separate embryos form and grow into two individual almonds located in the same shell. Twin is when a single almond has two radicals. Blank is when a kernel did not develop within the shell. Gum is a rust-colored hard and shiny resin that sometimes is clear. Almond kernel shrivel can occur on almond trees

planted on peach rootstock and is caused by the Peach yellow leafroll phytoplasma (Adaskaveg et al., 2017).

Kernel irrigation water use efficiency (KIWUE) was calculated as the ratio of marketable almond yield (the kernels), Y [kg], divided by the total amount of irrigation from March 1st to harvest, I [mm], as shown in equation 4.2.

$$KIWUE = \frac{Y}{I} \qquad \textit{Equation 4.2}$$

4.2.6. Light interception

Photosynthetically active radiation (PAR) intercepted by the canopy was measured at solar noon in each subplot of the experiment on June 14th and July 20th, 2019 and on June 8th and August 2nd, 2020 using a mobile PAR measurement system (Lampinen et al., 2012). The orchard was planted with alternating rows of three different varieties, so data from the left and right sides of the mobile PAR measurement system were kept separate to allow partitioning of canopy PAR interception for each variety independently.

4.2.7. Statistical analysis

Statistical comparisons were made across the irrigation treatments of each variety to assess differences in marketable kernel yield, various almond physical quality measurements, and canopy PAR interception using analysis of variance (ANOVA). The main objective of the statistical comparisons was to identify significant differences in the response variables due to irrigation treatment for each variety. Equation 4.3 shows the ANOVA model used in this study where y_{ij} is the response variable, μ is the overall mean, ρ_i is the block effect, β_j is the irrigation

effect, $(\rho\beta)_{ij}$ is the interaction between the block effect and the irrigation effect, and ε_{ij} is the experimental error term.

$$y_{ij} = \mu + \rho_i + \beta_j + (\rho\beta)_{ij} + \varepsilon_{ij} \qquad \textit{Equation 4.3}$$

Separate ANOVA tests following the model in equation 4.3 were done on each of the three varieties to optimize precision of the irrigation effect. For the Aldrich and Butte varieties, the irrigation factor levels were S1, S2, S3, and S4. For the Nonpareil variety, the irrigation factor levels were S1, S3, and S5. The block effect was included because there was a pre-existing yield and plant canopy size gradient with larger yields and canopy going from east to west. Furthermore, a previous experiment in 2016-2017 involved RDI treatments in blocks 1-3 and full irrigation in blocks 4-5 in the Nonpareil rows (Kizer et al., 2017). Data were analyzed using the Proc GLIMMIX procedure in SAS (https://support.sas.com/rnd/app/stat/procedures/glimmix.html) . Means were separated at the 0.05 significance level using the Tukey type least squares means (LSMEANS) procedure in SAS.

An alternative two-factor strip plot ANOVA model with variety and irrigation factors shown in equation 4.4 was tested but did not detect significant differences across irrigation treatments. In equation 4.4, y_{ijk} is the response variable, μ is the overall mean, ρ_i is the block effect, α_j is the variety effect, δ_{ij} is the whole plot error of the variety factor, β_k is the irrigation effect, λ_{ik} is the whole plot error of the irrigation factor, $(\alpha\beta)_{ij}$ is the interaction between variety and irrigation factors, and ε_{ijk} is the experimental error term. Significant differences not detected by the two-factor strip plot ANOVA model from equation 4.4 were detected in the single-factor ANOVA model from equation 4.3. The variety factor in the two-factor strip plot ANOVA model had an overwhelming effect on the almond physical quality and marketable kernel yield, so differences within a variety due to the irrigation treatments were less detectable by the two-

factor strip plot ANOVA model. Therefore, it made sense to do a single-factor ANOVA on each variety to optimize the precision of the irrigation effect of a single variety at a time. Strong variety effects likely due to genetics were so dominant that irrigation effects played a small role in the overall effect on the physical quality parameters, so it was not possible see the irrigation effect on the physical quality parameters unless a single factor ANOVA was done on each variety. The purpose of the study was to identify the most optimal irrigation regime for each variety in terms of various response variables, so the variety main effect was not of primary interest to this study.

$$y_{ijk} = \mu + \rho_i + \alpha_j + (\alpha\rho)_{ij} + \beta_k + (\rho\beta)_{ik} + (\alpha\beta)_{ij} + \varepsilon_{ijk} \qquad \textit{Equation 4.4}$$

There are several implications to the strip-plot experimental design. The whole plot A treatment is confounded with the whole plots of factor A. The whole plot B treatment is confounded with the whole plots of factor B. The strip plot design tends to sacrifice precision in testing the main effects but improves precision in testing interaction effects.

4.3. Results

4.3.1. Precipitation and evapotranspiration

Figure 4.3 shows the monthly precipitation at the California Irrigation Management Information System (CIMIS) in Williams, CA, which was located approximately 11 miles from the experimental site. The monthly precipitation was organized by water year, where a water year begins on October 1st and ends on September 30th of the following calendar year. Precipitation in the months of January through March of 2019 was high, but low in 2020. An unusually dry winter occurred in 2020 with zero precipitation during February. Figure 4.3 shows the precipitation starting in October of the calendar year before each year of the study.

Although the precipitation was measured 11 miles from the experimental site, the data gives a general idea of the precipitation amount between 2019 and 2020.

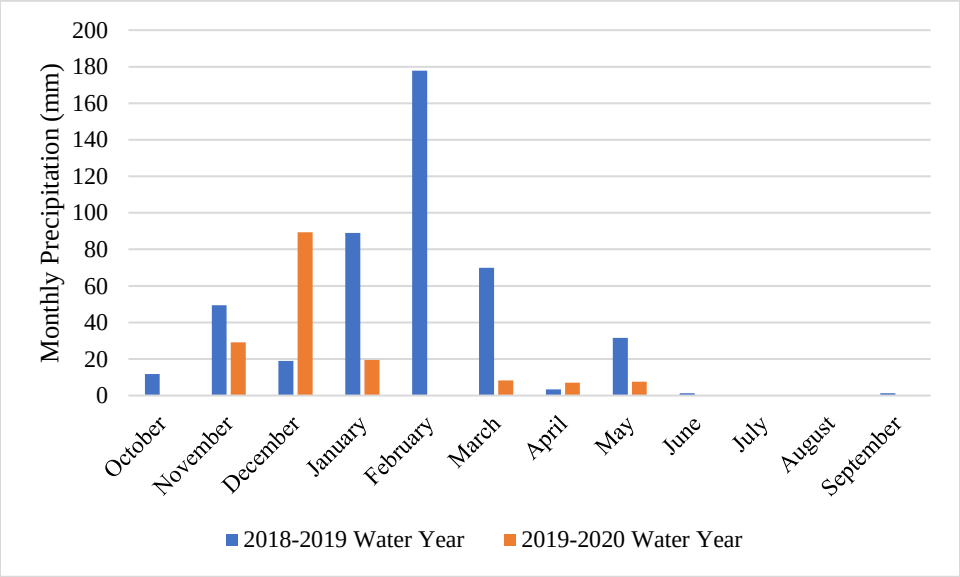

Figure 4.3. Monthly precipitation at the California Irrigation Management Information System station near Williams, CA during water years 2018-2019 and 2019-2020, where a water year begins on October 1st and ends on September 30th of the following calendar year.

Figure 4.4 shows the monthly evapotranspiration of a grass reference crop at the CIMIS station near Williams, CA. The monthly reference evapotranspiration was similar during both years of the experiment.

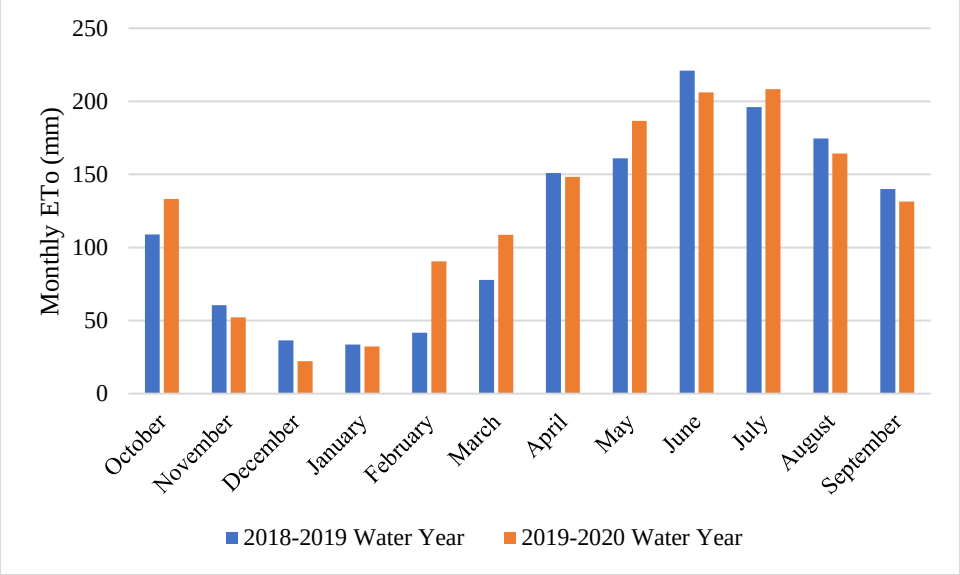

Figure 4.4. Monthly evapotranspiration of a grass reference crop at the California Irrigation Management Information System station near Williams, CA during water years 2018-2019 and 2019-2020, where a water year begins on October 1st and ends on September 30th of the following calendar year.

4.3.2. *Cumulative irrigation*

In 2019, the grower began irrigation for the year in mid-April and applied 327 mm of water between April 12, 2019 and the start of the experimental irrigation treatments in July. In 2020, the grower started irrigation at the beginning of March due to an unusual winter drought and applied 554 mm of water between March 3, 2020 and the start of the experimental irrigation treatments in July. Table 4.2 shows the total water applied from leaf out to harvest in all the irrigation treatments of each variety. Differences in total water applied between irrigation treatments were small because the RDI periods of the experimental irrigation treatments ranged between only 32 to 46 days as shown in Table 4.1, compared to the total irrigation season for the year of approximately 240 days (March to October). The total water applied shown in Table 4.2 does not include post-harvest irrigation (between September and November). Less total water

was applied before harvest in 2019 than in 2020 because there was more precipitation in the spring in 2019, so the grower did not irrigate as much in the spring compared to in 2020.

Table 4.2. Total water applied from leaf out to harvest in different irrigation regimes (mm)

Irrigation Schedule	Total water applied from leaf out to harvest (mm)[a]		
2019	Aldrich	Butte	Nonpareil
S1: 75% ETc during Nonpareil hull-split period	522	525	498
S2: 75% ETc during variety-specific hull-split period	561	608	
S3: 50% ETc during Nonpareil hull-split period	495	497	475
S4: 50% ETc during variety-specific hull-split period	542	580	
S5: 100% ETc during Nonpareil hull-split period			553
2020[b]	Aldrich	Butte	Nonpareil
S1: 75% ETc during Nonpareil hull-split period	786	792	731
S2: 75% ETc during variety-specific hull-split period	836	804	
S3: 50% ETc during Nonpareil hull-split period	727	724	661
S4: 50% ETc during variety-specific hull-split period	738	792	
S5: 100% ETc during Nonpareil hull-split period			774

[a]The mean of five replicates of each irrigation schedule of the total applied water was calculated.
[b]More irrigation was applied in 2020 because minimal rainfall occurred in the winter and spring that year.

Figure 4.5 show the cumulative water applied since the grower began irrigation in the spring from each irrigation treatment in each variety as the average of five replicates in 2019. In the Aldrich variety, S2 and S4 were at 100% ET_c until Aldrich hull-split started on July 27th, so S2 and S4 trees received more water in the beginning of the season than S1 and S3, which were at 75% ET_c and 50% ET_c beginning on July 9th when Nonpareil hull-split initiated. By harvest on

September 11th, S2 received the most water of the irrigation treatments in Aldrich because it was irrigated at the 75% ET_c rate during hull-split and the RDI treatment was initiated for fewer days than S1 and S3 due to variety differences in the period between 1% hull-split initiation and harvest, as shown in Table 4.1. There were some differences in water applied between S2 and S4 prior to Aldrich hull-split due to malfunctions with the irrigation system on July 25th, although they should have both received the same amount of water at the 100% ET_c rate.

In the Butte variety, S2 and S4 were at 100% ET_c until Butte hull-split started on August 7th, so S2 and S4 trees received more water in the beginning of the season than S1 and S3, which were at 75% ET_c and 50% ET_c beginning on July 9th when Nonpareil hull-split initiated. Water applied increased in S1 and S3 after the Nonpareil trees were harvested on August 22nd. By harvest on September 11th, S2 received the most water of the irrigation treatments in Butte because it was irrigated at the 75% ET_c rate during hull-split and the RDI treatment was initiated for fewer days than S1 and S3 due to variety differences in the period between 1% hull-split initiation and harvest, as shown in Table 4.1.

In the Nonpareil variety, S5 was irrigated at 100% ET_c and received the most water of all the treatments. S1 received 75% ET_c and S3 received 50% ET_c Nonpareil during hull-split, which began on July 9th. A plateau in cumulative water applied in all the irrigation treatments began around August 3rd as the grower restricted irrigation to dry the orchard ground in preparation for the harvest activities. Graphs of the cumulative water applied in 2020 are shown in the appendix.

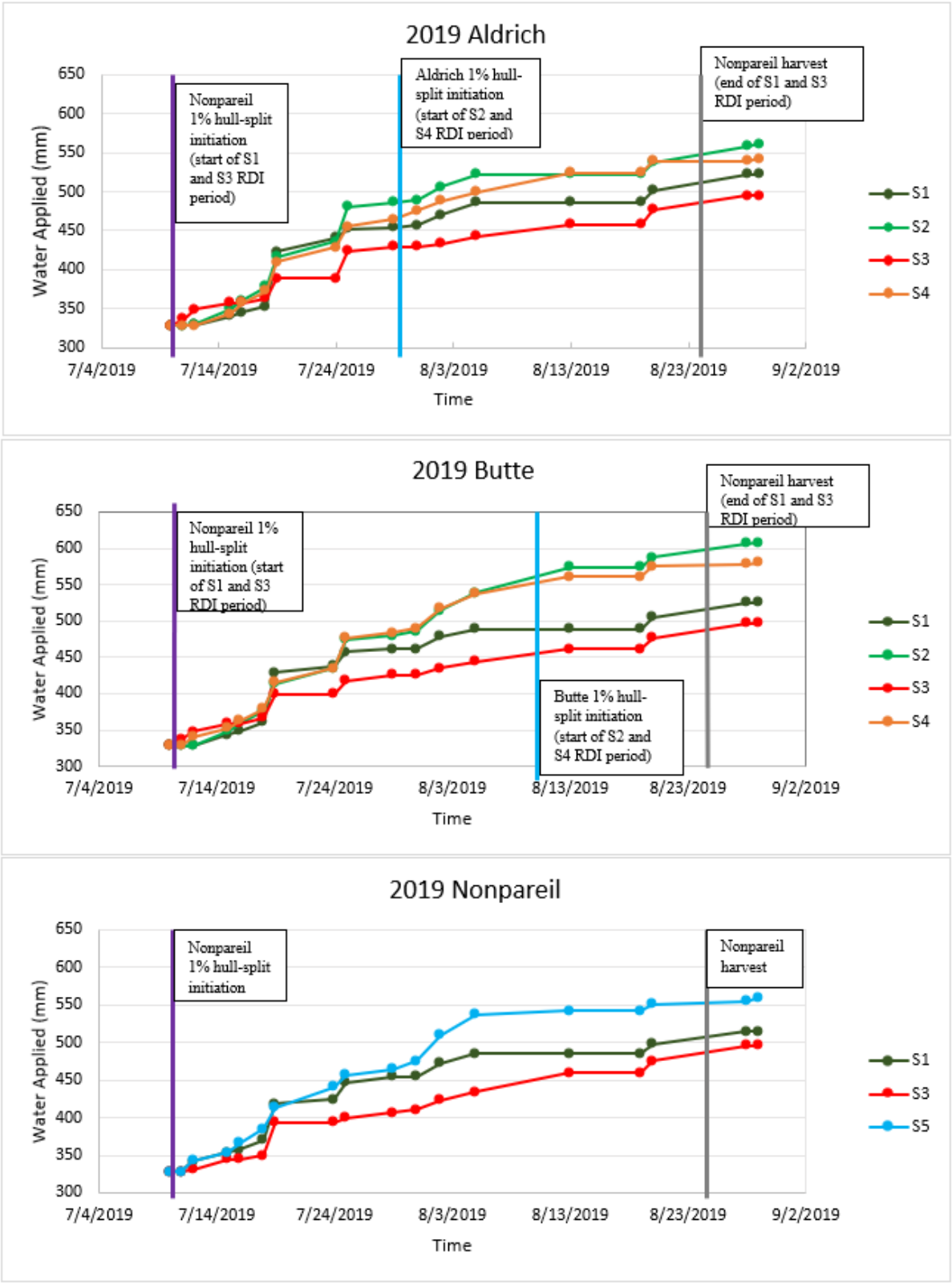

Figure 4.5. Cumulative water applied in the Aldrich, Butte, and Nonpareil varieties under various irrigation regimes in 2019 at the Nickels Soil Lab near Arbuckle, CA.

4.3.3. Irrigation effect on soil water content

Figure 4.6 shows the soil water content in all the irrigation treatments of each variety. Most soil water content measurements were taken immediately before irrigation when the soil water content was expected to be low. Large standard deviations were found in the soil water content in each treatment, likely due to spatial variations in water-holding capacity due to heterogeneity in the soil texture or topographic influences on distribution uniformity. In the Aldrich variety, there was a malfunction with the irrigation system on July 25th, so S1 had a large unintended spike in soil water content. In general, the soil water content followed the schedule of the water applied from irrigation. Between Nonpareil 1% hull-split initiation (July 9th) and Aldrich 1% hull-split initiation (July 27th) , the soil water content in treatments S2 and S4 (100% ET_c) were maintained at a higher level than in S3 (50% ET_c) due to the additional irrigation. After Aldrich hull-split began on July 27th, the soil water contents of S2 and S4 were reduced in response to the deficit irrigation, with S4 (50% ET_c) under more soil water deficit than S2 (75% ET_c) for most of the remainder of the season. The grower irrigated on August 19th, so all the treatments had approximately the same soil water content on that day. After the Nonpareil harvest on August 22nd, treatments S1 and S3 entered the 100% ET_c irrigation stage and soil water content increased, although it took longer for S3 to replenish the soil water content due to having been under more limited irrigation prior to harvest. Unlike the two Nonpareil-based hull-split treatments (S1 and S3), the soil water content of S4 remained low until the Aldrich harvest on September 11th. A malfunction with the irrigation system resulted in unintended extra irrigation in S2 on September 7th, although it should have followed the trend of S4. Graphs of the soil water content in each variety in response to the various irrigation treatments in 2020 can be found in the appendix.

In the Butte variety, the soil water contents in treatments S2 and S4 were maintained between 0.1 cm/cm and 0.2 cm/cm when they were in the 100% ET_c stage before dropping below 0.1 cm/cm after Butte hull-split started on August 7th. Differences in soil water content between S2 and S4 between Butte 1% hull-split (August 7th) and Butte harvest (September 11th) were small despite different applied water amounts. The soil water contents in treatments S1 and S3 were lower than in S2 and S4 between Nonpareil 1% hull-split (July 9th) and Butte 1% hull-split (August 7th) due to the deficit irrigation during that period. The grower irrigated on August 19th, so all the treatments had approximately the same soil water content on that day. After Nonpareil harvest (August 22nd), the S1 and S3 treatments entered the 100% ET_c stage, increasing the soil water contents.

Figure 4.6 (bottom) shows the soil water content in response to the irrigation treatments in the Nonpareil variety. Between Nonpareil 1% hull-split (July 9th) and August 13th, increased water applied led to higher soil water content with the highest soil water content in S5 (100% ET_c), followed by S1 (75% ET_c), and then by S3 (50% ET_c). The grower irrigated on August 19th, so all the treatments had approximately the same soil water content on that day and on August 21st. After the Nonpareil harvest, all treatments entered the 100% ET_c stage and soil water content increased on September 7th to the almost same soil water content as on April 12th prior to RDI treatments.

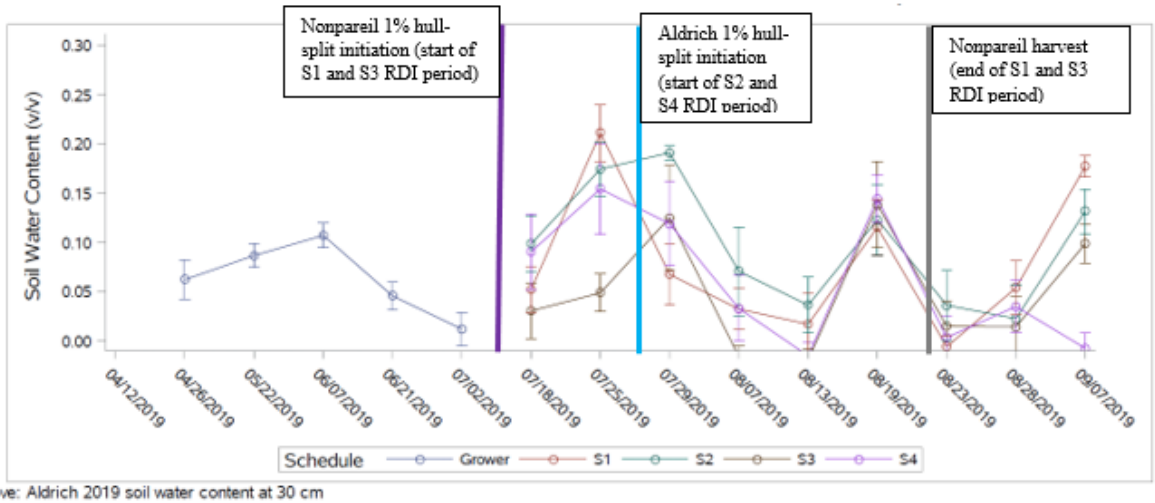

Above: Aldrich 2019 soil water content at 30 cm

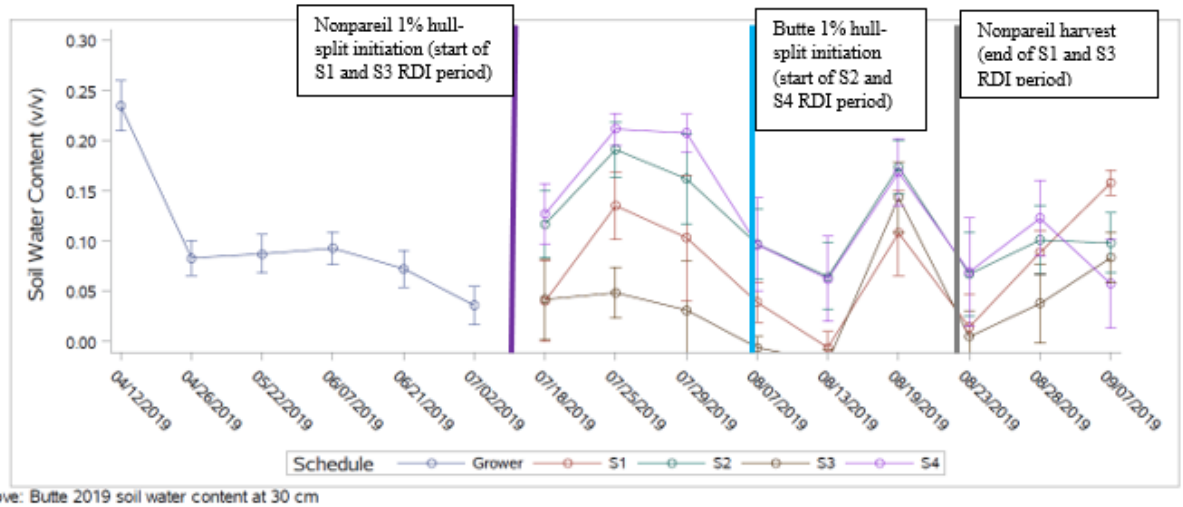

Above: Butte 2019 soil water content at 30 cm

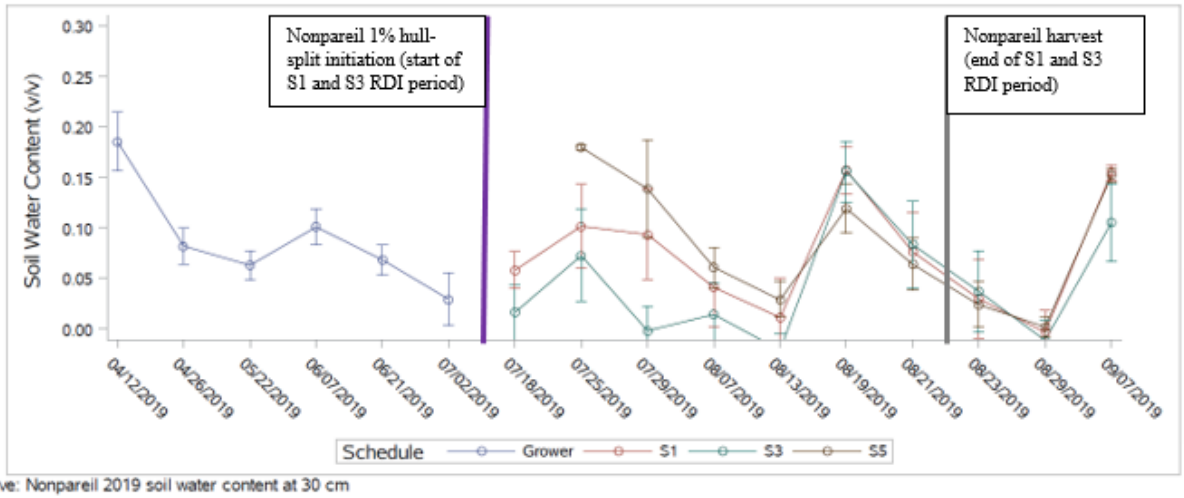

Above: Nonpareil 2019 soil water content at 30 cm

Figure 4.6. Soil water content under different irrigation schedules in the Aldrich (top), Butte (middle), and Nonpareil (bottom) varieties in 2019. S1 = 75% ET_c during Nonpareil hull-split period. S3 = 50% ET_c during Nonpareil hull-split period. S5 = 100% ET_c during Nonpareil hull-split period. S5 = 100% ET_c throughout the season. Error bars are standard deviations.

4.3.4. Irrigation effect on midday stem water potential

Figure 4.7 shows the midday stem water potential (MSWP) in the Aldrich, Butte, and Nonpareil varieties under the various irrigation treatments between July and September. The MSWP measurements are shown in MPa, where 1 MPa is equal to 10 bars. Most MSWP measurements were taken immediately before irrigation when the MSWP was expected to be low (high water stress). In the Aldrich variety, the average MSWP in 2019 and 2020, respectively, were -1.6 and -1.5 MPa in S1, -1.3 and -1.2 MPa in S2, -1.7 and -1.6 MPa in S3, and -1.6 and -1.6 MPa in S4. In both years in the Aldrich variety, 75% ET_c during variety-specific hull-split period (S2) resulted in the least water stress whereas 50% ET_c during Nonpareil hull-split period (S3) resulted in the most water stress. In the Butte variety, the average MSWP in 2019 and 2020, respectively, were -1.6 and -1.2 MPa in S1, -1.2 and -1.0 MPa in S2, -1.8 and -1.3 MPa in S3, and -1.5 and -1.1 MPa in S4. There was more water stress in 2019 than in 2020 in the Butte variety. In both years in the Butte variety, 75% ET_c during variety-specific hull-split period (S2) resulted in the least water stress whereas 50% ET_c during Nonpareil hull-split period (S3) resulted in the most water stress, which was the same result as in the Aldrich variety. In the Nonpareil variety, the average MSWP in 2019 and 2020, respectively, were -1.5 and -1.1 MPa in S1, -1.6 and -1.5 in S3, and -1.3 and -1.1 in S5. Between the two years of the study, S5 (100% ET_c) resulted in the least water stress, followed by S1 (75% ET_c), and then by S3 (50% ET_c). The grower irrigated the orchard on August 19th, 2019, so the MSWP was approximately the same in all subplots.

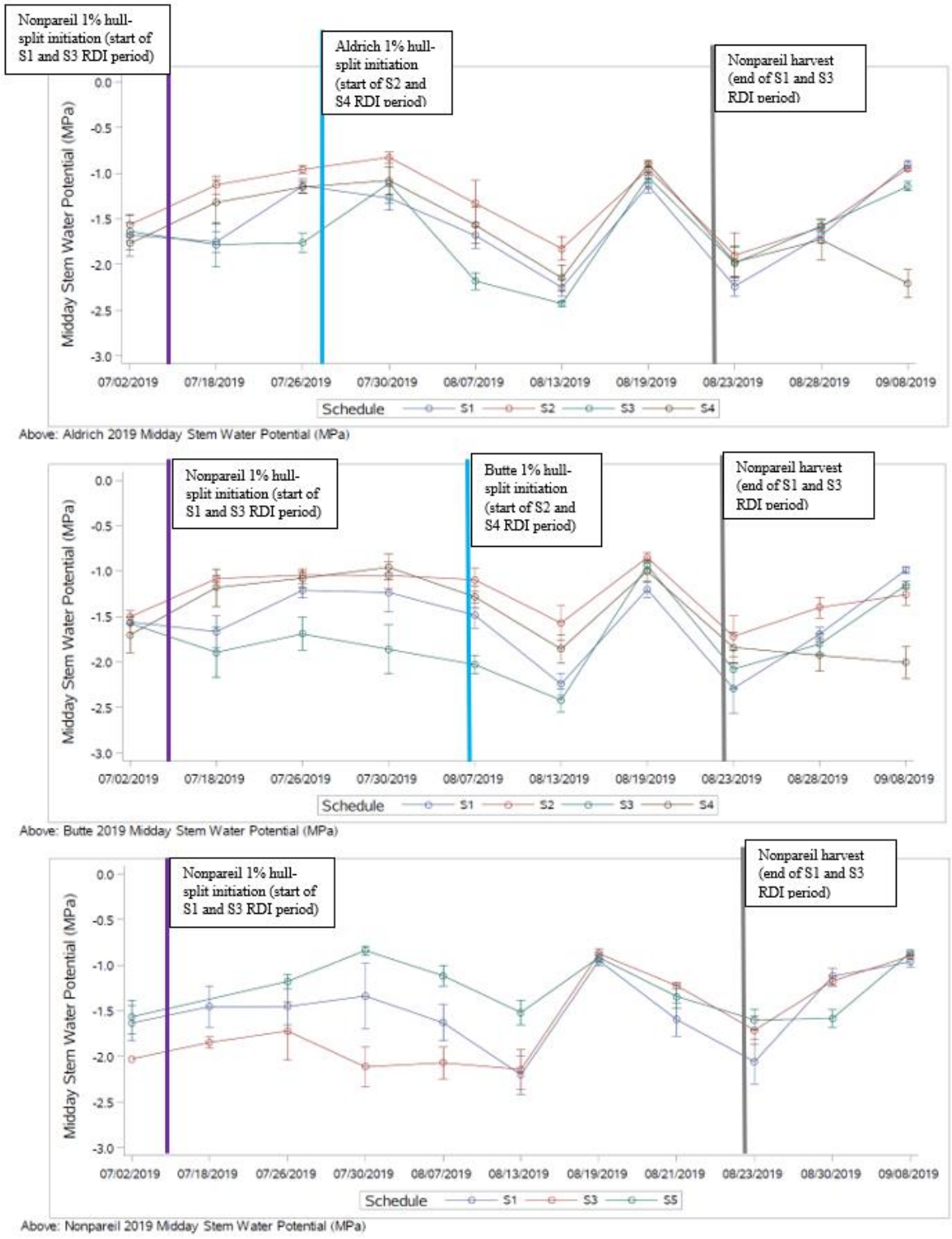

Figure 4.7. Midday stem water potential under different irrigation schedules in the Aldrich (top), Butte (middle), and Nonpareil (bottom) varieties in 2019. S1 = 75% ET_c during Nonpareil hull-split period. S2 = 75% ET_c during variety-specific hull-split period. S3 = 50% ET_c during Nonpareil hull-split period. S4 = 50% ET_c during variety-specific hull-split period. S5 = 100% ET_c throughout the season. Error bars are standard deviations.

4.3.5. Irrigation effect on almond physical quality

Table 4.3 shows the physical quality results of the Aldrich almond samples under different irrigation regimes. In the Aldrich variety, the thickness per 10 kernels was significantly higher in S2 than S3 in 2019 and significantly higher in S2 than both S1 and S3 in 2020 at the 95% confidence level. This means that 75% ET_c during variety-specific hull-split period (S2) in Aldrich resulted significantly thicker kernels than 75% ET_c and 50% ET_c during Nonpareil hull-split period (S1 and S3). In the Aldrich variety, S3 resulted in significantly higher occurrence of severe shrivel in S3 than in S1 and S4 in 2020. Although not significant, both Nonpareil-based hull-split RDI treatments resulted in higher occurrence of severe shrivel than both variety-specific hull-split RDI treatments in 2019. No significant differences were found across irrigation treatments in the Aldrich variety in the length and width per 10 kernels, sealed shells per 50 shells, grams per 50 kernels, double, twin, blank, gum, or insect damage at the 95% confidence level. S1 resulted in significantly fewer sealed shells out of 50 shells than S3 in 2019 at the 90% confidence level.

Table 4.4 shows the physical quality results of the Butte almond samples under different irrigation regimes. In 2019, both variety-specific hull-split RDI treatments (S2 and S4) resulted in significantly fewer sealed shells out of 50 shells than both Nonpareil-based hull-split RDI treatments (S1 and S3). In 2020, although only S2 had significantly fewer sealed shells out of 50 shells than S3, both variety-specific hull-split RDI treatments (S2 and S4) resulted in fewer sealed shells out of 50 shells than both Nonpareil-based hull-split RDI treatments (S1 and S3). No significant differences were found across irrigation treatments in the Butte variety in the thickness, length, width per 10 kernels, grams per 50 kernels, shrivel, double, twin, blank, gum, or insect damage at the 95% confidence level. However, the occurrence of severe shrivel was significantly higher in S2 than S1 in 2019 at 90% confidence level. S2 and S4 (according to

variety specific hull-split) tended to have more shrivel than S1 and S3 (according to Nonpareil hull-split), although not significant.

Table 4.5 shows the physical quality results of the Nonpareil variety under different irrigation regimes. No significant differences were found across irrigation treatments in the Nonpareil variety in the thickness, length, width per 10 kernels, sealed shells per 50 shells, grams per 50 kernels, shrivel, double, twin, blank, gum, or insect damage at the 95% confidence level. However, S5 resulted in significantly higher thickness per 10 kernels than S3 in 2020 at the 90% confidence level. Also, S1 resulted in significantly higher occurrence of severe shrivel than S5 in 2020 at the 90% confidence level.

Table 4.3. Aldrich variety physical quality under different irrigation regimes at Nickels Soil Lab near Arbuckle, CA[a]

Irrigation Schedule	Almond physical quality parameter									
	Thickness per 10 kernels (cm)[b]	Length per 10 kernels (cm)[b]	Width per 10 kernels (cm)[b]	Sealed shells per 50 shells	Grams per 50 Kernels	Shrivel[c]	Double[c]	Twin[c]	Blank[c]	Gum[c]
2019										
S1: 75% ET_c during Nonpareil hull-split period	7.94 ab	22.9 a	11.7 a	22 a	50 a	2.0 a	3.0 a	0.4 a	0.2 a	0.2 a
S2: 75% ET_c during variety-specific hull-split period	8.14 a	23.2 a	11.8 a	27 a	51 a	0.4 a	3.8 a	0.2 a	0.2 a	0.8 a
S3: 50% ET_c during Nonpareil hull-split period	7.78 b	23.1 a	12.0 a	37 a	50 a	2.0 a	4.6 a	0.6 a	0.2 a	0 a
S4: 50% ET_c during variety-specific hull-split period	8.06 ab	23.1 a	12.0 a	35 a	50 a	0.8 a	3.4 a	1.2 a	0.8 a	0.6 a
p-value	0.0458	0.6748	0.3757	0.0716	0.7391	0.091	0.6642	0.1102	0.3425	0.0951
2020										
S1: 75% ET_c during Nonpareil hull-split period	8.20 b	20.0 a	10.6 a	39 a	42 a	0 b	0.4 a	2.2 a	0.4 a	0 a
S2: 75% ET_c during variety-specific hull-split period	8.48 a	20.6 a	10.9 a	39 a	42 a	0.4 ab	0.6 a	0.8 a	0 a	0 a
S3: 50% ET_c during Nonpareil hull-split period	8.24 b	20.3 a	10.8 a	39 a	41 a	0.8 a	0.4 a	1.4 a	0.4 a	0 a
S4: 50% ET_c during variety-specific hull-split period	8.32 ab	19.8 a	10.7 a	39 a	41 a	0 b	1.2 a	1.6 a	0.4 a	0 a
p-value	0.008	0.0989	0.4512	0.9996	0.2395	0.0064	0.3477	0.5479	0.7413	NA

[a] Average values of five replicates for each irrigation schedule for 2019 and 2020. Different letters represent significant differences between irrigation schedule according to the Tukey multiple comparison adjustment at $p<0.05$.

[b] Ten kernels were lined up end to end in a row side by side and flipped each possible way to measure thickness, length, and width of ten kernels in centimeters.

[c] Shrivel, double, twin, blank, and gum were counted out of 50 kernels. Only severe shrivel was counted.

Table 4.4. Butte variety physical quality under different irrigation regimes at Nickels Soil Lab near Arbuckle, CA[a]

Irrigation Schedule	Almond physical quality parameter									
	Thickness per 10 kernels (cm)[b]	Length per 10 kernels (cm)[b]	Width per 10 kernels (cm)[b]	Sealed shells per 50 shells	Grams per 50 Kernels	Shrivel[c]	Double[c]	Twin[c]	Blank[c]	Gum[c]
2019										
S1: 75% ET_c during Nonpareil hull-split period	8.3 a	20.5 a	11.6 a	40 a	44 a	0 a	5.2 a	0.6 a	0.2 a	0.6 a
S2: 75% ET_c during variety-specific hull-split period	8.2 a	20.9 a	12.1 a	25 b	47 a	1.4 a	5.4 a	0.8 a	0 a	0 a
S3: 50% ET_c during Nonpareil hull-split period	8.3 a	20.5 a	11.8 a	37 a	45 a	0.2 a	4.2 a	0.2 a	0.2 a	0.2 a
S4: 50% ET_c during variety-specific hull-split period	8.4 a	20.5 a	11.7 a	26 b	46 a	0.6 a	6.0 a	0.4 a	0.8 a	0 a
p-value	0.35	0.14	0.10	0.001	0.12	0.06	0.59	0.47	0.37	0.16
2020										
S1: 75% ET_c during Nonpareil hull-split period	8.9 a	19.4 a	12.0 a	43 ab	48 a	0.8 a	2.5 a	4.0 a	0 a	0 a
S2: 75% ET_c during variety-specific hull-split period	9.0 a	19.7 a	12.2 a	40 b	50 a	1.4 a	0.8 a	1.8 a	0 a	0 a
S3: 50% ET_c during Nonpareil hull-split period	9.1 a	19.5 a	12.1 a	45 a	51 a	0.6 a	1.2 a	2.8 a	0.6 a	0.2 a
S4: 50% ET_c during variety-specific hull-split period	9.2 a	19.6 a	12.4 a	42 ab	49 a	0.8 a	0.5 a	2.0 a	0.3 a	0.3 a
p-value	0.71	0.79	0.39	0.05	0.40	0.66	0.30	0.33	0.10	0.58

[a] Average values of five replicates for each irrigation schedule for 2019 and 2020. In 2020, S1 and S4 had only four replicates due to a mistake during the almond sample collection. Different letters represent significant differences between irrigation schedule according to the Tukey multiple comparison adjustment in 2019 and the Tukey-Kramer multiple comparison adjustment in 2020 at $p<0.05$.

[b] Ten kernels were lined up end to end in a row side by side and flipped each possible way to measure thickness, length, and width of ten kernels in centimeters.

[c] Shrivel, double, twin, blank, and gum were counted out of 50 kernels. Only severe shrivel was counted.

Table 4.5. Nonpareil variety physical quality under different irrigation regimes at Nickels Soil Lab near Arbuckle, CA[a]

Irrigation Schedule	Almond physical quality parameter									
	Thickness per 10 kernels (cm)[b]	Length per 10 kernels (cm)[b]	Width per 10 kernels (cm)[b]	Sealed shells per 50 shells	Grams per 50 Kernels	Shrivel[c]	Double[c]	Twin[c]	Blank[c]	Gum[c]
2019										
S1/S2: 75% ET_c during Nonpareil hull-split period	7.7 a	24.3 a	13.4 a	22 a	63 a	2.6 a	0.4 a	8.4 a	0.2 a	0 a
S3/S4: 50% ET_c during Nonpareil hull-split period	7.4 a	24.6 a	13.3 a	26 a	60 a	1.4 a	1.0 a	6.4 a	1.2 a	0 a
S5: 100% ET_c during Nonpareil hull-split period	7.6 a	24.2 a	13.4 a	23 a	60 a	1.8 a	0.8 a	5.3 a	1.1 a	0.2 a
p-value	0.2256	0.3037	0.878	0.688	0.1447	0.367	0.4382	0.102	0.1495	0.3897
2020										
S1/S2: 75% ET_c during Nonpareil hull-split period	8.4 a	22.9 a	12.6 a	17 a	61 a	2.8 a	0.6 a	3.8 a	1.4 a	0.2 a
S3/S4: 50% ET_c during Nonpareil hull-split period	8.2 a	23.1 a	12.9 a	29 a	60 a	1.6 a	1.8 a	2.8 a	0.6 a	0 a
S5: 100% ET_c during Nonpareil hull-split period	8.6 a	23.1 a	12.9 a	22 a	60 a	0.9 a	0.7 a	2.5 a	0.5 a	0 a
p-value	0.0758	0.7934	0.34	0.1306	0.8418	0.0721	0.1924	0.4205	0.2145	0.2777

[a] Average values of five replicates for each irrigation schedule for 2019 and 2020. Different letters represent significant differences between irrigation schedule according to the Tukey multiple comparison adjustment at $p<0.05$.

[b] Ten kernels were lined up end to end in a row side by side and flipped each possible way to measure thickness, length, and width of ten kernels in centimeters.

[c] Shrivel, double, twin, blank, and gum were counted out of 50 kernels. Only severe shrivel was counted.

4.3.6. Yield

Table 4.6 shows the marketable kernel yield of almond trees under different irrigation regimes in 2019 and 2020. No significant differences were found across any of the irrigation treatments in the Aldrich, Butte, and Nonpareil varieties in 2019 and 2020 at the 90% or 95% confidence levels. Although not statistically significant, the marketable kernel yield of the Aldrich variety under both variety-specific hull-split RDI regimes (S2 at 4048 kg/hectare and S4 at 4180 kg/hectare) was higher than the marketable kernel yield of the Aldrich variety under the Nonpareil-based hull-split RDI regimes (S1 at 3993 kg/hectare and S3 at 3825 kg/hectare). The marketable kernel yield in 2020 was considerably higher than in 2019 in the Aldrich and Nonpareil varieties (between 123% and 147% increase in Aldrich and between 37% and 45% increase in Nonpareil), which was likely due to no rainfall during peak bloom in 2020 and was corroborated by record-breaking almond yields across California. The Aldrich variety is known for a strong alternate bearing response and usually alternates between high yield and low yield from year to year, which partly explains the large increase in marketable kernel yield from 2019 to 2020. The Butte variety showed minimal increase in marketable kernel yield between 2019 and 2020, possibly related to its later maturity. In 2019 and 2020, the marketable kernel yield of the Nonpareil variety was the highest in S5 (100% ET_c during Nonpareil hull-split period), followed by S1 (75% ET_c during Nonpareil hull-split period), and then by S3 (50% ET_c during Nonpareil hull-split period), meaning that marketable kernel yield increased with increased water applied, although the differences were not statistically significant.

Table 4.6. Marketable kernel yield of almond trees under different irrigation regimes in 2019 and 2020 at Nickels Soil Lab near Arbuckle, CA[a]

Irrigation Schedule	Kernel Yield (kg/hectare)		
2019	Aldrich	Butte	Nonpareil
S1: 75% ETc during Nonpareil hull-split period	1789 a	2937 a	3072 a
S2: 75% ETc during variety-specific hull-split period	1694 a	2820 a	
S3: 50% ETc during Nonpareil hull-split period	1608 a	2731 a	2769 a
S4: 50% ETc during variety-specific hull-split period	1691 a	2649 a	
S5: 100% ETc during Nonpareil hull-split period			3275 a
p-value	0.5229	0.3153	0.1533
2020	Aldrich	Butte	Nonpareil
S1: 75% ETc during Nonpareil hull-split period	3993 a	2998 a	4194 a
S2: 75% ETc during variety-specific hull-split period	4048 a	2829 a	
S3: 50% ETc during Nonpareil hull-split period	3825 a	2936 a	3855 a
S4: 50% ETc during variety-specific hull-split period	4180 a	2695 a	
S5: 100% ETc during Nonpareil hull-split period			4221 a
p-value	0.6255	0.2302	0.2551
Percent increase in yield from 2019 to 2020	Aldrich	Butte	Nonpareil
S1: 75% ETc during Nonpareil hull-split period	123 a	2 a	37 a
S2: 75% ETc during variety-specific hull-split period	139 a	0 a	
S3: 50% ETc during Nonpareil hull-split period	138 a	7 a	39 a
S4: 50% ETc during variety-specific hull-split period	147 a	2 a	
S5: 100% ETc during Nonpareil hull-split period			29 a
p-value	0.3005	0.5901	0.3415

[a] The marketable kernel yield measurements have been reduced by 10% to account for rocks, leaves, and other debris collected with the almonds. The total yield of each subplot was collected with a scale at the orchard and then multiplied by the fraction of kernel weight to total weight (hulls, shells, and kernels) to determine the kernel yield of each subplot.

4.3.7. Kernel irrigation water use efficiency

Table 4.7 shows the kernel irrigation water use efficiency of Aldrich, Butte, and Nonpareil almond trees under various irrigation regimes in 2019 and 2020. In 2019 and 2020, the kernel irrigation water use efficiency of the Butte variety was higher in both Nonpareil-based hull-split RDI treatments, S1 and S3, than the two variety-specific hull-split RDI treatments, S2 and S4, meaning that more marketable kernel yield was produced per volume of water applied when irrigating the Butte trees according to Nonpareil hull-split schedule. Earlier RDI application in both Nonpareil-based hull-split RDI treatments (S1 and S3) resulted in less total water applied during the growing season than RDI application according to variety-specific hull-split (S2 and S4) due to variety differences in the duration between hull-split initiation and harvest. In 2019, the kernel irrigation water use efficiency in Butte of S1 was significantly higher than in S2 and S4 at the 95% confidence level. In 2020, the kernel irrigation water use efficiency in Butte of S3 was significantly higher than in S2 and S4 at the 95% confidence level. No significant differences in kernel irrigation water use efficiency were found across irrigation treatments in the Aldrich and Nonpareil varieties in 2019 and 2020.

Table 4.7. Kernel irrigation water use efficiency of almond trees under various irrigation regimes in 2019 and 2020

Irrigation Schedule	Kernel Irrigation Water Use Efficiency (kg/m^3)		
2019	Aldrich	Butte	Nonpareil
S1: 75% ETc during Nonpareil hull-split period	0.34 a	0.54 a	0.62 a
S2: 75% ETc during variety-specific hull-split period	0.30 a	0.46 bc	
S3: 50% ETc during Nonpareil hull-split period	0.32 a	0.55 ab	0.59 a
S4: 50% ETc during variety-specific hull-split period	0.31 a	0.46 c	
S5: 100% ETc during Nonpareil hull-split period			0.58 a
p-value	0.32	0.01	0.68
2020	Aldrich	Butte	Nonpareil
S1: 75% ETc during Nonpareil hull-split period	0.51 a	0.38 ab	0.57 a
S2: 75% ETc during variety-specific hull-split period	0.49 a	0.35 b	
S3: 50% ETc during Nonpareil hull-split period	0.52 a	0.41 a	0.58 a
S4: 50% ETc during variety-specific hull-split period	0.57 a	0.34 b	
S5: 100% ETc during Nonpareil hull-split period			0.50 a
p-value	0.11	0.01	0.42

4.3.8. Light interception

Table 4.8 shows the percent of photosynthetically active radiation intercepted by the canopy (percent PAR) of almond trees under various irrigation regimes. On the 6/14/19, 7/20/19, and 8/2/20, no significant differences in percent PAR were found across irrigation treatments light interception measurements in any of the varieties at the 90% or 95% confidence levels. However, the p-value decreased between 6/14/2019 and 6/8/2020 (mid-season dates) as well as between 7/20/2019 and 8/2/2020 (late-season dates) in all varieties, indicating that the significance of the irrigation effect on percent PAR increased over the two years of the experiment.

On 6/8/20, the percent PAR of the Aldrich variety was significantly higher in S4 (50% ET_c during variety-specific hull-split period) compared to S1 (75% ET_c during Nonpareil hull-

split period) at the 95% confidence level. However, this significant difference was not repeated on any of the other dates of light interception measurements and does not align with the expectation that more water applied leads to higher percent PAR.

No significant differences across irrigation treatments were found in the percent difference in percent PAR between 6/14/2019 and 6/8/2020 (mid-season dates) as well as between 7/20/2019 and 8/2/2020 (late-season dates) at the 90% or 95% confidence levels. In the Aldrich variety, the percent difference in percent PAR was higher in both 50% ET_c treatments (S3 at 17% and S4 at 10%) than the two 75% ET_c treatments (S1 at 5% and S2 at 8%) between 6/14/2019 and 6/8/2020 (mid-season dates). Similarly, the percent PAR of the Aldrich variety slightly decreased between 7/20/2019 and 8/2/2020 in the two 75% ET_c treatments (S1 at -1% and S2 at -2%) but increased between 7/20/2019 and 8/2/2020 in both 50% ET_c treatments (S3 at 6% and S4 at 3%). In the Butte variety, the percent PAR increased between 6/14/2019 and 6/8/2020 as well as between 7/20/2019 and 8/2/2020 in all the irrigation treatments except for S3 (50% ET_c during Nonpareil hull-split period) which resulted in 0% change between both sets of dates.

Table 4.8. Percent of photosynthetically active radiation intercepted by almond trees under different irrigation regimes at Nickels Soil Lab near Arbuckle, CA

2019	6/14/2019	7/20/2019	6/14/2019	7/20/2019	6/14/2019	7/20/2019
Irrigation Schedule	Aldrich	Aldrich	Butte	Butte	Nonpareil	Nonpareil
S1: 75% ETc during Nonpareil hull-split period	64 a	70 a	67 a	71 a	73 a	79 a
S2: 75% ETc during variety-specific hull-split period	66 a	73 a	68 a	73 a		
S3: 50% ETc during Nonpareil hull-split period	61 a	68 a	68 a	72 a	70 a	77 a
S4: 50% ETc during variety-specific hull-split period	64 a	70 a	66 a	69 a		
S5: 100% ETc during Nonpareil hull-split period					72 a	78 a
p-value	0.3382	0.289	0.9531	0.7817	0.6651	0.6832
2020	6/8/2020	8/2/2020	6/8/2020	8/2/2020	6/8/2020	8/2/2020
Irrigation Schedule	Aldrich	Aldrich	Butte	Butte	Nonpareil	Nonpareil
S1: 75% ETc during Nonpareil hull-split period	67.3 b	69 a	71 a	73 a	80 a	81 a
S2: 75% ETc during variety-specific hull-split period	70.5 ab	71 a	73 a	76 a		
S3: 50% ETc during Nonpareil hull-split period	70.7 ab	72 a	68 a	72 a	77 a	78 a
S4: 50% ETc during variety-specific hull-split period	70.9 a	72 a	71 a	73 a		
S5: 100% ETc during Nonpareil hull-split period					78 a	80 a
p-value	0.0333	0.2175	0.4728	0.6866	0.312	0.4832
	6/14/20 to 6/8/20	7/20/19 to 8/2/20	6/14/20 to 6/8/20	7/20/19 to 8/2/20	6/14/20 to 6/8/20	7/20/19 to 8/2/20
Percent difference	Aldrich	Aldrich	Butte	Butte	Nonpareil	Nonpareil
S1: 75% ETc during Nonpareil hull-split period	5 a	-1 a	7 a	3 a	9 a	2 a
S2: 75% ETc during variety-specific hull-split period	8 a	-2 a	8 a	4 a		
S3: 50% ETc during Nonpareil hull-split period	17 a	6 a	0 a	0 a	9 a	1 a
S4: 50% ETc during variety-specific hull-split period	10 a	3 a	9 a	6 a		
S5: 100% ETc during Nonpareil hull-split period					9 a	3 a
p-value	0.2845	0.2822	0.6976	0.7571	0.9488	0.9195

4.4. Discussion

The RDI treatments in this study resulted in minor reductions in total water applied because the hull-split period when RDI was implemented is short (between 32 and 46 days) compared to the total irrigation season for the year of approximately 240 days (March to October). For example, 50% ET_c during hull-split in Nonpareil resulted in 14-15% less total water applied than 100% ET_c in Nonpareil. RDI according to variety-specific hull-split in later splitting varieties, such as Aldrich and Butte, resulted in more total water applied than RDI according to Nonpareil-based hull-split, as shown in Table 4.2. In the Aldrich and Butte varieties, S2 (75% ET_c rate during variety-specific hull-split) resulted in the most total water applied of all the irrigation treatments in this study and more total water applied than the similar treatment S1 (75% ET_c rate during Nonpareil hull-split) due to differences in the length of the hull-split period across the varieties.

Implementing RDI in Butte during Butte hull-split resulted in lower water use efficiency due to fewer days in between 1% hull-split initiation and harvest. The Butte variety had only 35 and 32 days between 1% hull-split initiation and harvest in 2019 and 2020, respectively, whereas the Aldrich variety had 46 and 43 days and the Nonpareil variety had 44 and 37 days in 2019 and 2020, respectively, as shown in Table 4.1. A farmer may use significantly more water per weight of Butte almonds produced by implementing RDI during Butte hull-split as opposed to during Nonpareil hull-split, which is the opposite of the Almond Board of California's goal of reducing the amount of water used to produce a pound of almonds by 20% by 2025.

A reduction in the fraction of sealed shells induced by RDI during variety-specific hull-split in Butte increases exposure of the edible kernel to the environment and may have implications on kernel damage. Lower percentage of sealed shells has been correlated with a higher percentage of navel orangeworm (*Amyelois transitella*) infestation of the kernel (Hamby et al.,

2011; Hamby and Zalom, 2013). Lower percentage of navel orangeworm infestation has been correlated with later splitting varieties, such as Butte (Hamby et al., 2011). This study did not detect significant differences in insect damage to the kernel (which mostly included the occurrence of navel orangeworm and ant damage) across irrigation treatments. The orchard used in this study did not have a recent history of navel orangeworm infestation because it was sprayed with insecticide and mummy nuts were removed each winter. Further research should investigate RDI during Butte hull-split period in Butte at an almond orchard with a history of navel orangeworm infestation to quantify the effects of irrigation induced changes in the fraction of sealed shells on navel orangeworm occurrence. Further research should also investigate possible functional explanations for the reduction in sealed shells induced by RDI during variety-specific hull-split in Butte almonds.

An increase in the thickness of the kernel induced by RDI during variety-specific hull-split in Aldrich may have implications on its marketability and storage requirements. Other physical quality measurements such as kernel length and width, grams per 50 kernels, double, twin, blank, and gum did not show significant differences after two years of the RDI irrigation treatments and do not seem to be affected by the variations in RDI schedules from this study.

The marketable kernel yield data was higher than in the literature for California almond varieties, likely because most of the literature was from many years ago when almond yields were considerably lower (Goldhamer et al., 2006; Goldhamer and Fereres, 2017). Management practices of almond orchards have improved marketable kernel yield in recent years. Light interception results aligned with yield results with no significant differences across irrigation treatments. The lack of significant effect of irrigation treatments on marketable kernel yield indicates that outlying variables other than irrigation contribute to the yield response of almonds.

The soil water content and midday stem water potential responded to the various RDI treatments in each variety, as shown in Figures 4.6 and 4.7, indicating that both measurements could be used as feedback on irrigation scheduling regimes based on phenological schedules such as hull-split. The effect of soil texture was observed to affect the midday stem water potential. Further research should evaluate the coupled roles of soil properties and variety differences that may together impact the productivity of almond orchards for a more robust understanding of how to improve water use.

Implementing the intended irrigation treatments was cumbersome under the strip plot experimental design due to the involvement of 60 independently irrigated subplots that required precise amounts of irrigation water to be applied. The wireless communication system and solenoid valves were intended to ease the labor involved in independently controlling the irrigation amounts in 60 subplots in this study, but they were not reliable enough, resulting in frequent manual irrigations to keep the irrigation on track to meet the requirements of the experimental irrigation treatments. Problems that occurred included valves not opening or closing due to broken solenoids, frequent low battery voltage in the controllers, communication issues in the wireless communication system, and web server outages. Further research and development should refine the technology of remote irrigation control systems to achieve a high level of reliability for the application of irrigating by variety by row to reduce the labor and time for the farmer to implement RDI by variety.

4.5. Conclusions

Regulated deficit irrigation (RDI) during hull-split was implemented in Butte, Aldrich, and Nonpareil almond varieties with varying hull-split schedules in the same orchard and compared against RDI during Nonpareil hull-split in terms of marketable kernel yield, total water applied, water use efficiency, nut physical quality, light interception, soil water content, and midday stem water potential. RDI during Butte hull-split in Butte reduced the fraction of sealed shells compared to RDI during Nonpareil hull-split in Butte, increasing the vulnerability of the kernel to the environment and possible pests. Kernel thickness increased in the Aldrich variety when RDI was implemented during Aldrich hull-split instead of Nonpareil hull-split period. Water use efficiency decreased in the Butte variety when it was irrigated during Butte hull-split instead of Nonpareil hull-split due to fewer number of days in between the initiation of Butte hull-split and harvest compared to Nonpareil. RDI during hull-split in Aldrich, Butte, and Nonpareil varieties did not significantly decrease marketable kernel yield, showing that RDI is a promising strategy for reducing water use in almond orchards with multiple varieties while minimizing yield losses. No increase in marketable kernel yield was achieved by implementing RDI according to variety-specific hull-split compared to scheduling RDI in all three varieties according to Nonpareil hull-split. In terms of yield only, the best strategy for implementing RDI in almond orchards with multiple varieties would the least labor-intensive method of irrigating all varieties in the same orchard according to the Nonpareil variety hull-split schedule. More research is needed for different orchard designs, varieties, and climates.

Acknowledgments

Thanks to the Almond Board of California for funding this research. Thanks to Franz Niederholzer. Stan Cutter, Ubaldo Salud, and the Nickels Soil Lab crew for providing and maintaining an almond orchard to conduct this research. Thanks to Aya Suzuki, David Moyers, Jazmin Melendez, Kyle Johnson, Marcoluis Garcia, Fatemeh Mehrabi, Prudentia Gugulethu Zikalala, Jingyuan Xue, Iael Raij Hoffman, Omar Samara, Floyid Nicolas, Usama Al-Dughaishi, Julie Meyers, Yangyang Li, Mackenzie Guilliams, Jae Sung Kim, Tibin Zhang, Carson Fogg, and Matt Read for assistance with field work. Thanks to Sam Metcalf for collecting lightbar measurements and Tran Nguyen for processing the lightbar data.

4.6. Appendix

4.6.1. Cumulative water applied in 2020

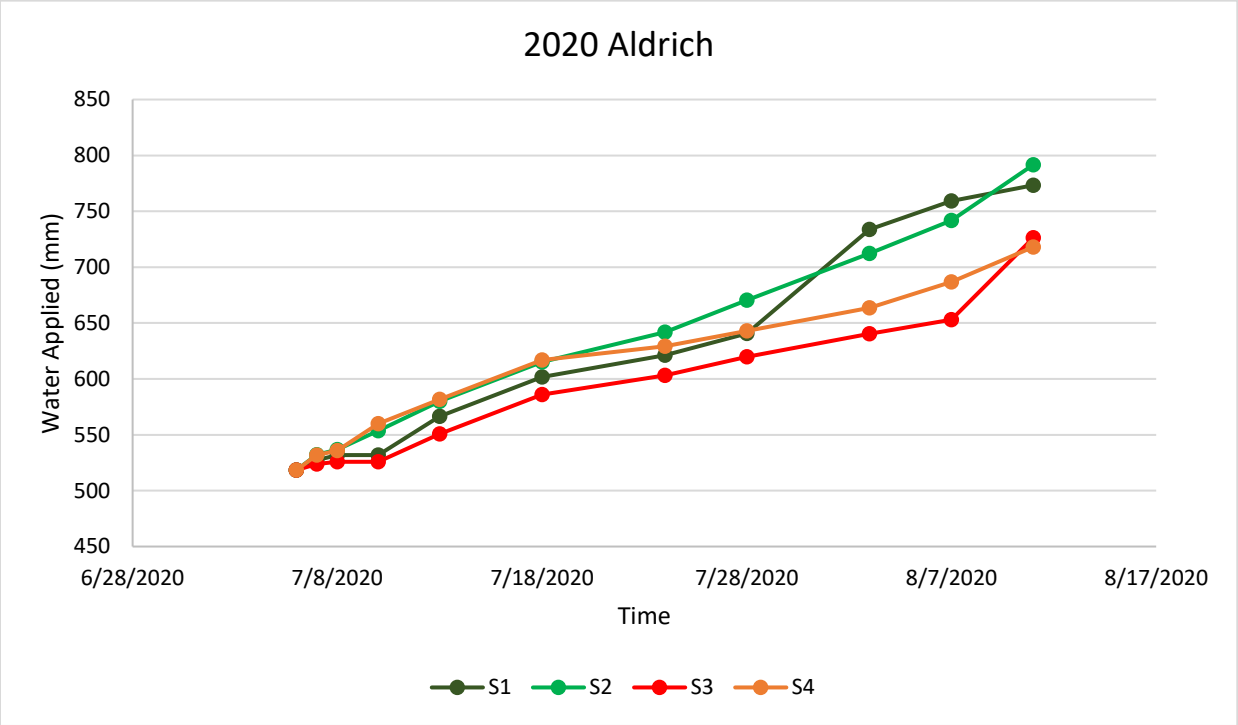

Figure 4.8. Cumulative water applied in the Aldrich variety under various irrigation regimes in 2020.

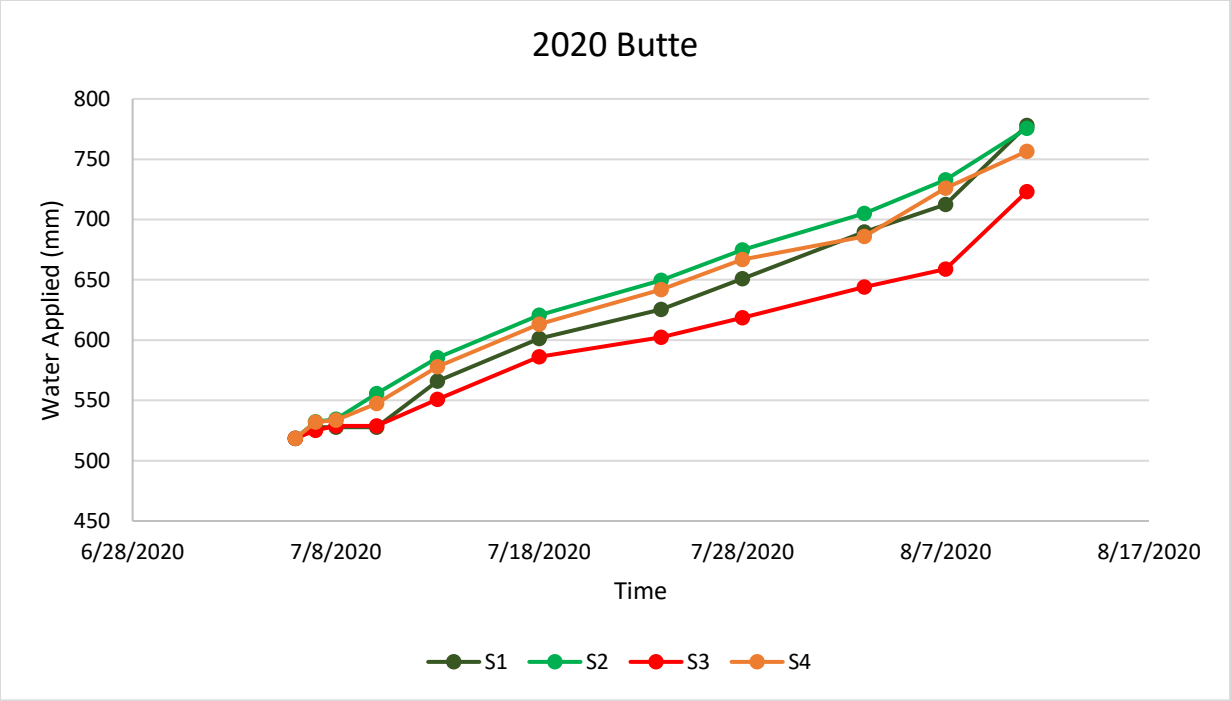

Figure 4.9. Cumulative water applied in the Butte variety under various irrigation regimes in 2020.

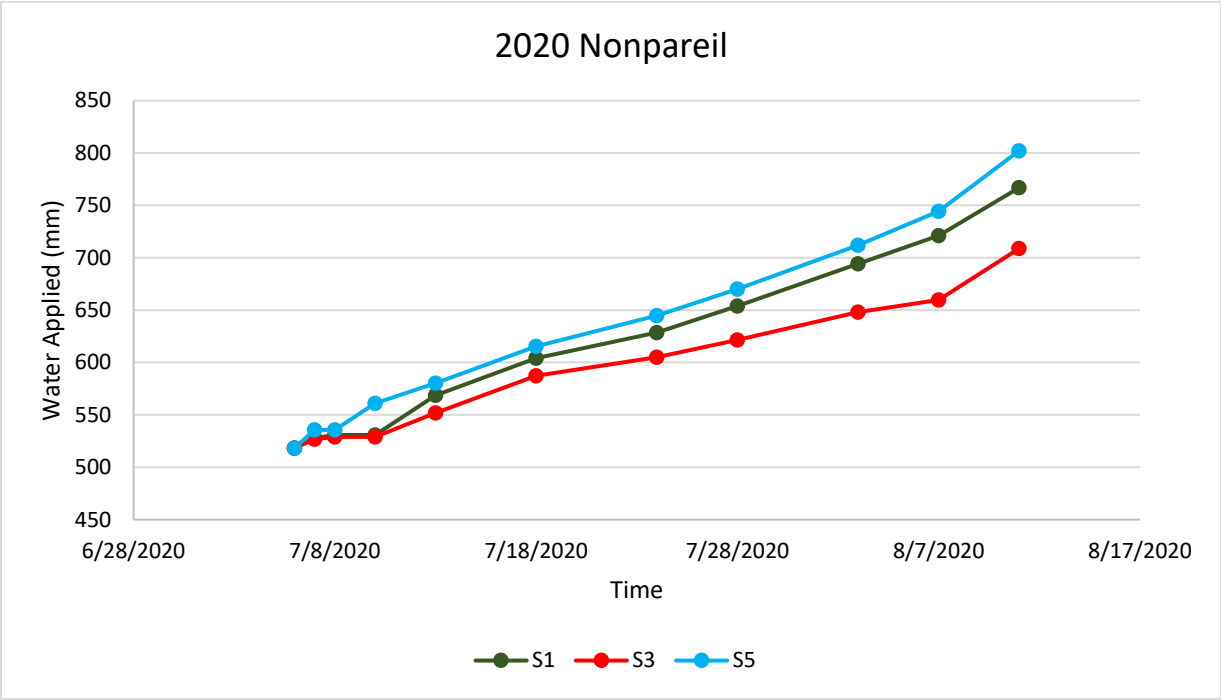

Figure 4.10. Cumulative water applied in the Nonpareil variety under various irrigation regimes in 2020.

4.6.2. Soil water content in 2020

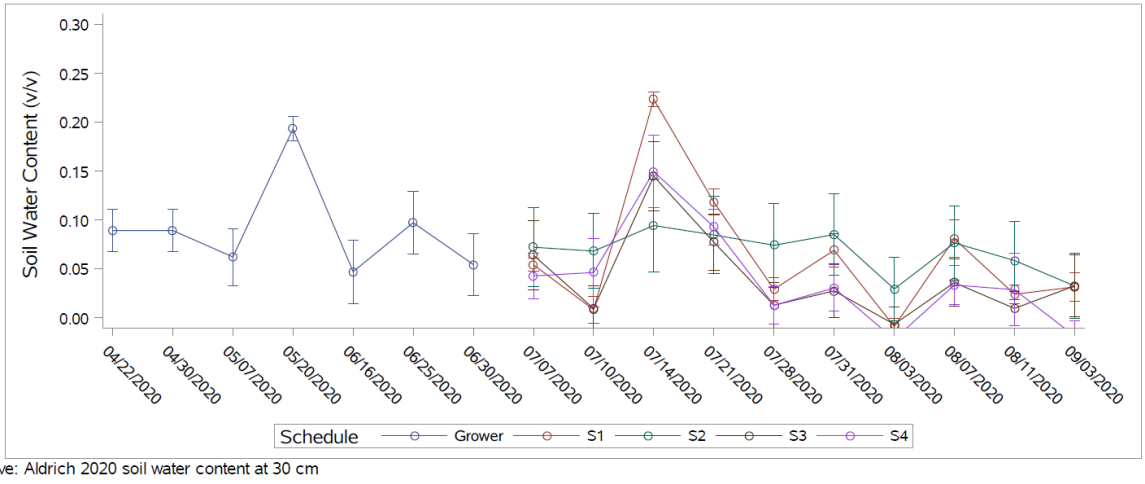

Figure 4.11. Soil water content under different irrigation schedules in the Aldrich variety in 2020. S1 = 75% ET_c during Nonpareil hull-split period. S2 = 75% ET_c during variety-specific hull-split period. S3 = 50% ET_c during Nonpareil hull-split period. S4 = 50% ET_c during variety-specific hull-split period. Error bars are standard deviations.

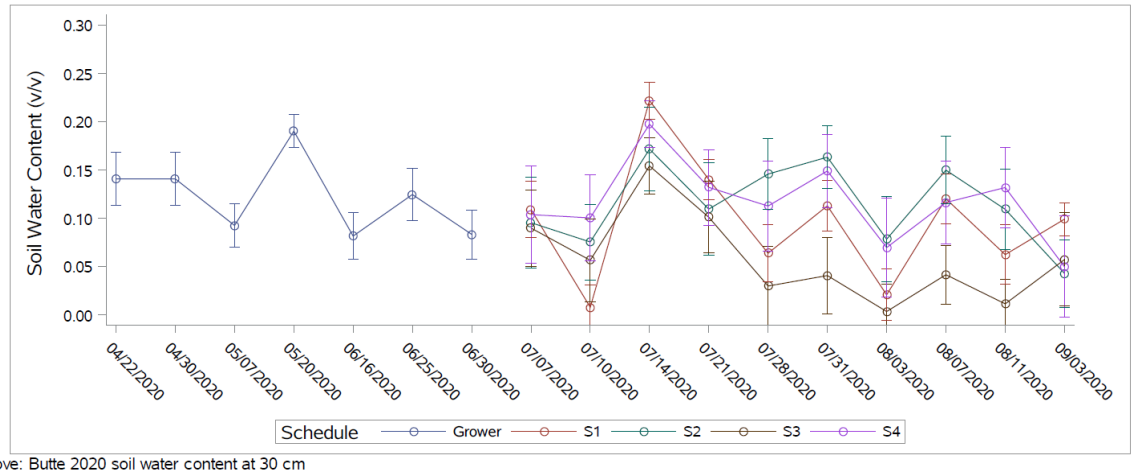

Above: Butte 2020 soil water content at 30 cm

Figure 4.12. Soil water content under different irrigation schedules in the Butte variety in 2020. S1 = 75% ET_c during Nonpareil hull-split period. S2 = 75% ET_c during variety-specific hull-split period. S3 = 50% ET_c during Nonpareil hull-split period. S4 = 50% ET_c during variety-specific hull-split period. Error bars are standard deviations.

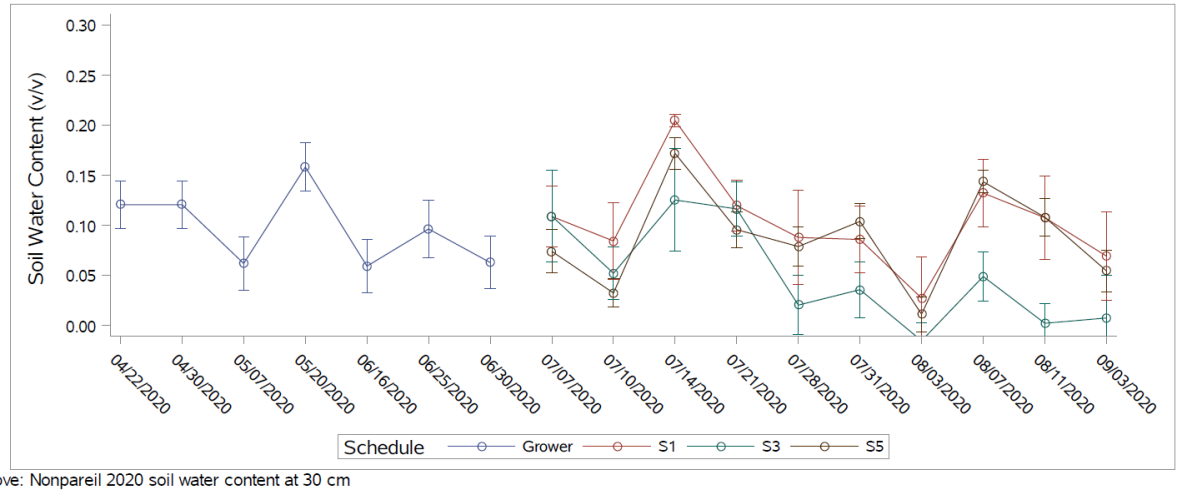

Above: Nonpareil 2020 soil water content at 30 cm

Figure 4.13. Soil water content under different irrigation schedules in the Nonpareil variety in 2020. S1 = 75% ET_c during Nonpareil hull-split period. S3 = 50% ET_c during Nonpareil hull-split period. S5 = 100% ETc during Nonpareil hull-split period. Error bars are standard deviations.

4.6.3. *Midday stem water potential in 2020*

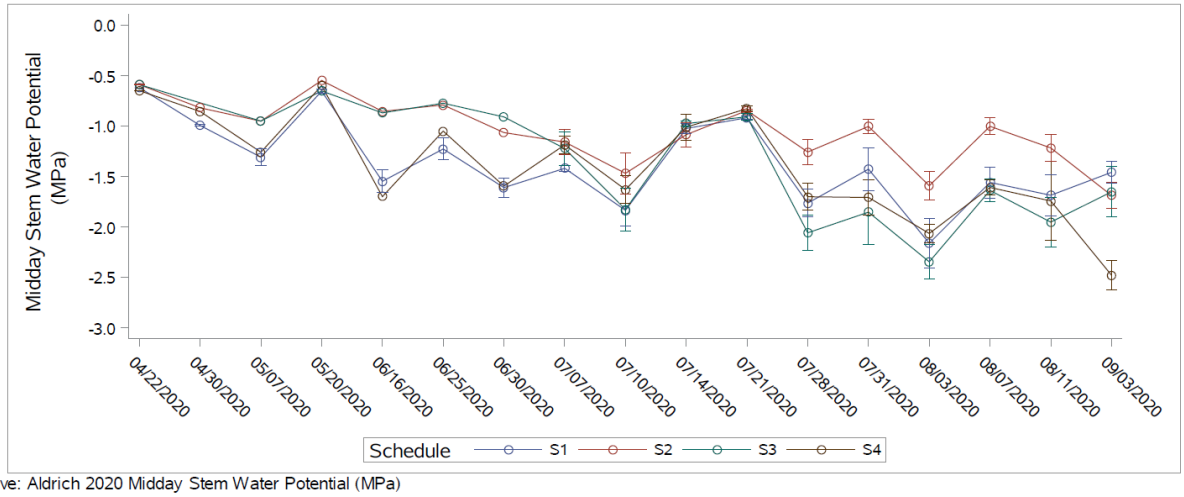

Above: Aldrich 2020 Midday Stem Water Potential (MPa)

Figure 4.14. Midday stem water potential under different irrigation schedules in the Aldrich variety in 2020. S1 = 75% ET_c during Nonpareil hull-split period. S2 = 75% ET_c during variety-specific hull-split period. S3 = 50% ET_c during Nonpareil hull-split period. S4 = 50% ET_c during variety-specific hull-split period. Error bars are standard deviations.

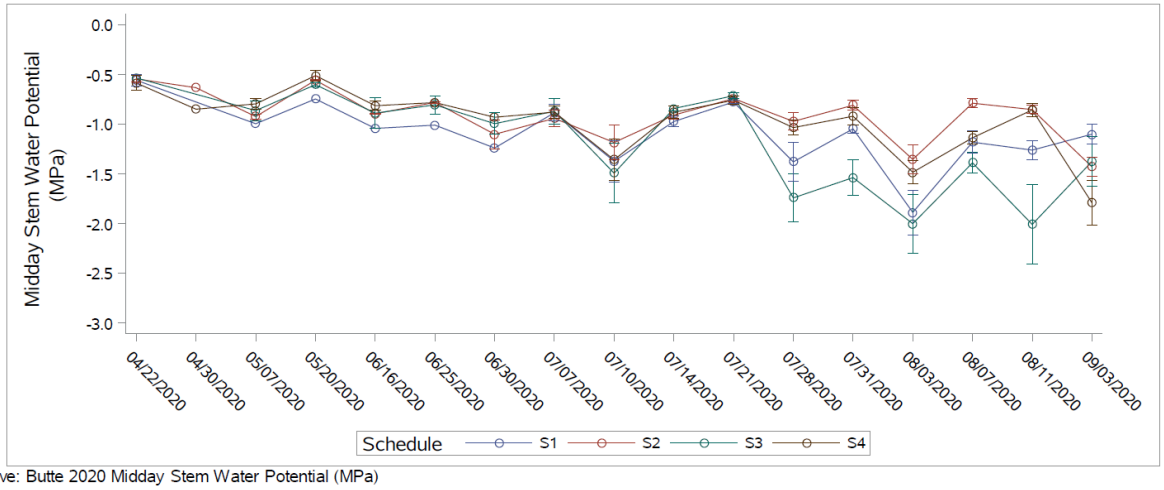

Above: Butte 2020 Midday Stem Water Potential (MPa)

Figure 4.15. Midday stem water potential under different irrigation schedules in the Butte variety in 2020. S1 = 75% ET_c during Nonpareil hull-split period. S2 = 75% ET_c during variety-specific hull-split period. S3 = 50% ET_c during Nonpareil hull-split period. S4 = 50% ET_c during variety-specific hull-split period. Error bars are standard deviations.

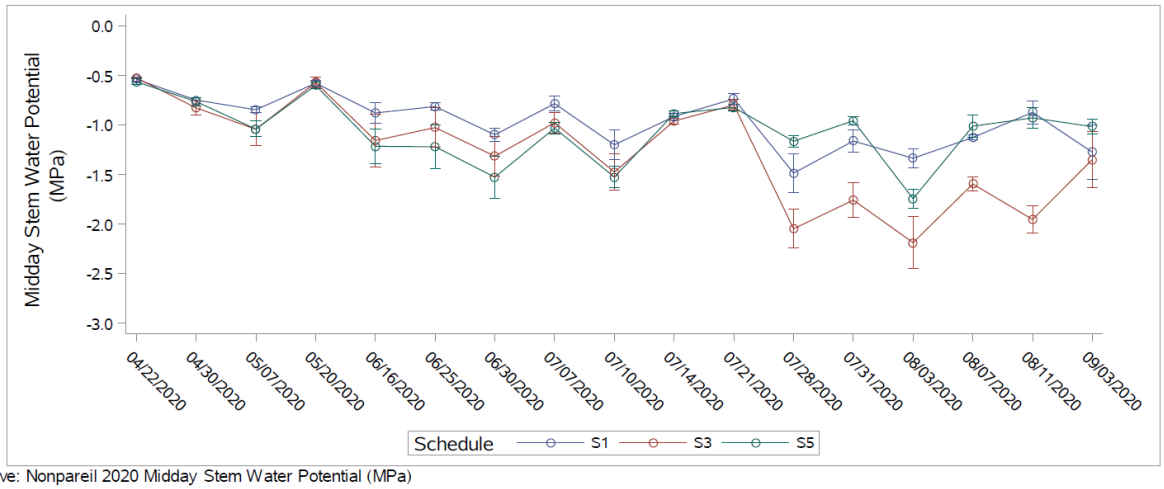

Above: Nonpareil 2020 Midday Stem Water Potential (MPa)

Figure 4.16. Midday stem water potential under different irrigation schedules in the Nonpareil variety in 2020. S1 = 75% ET_c during Nonpareil hull-split period. S2 = 75% ET_c during variety-specific hull-split period. S3 = 50% ET_c during Nonpareil hull-split period. S4 = 50% ET_c during variety-specific hull-split period. Error bars are standard deviations.

Chapter 5

Site-specific data-driven modeling of midday stem water potential in almond trees

Abstract

Midday stem water potential (MSWP) is a valuable measurement of plant water status for guiding advanced regulated deficit irrigation regimes. In almond orchards, regulated deficit irrigation during hull-split to achieve MSWP between -1.4 and -1.8 MPa has been showed to reduce water use without significantly reducing yield, so it is important for almond farmers to have access to estimates of MSWP as a guide for irrigation scheduling. The objective of this research was to develop a site-specific low-cost data-driven model to estimate MSWP using environmental data that might be available to a farmer at a five-acre almond orchard with Nonpareil, Butte, and Aldrich varieties. Available data as potential explanatory variables of MSWP include soil water content at 30 cm, 60 cm, 90 cm, 120 cm, and 150 cm, solar radiation, air temperature, relative humidity, soil texture and gravel content at four layers, and fraction of photosynthetically active radiation intercepted by the canopy. Soil water content at 30 cm was the most significant explanatory variable of MSWP and showed a nonlinear relationship with MSWP, so the square of soil water content at 30 cm was included in the model. When all varieties were combined, the best regression model included the following explanatory variables of MSWP that were significant to enter and exit the model at the 0.001 significance level: soil water content at 30 cm, the square of soil water content at 30 cm, daily minimum air temperature, daily maximum relative humidity, daily minimum relative humidity, fraction of photosynthetically active radiation, and soil texture class between 10 to 86 cm (adjusted R^2=0.66, RMSE=0.31). Separate regression models for each variety improved the correlations in the Aldrich and Butte varieties with explanatory inputs selected at the 0.05 significance level to

enter and exit the model (adjusted R^2=0.74, RMSE=0.27 and adjusted R^2=0.73, RMSE=0.28, respectively), but slightly worsened in the Nonpareil variety (R^2=0.64, RMSE=0.30). This work decompresses midday stem water potential into explanatory data that might be available to a farmer.

5.1. Introduction

The Sustainable Groundwater Management Act of California (SGMA) has called for major limitations on groundwater pumping in overdrafted basins, many of which are agriculturally important areas. This new legislation places considerable pressure on almond farmers, many of whom have traditionally relied on groundwater, to re-evaluate their irrigation management practices. Regulated deficit irrigation (RDI) at hull-split is an irrigation strategy than can decrease water use while minimally affecting yield and possibly reducing hull rot, a pathogenic disease that can result in irreversible spur and shoot mortality (Goldhamer et al., 2006; Teviotdale et al., 2001). RDI involves applying a percentage of the hypothetical crop water use of a well-watered plant of the same species during strategic growth stages that have potential for optimizing the water applied per pound of crop produced.

The best way to implement RDI is to use a pressure chamber to target specific plant water status levels during hull-split in each variety. A pressure chamber measures stem water potential, which can be thought of as the "blood pressure of the plant" and is a sensitive indicator of the plant water status (A. Fulton et al., 2017; Harold McCutchan and Shackel, 1992; Shackel et al., 2010). Table 5.1 shows an example RDI scheme driven by midday stem water potential measurements for a multi-variety almond orchard (Fulton et al., 2003):

Table 5.1: Example regulated deficit irrigation scheme guided by pressure chamber measurements in three almond varieties

Phenological Stage	Target Stem Water Potential (MPa)	Nonpareil	Aldrich	Butte
Shoot growth period	-0.6 to -0.8	Early March to late June	Mid-March to Mid-July	Late-March to late July
Just before hull-split initiation	-1.0 to -1.2	Late June to early July	Mid-July to late July	Late July to early August
Hull-split period	-1.4 to -1.8	Early July to mid-August	Late July to mid-September	Early August to late September
Post-Harvest	-0.6 to -0.8	Mid-August to late November	Mid-September to late November	Late-September to late November

Stem water potential is driven by effective gradients in water potential through the soil, roots, stems, leaves, and atmosphere (Hillel, 2004). Soil water potential will be affected by soil water content, soil texture, and gravel content. Atmospheric evaporative demand will be driven by meteorological conditions, such as solar radiation, air temperature, relative humidity, and wind speed.

The pressure chamber is the standard instrument for measuring MSWP, but it is labor-intensive and time-consuming (Jones, 2004). The pressure chamber has a sealed chamber where a leaf is inserted with the stem protruding through a rubber gasket. Pressure is increased in the chamber (often using a tank of nitrogen) until plant sap gushes out of the xylem to determine the leaf water potential (Sanden et al., 2010). Bagging shaded leaves for at least 20 minutes stops transpiration for the measurement of stem water potential (A. Fulton et al., 2017). Shaded bagged leaf water potential has been shown to be less variable due to changes in vapor pressure deficit (VPD) than unbagged leaf water potential and is more useful for irrigation scheduling (H McCutchan and Shackel, 1992). The labor-intensive nature of measuring MSWP and important of MSWP to optimizing water use efficiency in almond orchards has led to several efforts to model MSWP in almond trees. Prior research has focused on correlating leaf-temperature based

stress indices with MSWP in an attempt to develop a surrogate for the pressure chamber (Drechsler et al., 2019; Kizer et al., 2017). An artificial neural network approach attempted to model the relationship between environmental conditions and plant water status (Meyers et al., 2019). However, all those empirical modelling attempts required a specialized leaf monitoring system and were not easily transferable between fields, between seasons, or even between leaves.

Attempts to model MSWP using physics-based approaches have also been made. Van den Honert (1948) developed an Ohm's law electrical analogy of water movement through a plant that involves analyzing the water potentials and resistances along the water pathways through the plant, but this model is a steady-state oversimplification of a highly complex process of water movement through the soil-plant-atmosphere continuum. Rings et al. (2013) used a nonlinear hydrodynamic flow model to simulate unsaturated flow in the soil-tree domain to simulate stem water potential in a white fur tree with satisfactory agreement with stem water potential measurements. Correlations between volumetric soil water content in the upper 1.5 m and the difference between the observed MSWP and the baseline MSWP have been satisfactory in prune (Shackel et al., 2000).

Other efforts have focused on using artificial intelligence to estimate MSWP, but those models risk overfitting to the training data set and are often viewed as black boxes (Valdés-Vela et al., 2015). A machine learning approach to modeling MSWP in grapevine as a function of maximum and minimum air temperature, rainfall, soil texture, gravel, and slope using a gradient boosting machine yielded outstanding predicted performance (Brillante et al., 2016).

The work presented here uses data-driven modeling approaches to describe trends in midday stem water potential as a function of environmental data that might be available to an almond farmer. This environmental data includes soil water content, soil texture, gravel

content, fraction of photosynthetically active radiation intercepted by the canopy (fPAR), and air temperature and relative humidity from a local weather station, such as the California Irrigation Management Information System (CIMIS). This paper also investigates whether significant explanatory environmental variables of MSWP vary across almond varieties. The overall goal of this research is to determine what environmental data is important in developing site-specific data-driven models of MSWP in almond trees.

5.2. Materials and Method

5.2.1. Site description

The study area was a 1.6-acre almond [*Prunus dulcis*] orchard of mature cv. 'Nonpareil,' 'Aldrich,' and 'Butte' trees planted on peach rootstock (4.3 m tree spacing x 6 m row spacing) located near Arbuckle, California, United States (38.97 °N, 122.07° W). The study area was described in more detail in Drechsler and Kisekka (2021). This study area had considerable spatial variability in soil texture, as shown in Figure 5.1 and was the reason for another study that involved the creation of management zones (Kizer et al., 2017).

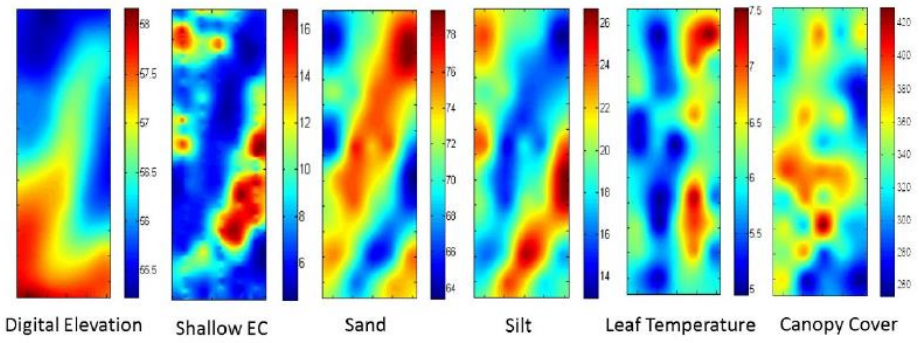

Figure 5.1. Digital elevation, shallow electrical conductivity, leaf temperature, canopy cover, and silt and sand content in the top 30 cm. Reproduced from Kizer et al. (2017).

5.2.2. Data collection

Midday stem water potential (MSWP) was measured at 60 trees using a pressure chamber (Model 615D, PMS Instruments, Albany, Oregon, USA) twice a week from June to September in 2019 and from April to September in 2020, usually immediately before an irrigation during a deficit irrigation experiment. One shaded leaf in the lower canopy of each of the 60 trees was covered with a mylar bag for at least 20 minutes prior to excision immediately (less than 30 seconds) before the pressure chamber measurement (between 12:00 and 16:00 hours). Table 5.3 shows the dates of all the MSWP measurements. Between April and May of 2020, MSWP was measured at only 8 to 19 of the 60 trees under the grower's irrigation regime prior to the deficit irrigation treatments of the experiment that started in July of 2020. In 2019, MSWP was measured during the grower's irrigation only once on 7/2/19. All the other dates in 2019 were under the deficit irrigation experiment. Figure 5.2 shows a map of the 60 locations of midday stem water potential and neutron probe measurements, denoting by black dots.

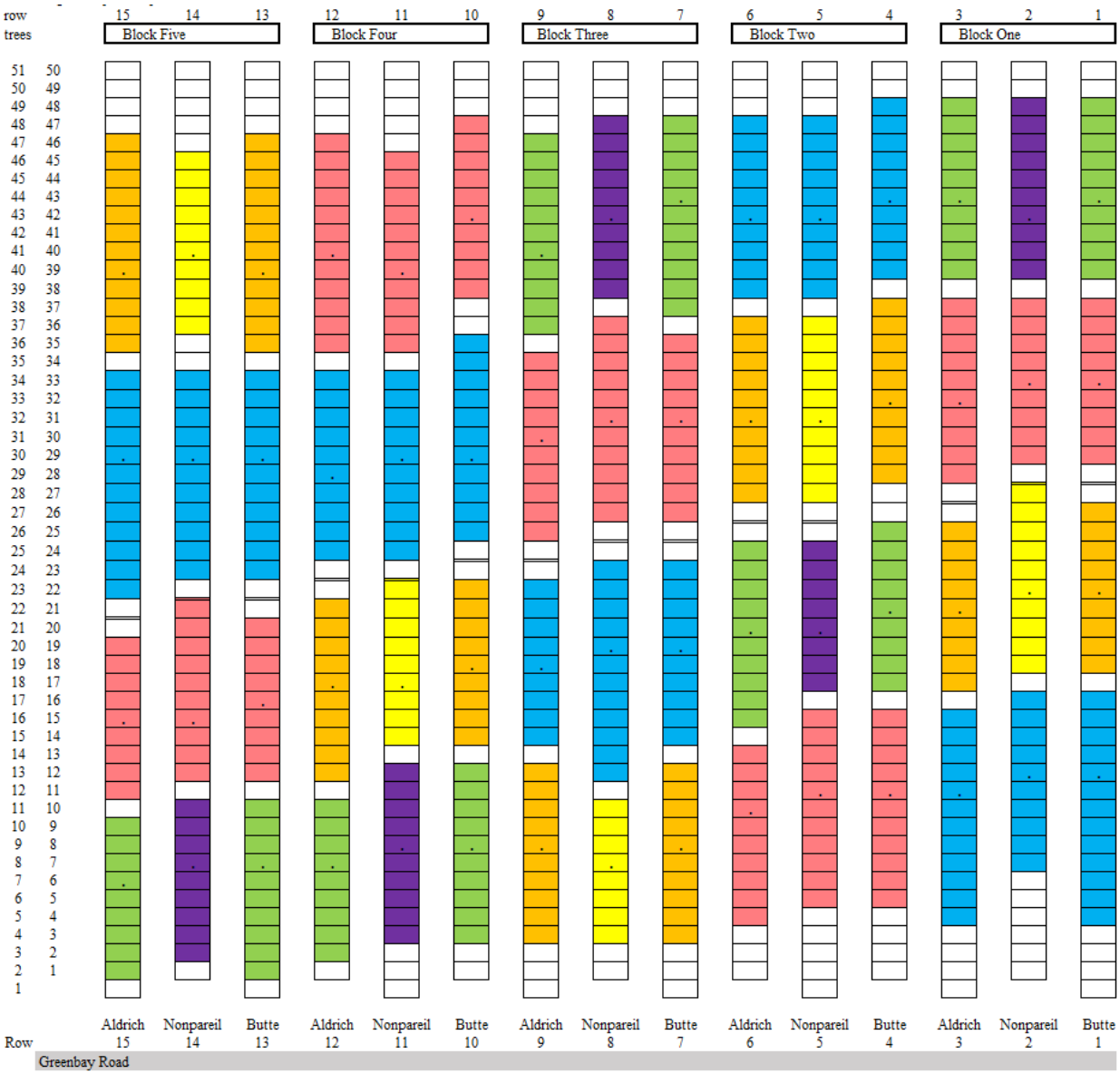

Figure 5.2. A map of the 15-row almond orchard with black dots indicating the 60 locations of the neutron probe and midday stem water potential measurements.

Neutron probe counts were measured at 30 cm, 60 cm, 90 cm, 120 cm, and 150 cm depths at 60 locations using a neutron probe (CPN 503 ELITE Hydroprobe, InstroTek, Raleigh, North Carolina, USA) at 60 locations in the orchard between April and September in 2019 and 2020 and usually immediately before irrigation. A local calibration equation was developed using volumetric soil samples taken at 30 cm and 60 cm depths from the study field in 2020 (N=11,

R^2=0.86). The neutron probe counts were converted into volumetric soil water content with the calibration equation.

Photosynthetically active radiation (PAR) intercepted by the canopy was measured at solar noon in each subplot of the experiment on June 14th and July 20th, 2019 and on June 8th and August 2nd, 2020 using a mobile PAR measurement system (Lampinen et al., 2012). The orchard was planted with alternating rows of three different varieties, so data from the left and right sides of the mobile PAR measurement system were kept separate to allow partitioning of canopy PAR interception for each variety independently.

Solar radiation (pyranometer), air temperature/relative humidity (HMP35), wind speed (anemometer), and reference evapotranspiration (Penman-Monteith equation) data were downloaded from the Williams CIMIS station. Soil texture was classified at 0-10, 10-86, 86-112, and 112-183 cm layers using the pipette method from soil cores obtained from a Geoprobe.

There were six Nonpareil trees that were intensively monitoring using affordable soil water content, soil water potential, and in-tree stem water potential sensors using the setup shown in Figure 5.3. At these six trees, soil water content was measured at 30 cm, 60 cm, and 90 cm at six locations using commercially available dielectric sensors (TEROS 10 and 12, METER Group, Pullman, WA) located approximately 1 m away from the neutron probe access tube. The neutron probe had a larger measurement volume of influence than the dielectric sensors, so the measurements were expected to possibly have different correlations with MSWP. Soil water potential was measured at 30 cm, 60 cm, and 90 cm at six locations using commercially available sensors (TEROS 21, METER Group, Pullman, WA) located approximately 10 cm away from the dielectric soil water content sensors. MSWP was also measured at these six trees in 2020 using commercially available sensors that were embedded into the tree trunk and connected to the vascular tissue (StemSense™, Saturas, Pasadena, CA and Migdal HaEemeq , Israel).

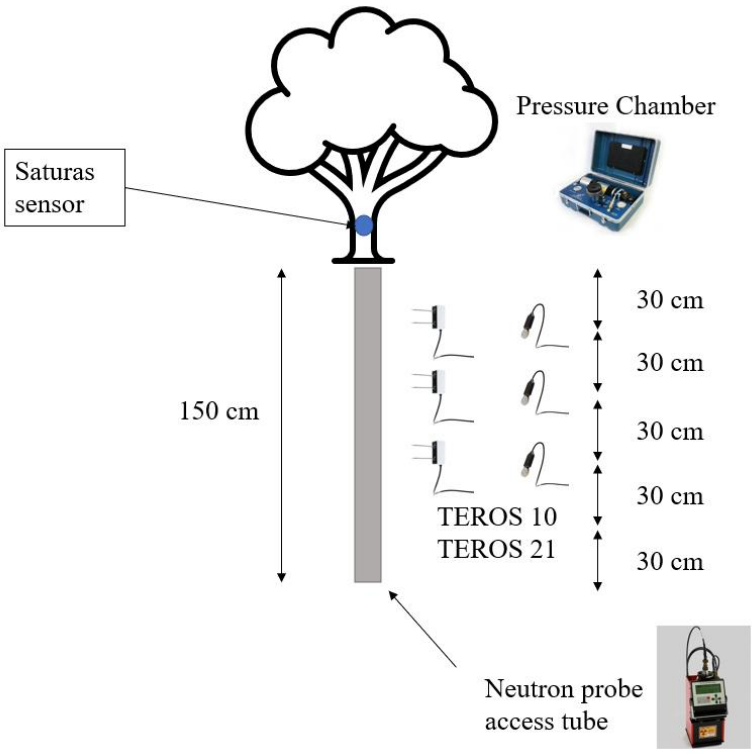

Figure 5.3. A conceptual diagram of the data collection setup in the six intensively monitored Nonpareil trees.

5.2.3. Variable input selection

Available data as possible predictor variables of midday stem water potential included: soil water content at 30 cm, 60 cm, 90 cm, 120 cm, and 150 cm measured using a neutron probe [m^3/m^3], soil water content at 30 cm, 60 cm, and 90 cm measuring using dielectric sensors [m^3/m^3], solar radiation [W/m^2], air temperature [°C], relative humidity [%], vapor pressure deficit [kPa], water potential of the air [MPa], percent sand, silt, clay, and gravel at four layers [%], and fraction of photosynthetically active radiation intercepted by the canopy (fPAR) [unitless]. The fPAR measurements can be thought of as a proxy of the canopy sizes of the various varieties in this study. The percent sand, silt, clay, and gravel at four layers were classified once during the study period and were assumed to not change during the study

period. The stepwise selection procedure in SAS was used for selecting the input variables for the multiple linear regression models. When severe multicollinearity (variance inflation factor > 10 or Pearson correlation coefficient > 0.95) was found between similar possible input variables (such as between solar radiation at solar noon and daily average solar radiation), the possible input variable with the better correlation with MSWP was used in the stepwise selection procedure. Vapor pressure deficit (VPD) and the water potential of the air (φ_a) had severe multicollinearity with air temperature and relative humidity, so only air temperature and relative humidity were used in the stepwise selection procedure. The average air temperature was severely correlated with the maximum and minimum air temperature (and similarly, relative humidity), so only minimum and maximum air temperature were used in the stepwise selection procedure. Both the significance level to enter the model (SLE) and the significance level to exit the model (SLE) in the stepwise selection procedure were tested at two different values: 0.001 (to allow fewer variables to enter the model) and 0.05 (to allow more variables to enter the model). More details about the stepwise selection procedure can be found in the SAS documentation on Proc Reg (https://documentation.sas.com/).

Table 5.2. Variable input selection for the data-driven modeling approach for estimating midday stem water potential

Type of variable	Variables
Meteorological variables	Daily minimum relative humidity Daily maximum relative humidity Daily minimum air temperature Daily maximum air temperature Daily solar radiation at solar noon
Soil water content	Soil water content at 30 cm Soil water content at 60 cm Soil water content at 90 cm Soil water content at 120 cm Soil water content at 150 cm
Canopy characteristics	Variety Fraction of photosynthetically active radiation intercepted by the canopy (fPAR)
Soil profile characteristics	Soil texture 0-10 cm (layer A) Soil texture 10-86 cm (layer B) Soil texture 86-112 cm (layer C) Soil texture 112-180 cm (layer D) Gravel content 0-10 cm (layer A) Gravel content 10-86 cm (layer B) Gravel content 86-112 cm (layer C) Gravel content 112-180 cm (layer D)

5.2.4. Model development

The regression models were developed using the Proc Reg procedure in SAS (https://documentation.sas.com/). Multiple linear regression models and nonlinear regression models were developed for each variety and for all varieties combined. An artificial neural network (ANN) was developed in MATLAB using the variables selected from the stepwise selection as input variables but correlation between predicted and measured MSWP was poor (less than R^2=0.3).

5.3. Results

5.3.1. Descriptive statistics

Table 5.3 shows the descriptive statistics of the MSWP measurements. Deficit irrigation treatments were applied on all the dates of MSWP measurements in 2019 and in July through September of 2020. The purpose of this paper was to develop a data-driven model of MSWP, so the deficit irrigation details are explained in another paper (Drechsler and Kisekka, 2021). The table shows that a wide range of MSWP values were obtained from 1233 measurements from a total of 29 different dates, making the data set suitable for data-driven modeling approaches. Figure 5.4 shows a distribution analysis of the MSWP data, indicating that there was a wide range of measurements collected.

Table 5.3. Descriptive statistics of midday stem water potential [MPa] on various dates

Analysis Variable : SWP (MPa)					
Date	Mean	Standard Deviation	Minimum	Maximum	Number of Observations
07/02/19	-1.63	0.27	-2.17	-0.80	24
07/18/19	-1.52	0.48	-2.70	-0.50	49
07/26/19	-1.32	0.41	-2.57	-0.80	51
07/30/19	-1.27	0.57	-2.88	-0.64	52
08/07/19	-1.58	0.48	-2.48	-0.74	55
08/13/19	-2.06	0.43	-2.79	-1.13	54
08/19/19	-0.97	0.17	-1.44	-0.68	59
08/21/19	-1.38	0.37	-2.23	-0.85	20
08/23/19	-1.92	0.46	-2.80	-0.93	59
08/28/19	-1.68	0.30	-2.55	-1.00	39
08/30/19	-1.37	0.32	-1.98	-0.87	20
09/08/19	-1.19	0.47	-2.64	-0.74	59
04/22/20	-0.57	0.05	-0.66	-0.50	21
04/30/20	-0.83	0.11	-1.00	-0.63	11
05/07/20	-1.01	0.21	-1.50	-0.70	24
05/20/20	-0.60	0.07	-0.75	-0.46	23
06/16/20	-1.10	0.35	-1.83	-0.61	24
06/25/20	-0.97	0.26	-1.59	-0.63	22
06/30/20	-1.25	0.31	-1.79	-0.78	22

Table 5.3 – continued

Date	Mean	Standard Deviation	Minimum	Maximum	Number of Observations
07/07/20	-1.03	0.27	-1.76	-0.58	59
07/10/20	-1.48	0.44	-2.36	-0.67	59
07/14/20	-0.95	0.15	-1.51	-0.76	59
07/21/20	-0.81	0.09	-1.02	-0.60	58
07/28/20	-1.49	0.48	-2.50	-0.76	56
07/31/20	-1.27	0.48	-2.77	-0.69	58
08/03/20	-1.83	0.43	-2.69	-0.96	38
08/07/20	-1.26	0.36	-2.10	-0.66	58
08/11/20	-1.35	0.57	-2.63	-0.67	44
09/03/20	-1.46	0.53	-2.88	-0.79	56

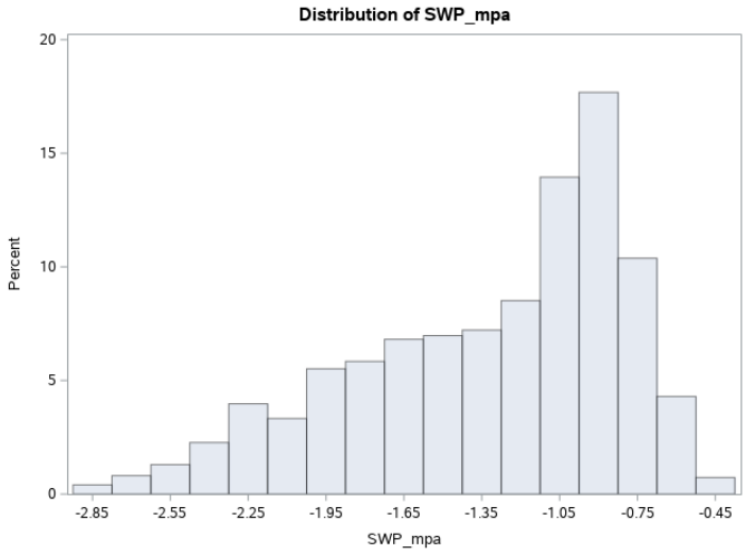

Figure 5.4. Distribution analysis of midday stem water potential.

5.3.2. Simple regression approach

There is a clear nonlinear relationship between MSWP and soil water content at 30 cm, as shown by the quadratic regression model in Figure 5.5. This model includes all the data from 2019 and 2020 from Nonpareil, Butte, and Aldrich varieties, totaling 1222 observations. As the soil water content at 30 cm increases, the MSWP increases until around 0.1 (v/v) when there is a diminishing increasing response to MSWP due to increases in soil water content at 30 cm. Although the model shows a negative relationship between MSWP and soil water content at 30 cm after around 0.2 (v/v), it makes more physical sense for the relationship to be flat, indicating no change in MSWP upon increases in soil water content at 30 cm. Low density of measurements at large soil water content at 30 cm resulted in more uncertainty in the model estimates of MSWP in that region.

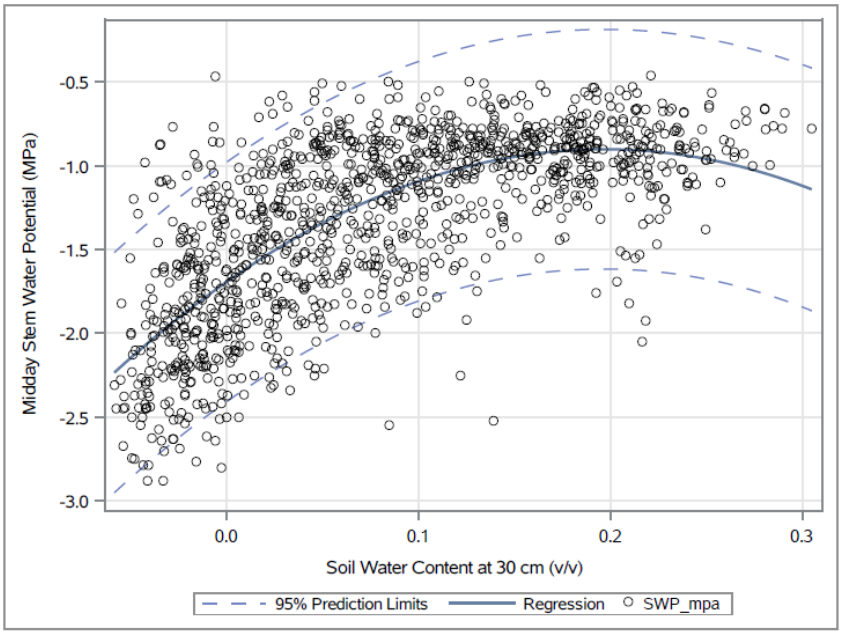

Figure 5.5. A quadratic regression model of midday stem water potential explained by soil water content measured at 30 cm below the soil surface. The dashed curves indicate the 95% prediction limits of the regression model.

Table 5.4 shows the parameter estimates from a quadratic regression model of MSWP with soil water content at 30 cm and the square of soil water content at 30 cm as explanatory variables. The adjusted R^2 was 0.5158, the RMSE was 0.36383, and the number of observations was 1222.

$$\varphi_{stem}\,[MPa] = -20.46\,[MPa] \times \theta_{30\,cm}^2 + 8.05\,[MPa] \times \theta_{30\,cm} - 1.69\,[MPa] \quad \textit{Equation 5.1}$$

where φ_{stem} is the midday stem water potential and $\theta_{30\,cm}$ is the soil water content at 30 cm.

Table 5.4. Coefficients of simple quadratic regression of midday stem water potential explained by soil water content measured at 30 cm below the soil surface.

Parameter Estimates					
Variable	DF	Parameter Estimate	Standard Error	t Value	Pr > |t|
Intercept	1	-1.69351	0.01469	-115.26	<.0001
Soil water content at 30 cm [v/v]	1	8.04888	0.31242	25.76	<.0001
Square of soil water content at 30 cm $[v/v]^2$	1	-20.45886	1.48906	-13.74	<.0001

5.3.3. Multiple linear regression of MSWP

This section shows candidate multiple linear regression models of MSWP with soil water content and meteorological data as possible explanatory variables (soil texture and gravel content as possible explanatory variables will be discussed later in this paper). All terms in these candidate models are linear. When all the available data from 2019 and 2020 were separated by variety, there were some differences in significant predictors of MSWP across the varieties. The stepwise selection procedure chose the following independent variables for the Aldrich variety: soil water content at 30 cm, daily maximum relative humidity, daily minimum relative humidity, and daily minimum air temperature. The adjusted R-square value was 0.6484, the RMSE was 0.31500, and the number of observations used in the model was 367. The

number of parameters in the selected model was 4 and the C(p) value was 10.58. Table 5.5 shows the multiple linear regression results for the Aldrich variety. Table 5.6 shows alternative multiple linear regression models involving explanatory variables that met SLE=0.05 and SLS=0.05.

Table 5.5. Multiple linear regression model of midday stem water potential in the Aldrich variety using soil water content and meteorological data

Parameter Estimates						
Variable	DF	Parameter Estimate	Standard Error	t Value	Pr > |t|	Variance Inflation
Intercept	1	2.15022	0.42286	5.08	<.0001	0
Soil water content at 30 cm [v/v]	1	4.43072	0.21200	20.90	<.0001	1.08912
Daily maximum relative humidity [%]	1	-0.03572	0.00438	-8.15	<.0001	1.55467
Daily minimum relative humidity [%]	1	0.01245	0.00249	5.00	<.0001	1.65610
Daily minimum air temperature [°C]	1	-0.07607	0.00933	-8.15	<.0001	1.29908

Table 5.6. Potential multiple linear regression models of midday stem water potential in the Aldrich variety using soil water content and meteorological data

Number in Model	R-Square	Adjusted R-Square	C(p)	MSE	Variables in Model
1	0.5596	0.5584	102.5092	0.12463	Soil water content at 30 cm [v/v]
1	0.0570	0.0544	633.6603	0.26683	Daily minimum air temperature [°C]
1	0.0392	0.0365	652.5265	0.27188	Daily maximum relative humidity [%]
2	0.5883	0.5860	74.1283	0.11681	Soil water content at 30 cm [v/v] Daily minimum air temperature [°C]
2	0.5860	0.5837	76.5809	0.11747	Soil water content at 30 cm [v/v] Daily maximum relative humidity [%]
2	0.5608	0.5584	103.1461	0.12460	Soil water content at 30 cm [v/v] Daily minimum relative humidity [%]
3	0.6282	0.6252	33.9163	0.10577	Soil water content at 30 cm [v/v] Daily maximum relative humidity [%] Daily minimum air temperature [°C]
3	0.5885	0.5850	75.9733	0.11709	Soil water content at 30 cm [v/v] Daily minimum relative humidity [%] Daily minimum air temperature [°C]
3	0.5884	0.5850	76.0370	0.11711	Soil water content at 30 cm [v/v] Daily maximum relative humidity [%] Daily minimum relative humidity [%]
4	0.6522	0.6484	10.5800	0.09923	Soil water content at 30 cm [v/v] Daily maximum relative humidity [%] Daily minimum relative humidity [%] Daily minimum air temperature [°C]

The stepwise selection procedure chose the following independent variables for the Butte variety: soil water content at 30 cm, fPAR, daily maximum relative humidity, daily minimum relative humidity, daily minimum air temperature, and daily average solar radiation. The adjusted R-square value was 0.5607, the RMSE was 0.34334, and the number of observations in the model was 383. The number of parameters in the model was 6 and the C(p) value was 17.8. Table 5.7 shows the multiple linear regression results for the Butte variety.

Table 5.8 shows alternative multiple linear regression models involving explanatory variables that met SLE=0.05 and SLS=0.05.

Table 5.7. Multiple linear regression model of midday stem water potential in the Butte variety using soil water content and meteorological data

Parameter Estimates						
Variable	DF	Parameter Estimate	Standard Error	t Value	Pr > |t|	Variance Inflation
Intercept	1	0.28546	0.53746	0.53	0.5956	0
Soil water content at 30 cm [v/v]	1	3.47550	0.21658	16.05	<.0001	1.20980
fPAR	1	0.01857	0.00260	7.13	<.0001	1.13025
Daily maximum relative humidity [%]	1	-0.03109	0.00466	-6.67	<.0001	1.61308
Daily minimum relative humidity [%]	1	0.00737	0.00262	2.81	0.0052	1.62936
Daily minimum air temperature [°C]	1	-0.07658	0.00999	-7.67	<.0001	1.31766
Daily average solar radiation [W m^{-2}]	1	0.00161	0.00049166	3.28	0.0011	1.21071

Table 5.8. Potential multiple linear regression models of midday stem water potential in the Butte variety using soil water content and meteorological data

Number in Model	R-Square	Adjusted R-Square	C(p)	MSE	Variables in Model
1	0.3611	0.3594	192.5966	0.17190	Soil water content at 30 cm [v/v]
1	0.0798	0.0774	444.1979	0.24757	Daily average solar radiation [W m^{-2}]
1	0.0777	0.0752	446.1312	0.24815	Daily maximum relative humidity [%]
2	0.4571	0.4542	108.7023	0.14645	Soil water content at 30 cm [v/v] fPAR
2	0.4191	0.4161	142.6545	0.15669	Soil water content at 30 cm [v/v] Daily maximum relative humidity [%]
2	0.4002	0.3970	159.5800	0.16180	Soil water content at 30 cm [v/v] Daily minimum air temperature [°C]
3	0.4956	0.4916	76.2393	0.13642	Soil water content at 30 cm [v/v] fPAR Daily maximum relative humidity [%]
3	0.4909	0.4868	80.4863	0.13771	Soil water content at 30 cm [v/v] fPAR Daily minimum air temperature [°C]
3	0.4824	0.4783	88.0646	0.14000	Soil water content at 30 cm [v/v] Daily maximum relative humidity [%] Daily minimum air temperature [°C]
4	0.5487	0.5439	30.7602	0.12239	Soil water content at 30 cm [v/v] fPAR Daily maximum relative humidity [%] Daily minimum air temperature [°C]
4	0.5154	0.5103	60.4902	0.13140	Soil water content at 30 cm [v/v] fPAR Daily minimum air temperature [°C] Daily average solar radiation [W m^{-2}]
4	0.4997	0.4944	74.5527	0.13567	Soil water content at 30 cm [v/v] fPAR Daily maximum relative humidity [%] Daily average solar radiation [W m^{-2}]
5	0.5585	0.5527	23.9503	0.12004	Soil water content at 30 cm [v/v] fPAR Daily maximum relative humidity [%] Daily minimum air temperature [°C] Daily average solar radiation [W m^{-2}]
5	0.5552	0.5493	26.9264	0.12094	Soil water content at 30 cm [v/v] fPAR Daily maximum relative humidity [%] Daily minimum relative humidity [%] Daily minimum air temperature [°C]

Table 5.8 – continued

Number in Model	R-Square	Adjusted R-Square	C(p)	MSE	Variables in Model
5	0.5164	0.5100	61.6344	0.13149	Soil water content at 30 cm [v/v] fPAR Daily minimum relative humidity [%] Daily minimum air temperature [°C] Daily average solar radiation [W m^{-2}]
6	0.5676	0.5607	17.8307	0.11788	Soil water content at 30 cm [v/v] fPAR Daily maximum relative humidity [%] Daily minimum relative humidity [%] Daily minimum air temperature [°C] Daily average solar radiation [W m^{-2}]

The stepwise selection procedure chose the following independent variables for the Nonpareil variety: soil water content at 30 cm and 150 cm, fPAR, daily maximum relative humidity, and daily minimum air temperature. The adjusted R-square value was 0.5465, the RMSE was 0.33851, the number of observations was 369, and the C(p) value was 13.65 (as opposed to 5 parameters in the model), indicating some bias in the best model. Table 5.9 shows the multiple linear regression results for the Nonpareil variety. Table 5.10 shows alternative multiple linear regression models involving explanatory variables that met SLE=0.05 and SLS=0.05.

Table 5.9. Multiple linear regression model of midday stem water potential in the Nonpareil variety using soil water content and meteorological data

Parameter Estimates						
Variable	DF	Parameter Estimate	Standard Error	t Value	Pr > |t|	Variance Inflation
Intercept	1	-0.21137	0.54987	-0.38	0.7009	0
Soil water content at 30 cm [v/v]	1	4.10268	0.23540	17.43	<.0001	1.22664
Soil water content at 150 cm [v/v]	1	-0.58418	0.25634	-2.28	0.0233	1.40726
fPAR	1	0.01387	0.00324	4.27	<.0001	1.32504
Daily maximum relative humidity [%]	1	-0.01425	0.00373	-3.82	0.0002	1.25906
Daily minimum air temperature [°C]	1	-0.06866	0.00907	-7.57	<.0001	1.07315

Table 5.10. Potential multiple linear regression models of midday stem water potential in the Nonpareil variety using soil water content and meteorological data

Number in Model	R-Square	Adjusted R-Square	C(p)	MSE	Variables in Model
1	0.4158	0.4142	119.0274	0.14801	Soil water content at 30 cm [v/v]
1	0.0901	0.0876	388.8970	0.23053	Daily minimum air temperature [°C]
1	0.0267	0.0240	441.4659	0.24661	Daily maximum relative humidity [%]
2	0.4738	0.4709	72.9673	0.13368	Soil water content at 30 cm [v/v] fPAR
2	0.4719	0.4691	74.5228	0.13416	Soil water content at 30 cm [v/v] Daily minimum air temperature [°C]
2	0.4338	0.4307	106.0964	0.14384	Soil water content at 30 cm [v/v] Daily maximum relative humidity [%]
3	0.5321	0.5283	26.6525	0.11919	Soil water content at 30 cm [v/v] fPAR Daily minimum air temperature [°C]
3	0.5097	0.5057	45.2459	0.12491	Soil water content at 30 cm [v/v] Daily maximum relative humidity [%] Daily minimum air temperature [°C]
3	0.4868	0.4825	64.2443	0.13075	Soil water content at 30 cm [v/v] Soil water content at 150 cm [v/v] Daily minimum air temperature [°C]
4	0.5463	0.5413	16.9546	0.11591	Soil water content at 30 cm [v/v] fPAR Daily maximum relative humidity [%] Daily minimum air temperature [°C]
4	0.5347	0.5296	26.5233	0.11886	Soil water content at 30 cm [v/v] Soil water content at 150 cm [v/v] fPAR Daily minimum air temperature [°C]
4	0.5301	0.5250	30.3069	0.12003	Soil water content at 30 cm [v/v] Soil water content at 150 cm [v/v] Daily maximum relative humidity [%] Daily minimum air temperature [°C]
5	0.5527	0.5465	13.6515	0.11459	Soil water content at 30 cm [v/v] Soil water content at 150 cm [v/v] fPAR Daily maximum relative humidity [%] Daily minimum air temperature [°C]

When all varieties were combined, the stepwise selection procedure chose the following independent variables: soil water content at 30, 60, and 90 cm, fPAR, daily minimum and maximum relative humidity, and daily minimum and maximum air temperature. The adjusted R-square value was 0.5839, the RMSE was 0.33825, the number of observations was 1119, and C(p) was 10.6. Table 5.11 shows the multiple linear regression results for all varieties combined. This model had the least bias of all the possible models with all or some of the selected input variables, so therefore it was the best model. Table 5.12 shows alternative multiple linear regression models involving explanatory variables that met SLE=0.05 and SLS=0.05. The soil water content data in this table were from the neutron probe. Soil water content at 30 cm had the best correlation with MSWP [adjusted R^2 of 0.4375], followed by soil water content at 60 cm [adjusted R^2 of 0.2325] and then by soil water content at 90 cm [adjusted R^2 of 0.0801]. This result suggests that measurements of soil water content at 30 cm could be useful to farmers in attempting to target specific MSWP values during certain growth stages. Improvements in correlation were achieved by including both fPAR, daily minimum and maximum air temperature, and daily minimum and maximum relative humidity. The addition of fPAR helps to factor in variety differences in canopy size that may affect MSWP. This result says that a farmer should install a soil water content at 30 cm, 60 cm, and 90 cm and have a relative humidity and air temperature sensor (or access to a nearby weather station with those sensors) for the best correlations with MSWP.

Table 5.11. Multiple linear regression model of midday stem water potential of all varieties combined using soil water content and meteorological data

Parameter Estimates						
Variable	DF	Parameter Estimate	Standard Error	t Value	Pr > |t|	Variance Inflation
Intercept	1	0.64322	0.29409	2.19	0.0289	0
Soil water content at 30 cm [v/v]	1	3.84713	0.18178	21.16	<.0001	2.34826
Soil water content at 60 cm [v/v]	1	0.42332	0.18107	2.34	0.0196	3.49750
Soil water content at 90 cm [v/v]	1	-0.46304	0.15566	-2.97	0.0030	2.30055
fPAR	1	0.01336	0.00139	9.60	<.0001	1.12809
Daily maximum relative humidity [%]	1	-0.03159	0.00290	-10.91	<.0001	1.99174
Daily minimum relative humidity [%]	1	0.01239	0.00214	5.79	<.0001	3.32550
Daily maximum air temperature [°C]	1	0.01580	0.00636	2.49	0.0131	2.82155
Daily minimum air temperature [°C]	1	-0.08918	0.00829	-10.76	<.0001	2.74022

Table 5.12. Potential multiple linear regression models of midday stem water potential using soil water content and meteorological data

Number in Model	R-Square	Adjusted R-Square	C(p)	MSE	Variables in Model
1	0.4380	0.4375	397.2091	0.15467	Soil water content at 30 cm [v/v]
1	0.2331	0.2325	948.4354	0.21104	Soil water content at 60 cm [v/v]
1	0.0809	0.0801	1358.022	0.25293	Soil water content at 90 cm [v/v]
2	0.5006	0.4997	230.6563	0.13755	Soil water content at 30 cm [v/v] fPAR
2	0.4811	0.4802	283.1416	0.14292	Soil water content at 30 cm [v/v] Daily minimum air temperature [°C]
2	0.4674	0.4665	320.0425	0.14670	Soil water content at 30 cm [v/v] Daily maximum relative humidity [%]
3	0.5371	0.5359	134.4849	0.12761	Soil water content at 30 cm [v/v] fPAR Daily minimum air temperature [°C]
3	0.5298	0.5285	154.1797	0.12963	Soil water content at 30 cm [v/v] Daily maximum relative humidity [%] Daily minimum air temperature [°C]
3	0.5176	0.5163	187.1118	0.13301	Soil water content at 30 cm [v/v] fPAR Daily maximum relative humidity [%]
4	0.5689	0.5674	50.8934	0.11895	Soil water content at 30 cm [v/v] fPAR Daily maximum relative humidity [%] Daily minimum air temperature [°C]
4	0.5396	0.5380	129.8087	0.12704	Soil water content at 30 cm [v/v] Daily maximum relative humidity [%] Daily minimum relative humidity [%] Daily minimum air temperature [°C]
4	0.5384	0.5367	133.1639	0.12739	Soil water content at 30 cm [v/v] Soil water content at 90 cm [v/v] fPAR Daily minimum air temperature [°C]
5	0.5811	0.5792	20.2303	0.11570	Soil water content at 30 cm [v/v] fPAR Daily maximum relative humidity [%] Daily minimum relative humidity [%] Daily minimum air temperature [°C]

Table 5.12 – continued

Number in Model	R-Square	Adjusted R-Square	C(p)	MSE	Variables in Model
5	0.5709	0.5690	47.5952	0.11851	Soil water content at 30 cm [v/v] Soil water content at 90 cm [v/v] fPAR Daily maximum relative humidity [%] Daily minimum air temperature [°C]
5	0.5709	0.5690	47.6294	0.11852	Soil water content at 30 cm [v/v] fPAR Daily maximum relative humidity [%] Daily maximum air temperature [°C] Daily minimum air temperature [°C]
6	0.5834	0.5811	15.9856	0.11517	Soil water content at 30 cm [v/v] fPAR Daily maximum relative humidity [%] Daily minimum relative humidity [%] Daily maximum air temperature [°C] Daily minimum air temperature [°C]
6	0.5823	0.5800	19.0270	0.11548	Soil water content at 30 cm [v/v] Soil water content at 90 cm [v/v] fPAR Daily maximum relative humidity [%] Daily minimum relative humidity [%] Daily minimum air temperature [°C]
6	0.5814	0.5791	21.3681	0.11572	Soil water content at 30 cm [v/v] Soil water content at 60 cm [v/v] fPAR Daily maximum relative humidity [%] Daily minimum relative humidity [%] Daily minimum air temperature [°C]
7	0.5848	0.5822	14.0995	0.11487	Soil water content at 30 cm [v/v] Soil water content at 90 cm [v/v] fPAR Daily maximum relative humidity [%] Daily minimum relative humidity [%] Daily maximum air temperature [°C] Daily minimum air temperature [°C]
7	0.5846	0.5820	14.8125	0.11494	Soil water content at 30 cm [v/v] Soil water content at 60 cm [v/v] Soil water content at 90 cm [v/v] fPAR Daily maximum relative humidity [%] Daily minimum relative humidity [%] Daily minimum air temperature [°C]

Table 5.12 – continued

Number in Model	R-Square	Adjusted R-Square	C(p)	MSE	Variables in Model
7	0.5836	0.5810	17.4867	0.11522	Soil water content at 30 cm [v/v] Soil water content at 60 cm [v/v] fPAR Daily maximum relative humidity [%] Daily minimum relative humidity [%] Daily maximum air temperature [°C] Daily minimum air temperature [°C]
8	0.5869	0.5839	10.6256	0.11441	Soil water content at 30 cm [v/v] Soil water content at 60 cm [v/v] Soil water content at 90 cm [v/v] fPAR Daily maximum relative humidity [%] Daily minimum relative humidity [%] Daily maximum air temperature [°C] Daily minimum air temperature [°C]

5.3.4. *Nonlinear regression of MSWP*

The simple nonlinear regression between MSWP and soil water content at 30 cm shown in Figure 5.5 that there is a nonlinear relationship between MSWP and soil water content at 30 cm. Therefore, the square of soil water content at 30 cm was tried as a possible explanatory variable in various nonlinear regression models of MSWP in addition to linear soil water content terms at various depths and linear meteorological terms. Because both soil water content at 30 cm and the square of soil water content at 30 cm were included in the model, the multicollinearity increased but the variance inflation factor was still less than 10 for all input variables, which was acceptable. A significance level to enter and exit the model was 0.001 (stricter than the previously used 0.05 to avoid too many predictor variables). The square of soil water content at 30 cm satisfied the SLE=0.001 and SLS=0.001 required in all varieties and in the "all varieties" model. The addition of the square of soil water content at 30 cm increased the

adjusted R^2 to 0.6338 in the selected "all varieties" model, 0.6902 in the selected Aldrich model, 0.6221 in the selected Butte model, and 0.5838 in the selected Nonpareil model. Tables 5.13 to 5.16 show the parameter estimates for the selected models for "all varieties", Aldrich, Butte, and Nonpareil. Table 5.17 shows detailed statistics about each of the selected models.

Table 5.13: Nonlinear regression of MSWP with all varieties combined using soil water content and meteorological data

Parameter Estimates						
Variable	DF	Parameter Estimate	Standard Error	t Value	Pr > |t|	Variance Inflation
Intercept	1	0.40989	0.26963	1.52	0.1287	0
Soil water content at 30 cm [v/v]	1	7.32367	0.28767	25.46	<.0001	6.68160
Square of the soil water content at 30 cm [v/v]	1	-17.47298	1.35248	-12.92	<.0001	6.53958
fPAR	1	0.01354	0.00127	10.66	<.0001	1.06861
Daily maximum relative humidity [%]	1	-0.02550	0.00247	-10.31	<.0001	1.65200
Daily minimum relative humidity [%]	1	0.00757	0.00142	5.34	<.0001	1.65621
Daily minimum air temperature [°C]	1	-0.06753	0.00533	-12.68	<.0001	1.28617

Table 5.14. Nonlinear regression of MSWP in the Aldrich variety using soil water content and meteorological data

Parameter Estimates						
Variable	DF	Parameter Estimate	Standard Error	t Value	Pr > |t|	Variance Inflation
Intercept	1	1.87359	0.39885	4.70	<.0001	0
Soil water content at 30 cm [v/v]	1	7.58681	0.48925	15.51	<.0001	6.58308
Square of the soil water content at 30 cm [v/v]	1	-17.63613	2.49752	-7.06	<.0001	6.38791
Daily maximum relative humidity [%]	1	-0.03335	0.00413	-8.08	<.0001	1.56504
Daily minimum relative humidity [%]	1	0.01151	0.00234	4.91	<.0001	1.66140
Daily minimum air temperature [°C]	1	-0.07083	0.00879	-8.06	<.0001	1.30842

Table 5.15. Nonlinear regression of MSWP in the Butte variety using soil water content and meteorological data

Parameter Estimates						
Variable	DF	Parameter Estimate	Standard Error	t Value	Pr > |t|	Variance Inflation
Intercept	1	-0.78840	0.47890	-1.65	0.1005	0
Soil water content at 30 cm [v/v]	1	7.42871	0.49830	14.91	<.0001	7.44518
Square of the soil water content at 30 cm [v/v]	1	-17.72218	2.11353	-8.39	<.0001	7.39130
fPAR	1	0.01784	0.00242	7.38	<.0001	1.13192
Daily maximum relative humidity [%]	1	-0.01958	0.00369	-5.31	<.0001	1.17368
Daily minimum air temperature [°C]	1	-0.05949	0.00840	-7.08	<.0001	1.08231
Daily average solar radiation [W m^{-2}]	1	0.00175	0.00045336	3.87	0.0001	1.19684

Table 5.16. Nonlinear regression of MSWP in the Nonpareil variety using soil water content and meteorological data

Parameter Estimates						
Variable	DF	Parameter Estimate	Standard Error	t Value	Pr > |t|	Variance Inflation
Intercept	1	-2.15109	0.24332	-8.84	<.0001	0
Soil water content at 30 cm [v/v]	1	7.30067	0.51292	14.23	<.0001	6.34523
Square of the soil water content at 30 cm [v/v]	1	-18.62090	2.64286	-7.05	<.0001	6.33524
fPAR	1	0.01880	0.00274	6.86	<.0001	1.02952
Daily minimum air temperature [°C]	1	-0.05730	0.00844	-6.79	<.0001	1.01341

Table 5.17: Detailed statistics of nonlinear regression of MSWP with SLE=0.001 and SLS=0.001

Variety	Selected Inputs	Output	Adjusted R^2	RMSE	C(p)	Number in the model
All varieties	Soil water content at 30 cm (Soil water content at 30 cm)^2 fPAR Daily maximum relative humidity Daily minimum relative humidity Daily minimum air temperature	MSWP	0.6338	0.31732	29.2	6
Aldrich	Soil water content at 30 cm (Soil water content at 30 cm)^2 Daily maximum relative humidity Daily minimum relative humidity Daily minimum air temperature	MSWP	0.6902	0.29568	11.4	5
Butte	Soil water content at 30 cm (Soil water content at 30 cm)^2 fPAR Daily maximum relative humidity Daily minimum air temperature Daily average solar radiation	MSWP	0.6221	0.31843	29.0	6
Nonpareil	Soil water content at 30 cm (Soil water content at 30 cm)^2 fPAR Daily minimum air temperature	MSWP	0.5838	0.32430	26.0	4

5.3.5. Soil texture and gravel as possible explanatory variables of MSWP

This section demonstrates how the nonlinear regression models can considerably improve when soil texture and gravel class are allowed as possible explanatory variables of MSWP. Soil texture and gravel content class at four layers were included as possible explanatory variables with (1) a strict SLS=0.001 and SLE=0.001 (Table 5.18), and (2) then later with a more flexible SLS=0.05 and SLS=0.05 (Table 5.23). Soil texture at layer B was significant in the "all varieties" model with SLS=0.001 and SLE=0.001. Soil texture at layer A was significant in the Butte model with SLS=0.001 and SLE=0.001. Soil texture at layer C was significant in the Aldrich model with SLS=0.001 and SLE=0.001. No soil texture layer was significant in the Nonpareil model with SLS=0.001 and SLE=0.001. None of the gravel class layers were significant in any of the varieties with SLS=0.001 and SLE=0.001. A variety class was tested in the "all varieties" model but was not significant with SLS=0.001 and SLE=0.001.

Table 5.18. Detailed statistics of nonlinear regression model with soil texture and gravel as possible predictors of MSWP with SLE=0.001 and SLS=0.001

Variety	Selected Inputs	Output	Adjusted R^2	RMSE	C(p)	Number in the model	Number of Observations
All varieties	Soil water content at 30 cm (Soil water content at 30 cm)^2 fPAR Daily maximum relative humidity Daily minimum relative humidity Daily minimum air temperature Soil texture at layer B	MSWP	0.6559	0.30732	44.44	7	834
Aldrich	Soil water content at 30 cm (Soil water content at 30 cm)^2 Daily maximum relative humidity Daily minimum relative humidity Daily minimum air temperature Soil class at layer C	MSWP	0.6958	0.2888	55.86	6	291

Table 5.18 – continued

Variety	Selected Inputs	Output	Adjusted R^2	RMSE	C(p)	Number in the model	Number of Observations
Butte	Soil water content at 30 cm (Soil water content at 30 cm)^2 fPAR Daily maximum relative humidity Daily minimum air temperature Soil class at layer A	MSWP	0.6821	0.30195	60.26	6	272
Nonpareil	Soil water content at 30 cm (Soil water content at 30 cm)^2 fPAR Daily minimum air temperature	MSWP	0.6191	0.30709	27.00	4	271

Table 5.19. Parameter estimates of nonlinear regression model with soil texture and gravel with all varieties combined (SLE, SLS = 0.001)

All Varieties: Parameter Estimates						
Variable	DF	Parameter Estimate	Standard Error	t Value	Pr > |t|	Variance Inflation
Intercept	1	0.61933	0.30178	2.05	0.0405	0
Soil water content at 30 cm [v/v]	1	7.39825	0.33227	22.27	<.0001	6.56596
Square of the soil water content at 30 cm [v/v]	1	-16.69394	1.61148	-10.36	<.0001	6.34504
fPAR	1	0.01228	0.00159	7.72	<.0001	1.04867
Daily maximum relative humidity [%]	1	-0.02530	0.00276	-9.18	<.0001	1.68110
Daily minimum relative humidity [%]	1	0.00669	0.00160	4.17	<.0001	1.70383
Daily minimum air temperature [°C]	1	-0.06685	0.00596	-11.22	<.0001	1.29282
Soil class B	1	-0.04197	0.00895	-4.69	<.0001	1.08758

Table 5.20. Parameter estimates of nonlinear regression model with soil texture and gravel in Aldrich (SLE, SLS = 0.001)

Aldrich: Parameter Estimates						
Variable	DF	Parameter Estimate	Standard Error	t Value	Pr > |t|	Variance Inflation
Intercept	1	1.81008	0.43743	4.14	<.0001	0
Soil water content at 30 cm [v/v]	1	7.65952	0.58006	13.20	<.0001	7.88344
Square of the soil water content at 30 cm [v/v]	1	-17.70306	2.81251	-6.29	<.0001	7.53385
Daily maximum relative humidity [%]	1	-0.03058	0.00451	-6.78	<.0001	1.61236
Daily minimum relative humidity [%]	1	0.01267	0.00257	4.93	<.0001	1.68550
Daily minimum air temperature [°C]	1	-0.07596	0.00977	-7.77	<.0001	1.32941
Soil class C	1	-0.04040	0.00953	-4.24	<.0001	1.06035

Table 5.21. Parameter estimates of nonlinear regression model with soil texture and gravel in Butte (SLE, SLS = 0.001)

Butte: Parameter Estimates						
Variable	DF	Parameter Estimate	Standard Error	t Value	Pr > |t|	Variance Inflation
Intercept	1	0.62047	0.51855	1.20	0.2326	0
Soil water content at 30 cm [v/v]	1	8.84883	0.59172	14.95	<.0001	7.51092
Square of the soil water content at 30 cm [v/v]	1	-19.66814	2.56711	-7.66	<.0001	6.70706
fPAR	1	0.01872	0.00371	5.05	<.0001	1.14090
Daily maximum relative humidity [%]	1	-0.02511	0.00374	-6.71	<.0001	1.07561
Daily minimum air temperature [°C]	1	-0.05428	0.00915	-5.93	<.0001	1.05090
Soil class A	1	-0.23063	0.04116	-5.60	<.0001	1.22413

Table 5.22. Parameter estimates of nonlinear regression model with soil texture and gravel in Nonpareil (SLE, SLS = 0.001)

Parameter Estimates						
Variable	DF	Parameter Estimate	Standard Error	t Value	Pr > |t|	Variance Inflation
Intercept	1	-2.15268	0.26920	-8.00	<.0001	0
Soil water content at 30 cm [v/v]	1	7.77683	0.56534	13.76	<.0001	5.60227
Square of the soil water content at 30 cm [v/v]	1	-22.19709	3.05809	-7.26	<.0001	5.56068
fPAR	1	0.01849	0.00304	6.08	<.0001	1.00130
Daily minimum air temperature [°C]	1	-0.05551	0.00933	-5.95	<.0001	1.02505

Table 5.23 shows another version of the nonlinear regression model with soil texture and gravel as additional explanatory variables with a less strict SLE=0.05 and SLS=0.05. As opposed to the previous nonlinear regression model that had SLE=0.001 and SLS=0.001, the significance levels for possible explanatory variables to enter and exit the next model were less strict. Therefore, more explanatory variables entered and stayed in the model and the adjusted R^2 improved. The "all varieties" model included soil water content at 120 cm, daily maximum air

temperature, daily average solar radiation, soil texture at layer C, and gravel content at layer B, in addition to the same explanatory variables in the previous model (soil water content at 30 cm, the square of soil water content at 30 cm, fPAR, daily maximum relative humidity, daily minimum relative humidity, daily minimum air temperature, and soil texture at layer B). The adjusted R^2 increased to 0.67 and RMSE decreased to 0.30193.

The variety-specific models also improved with the addition of new explanatory variables when the SLE and SLS were increased to 0.05. In the Aldrich model, soil water content at 120 cm, soil class at layer A, soil class at layer D, gravel class at layer A, and gravel class at layer D, entered and stayed in the model at SLE and SLS of 0.05 (in addition to the same explanatory variables in the previous model: soil water content at 30 cm, the square of soil water content at 30 cm, daily maximum relative humidity, daily minimum relative humidity, daily minimum air temperature, and soil texture at layer C). The adjusted R^2 increased to 0.74 and RMSE decreased to 0.27, which were considered very good. In the Butte model, soil water content at 60 cm and 120 cm and soil class at layers B and C entered and stayed in the model at SLE and SLS of 0.05 (in addition to the same explanatory variables in the previous model: soil water content at 30 cm, the square of soil water content at 30 cm, fPAR, daily maximum relative humidity, daily minimum air temperature, and soil class at layer A). The adjusted R^2 increased to 0.73 and the RMSE decreased to 0.28, which were considered very good. In the Nonpareil model, daily maximum relative humidity and gravel class at layer B entered and stayed in the model at SLE and SLS of 0.05 (in addition to the same explanatory variables in the previous model: soil water content at 30 cm, the square of soil water content at 30 cm, fPAR, and daily minimum air temperature). The adjusted R^2 increased to 0.64 and the RMSE decreased to 0.30, which were considered satisfactory. Tables 5.24 to 5.27 show the parameter estimates for the models. The Butte model did have some multicollinearity in the soil water content at 30 cm

(VIF=10.95), evidently due to the correlation with the square of the soil water content at 30 cm (VIF=7.2) and soil water content at 60 cm (VIF=7.6). Figure 5.6 shows graphs of the predicted MSWP versus the measured MSWP for the Aldrich, Butte, Nonpareil, and "all varieties" models.

Table 5.23. Detailed statistics of nonlinear regression model with soil texture and gravel as possible predictors of MSWP with SLE=0.05 and SLS=0.05

Variety	Selected Inputs	Output	Adjusted R^2	RMSE	C(p)	Number of parameters in the model	Number of Observations
All varieties	Soil water content at 30 cm (Soil water content at 30 cm)^2 Soil water content at 120 cm fPAR Daily maximum relative humidity Daily minimum relative humidity Daily maximum air temperature Daily minimum air temperature Daily average solar radiation Soil texture at layer B Soil texture at layer C Gravel content at layer B	MSWP	0.6678	0.30193	19.4	12	834

Table 5.23 – continued

Variety	Selected Inputs	Output	Adjusted R^2	RMSE	C(p)	Number of parameters in the model	Number of Observations
Aldrich	Soil water content at 30 cm (Soil water content at 30 cm)^2 Soil water content at 120 cm Daily maximum relative humidity Daily minimum relative humidity Daily minimum air temperature Soil class at layer A Soil class at layer C Soil class at layer D Gravel class at layer A Gravel class at layer D	MSWP	0.7409	0.26650	11.46	11	291

Table 5.23 – continued

Variety	Selected Inputs	Output	Adjusted R^2	RMSE	C(p)	Number of parameters	Number of Observations
Butte	Soil water content at 30 cm (Soil water content at 30 cm)^2 Soil water content at 60 cm Soil water content at 120 cm fPAR Daily maximum relative humidity Daily minimum air temperature Soil class at layer A Soil class at layer B Soil class at layer C	MSWP	0.7260	0.28035	20.22	10	272
Nonpareil	Soil water content at 30 cm (Soil water content at 30 cm)^2 fPAR Daily minimum air temperature Daily maximum relative humidity Gravel class at layer B	MSWP	0.6419	0.29778	11.76	6	271

Table 5.24. Parameter estimates of nonlinear regression model with soil texture and gravel with all varieties combined (SLE, SLS = 0.05)

All Varieties: Parameter Estimates						
Variable	DF	Parameter Estimate	Standard Error	t Value	Pr > |t|	Variance Inflation
Intercept	1	0.04650	0.32755	0.14	0.8871	0
Soil water content at 30 cm [v/v]	1	7.40294	0.33695	21.97	<.0001	6.99547
Soil water content at 120 cm [v/v]	1	0.41241	0.17151	2.40	0.0164	1.88671
Square of the soil water content at 30 cm [v/v]	1	-16.99363	1.59954	-10.62	<.0001	6.47661
fPAR	1	0.01153	0.00171	6.75	<.0001	1.25333
Daily maximum relative humidity [%]	1	-0.02740	0.00301	-9.10	<.0001	2.08016
Daily minimum relative humidity [%]	1	0.01149	0.00226	5.09	<.0001	3.50140
Daily maximum air temperature [°C]	1	0.01783	0.00666	2.68	0.0076	2.93154
Daily minimum air temperature [°C]	1	-0.08598	0.00873	-9.85	<.0001	2.87952
Daily average solar radiation [W m^{-2}]	1	0.00060491	0.00029953	2.02	0.0438	1.29541
Soil class B	1	-0.02429	0.00964	-2.52	0.0119	1.30615
Soil class C	1	-0.02702	0.00724	-3.73	0.0002	1.55025
Gravel class B	1	0.06649	0.02043	3.26	0.0012	1.38233

Table 5.25. Parameter estimates of nonlinear regression model with soil texture and gravel in Aldrich (SLE, SLS = 0.05)

Aldrich: Parameter Estimates						
Variable	DF	Parameter Estimate	Standard Error	t Value	Pr > |t|	Variance Inflation
Intercept	1	1.41013	0.42215	3.34	0.0010	0
Soil water content at 30 cm [v/v]	1	8.51186	0.56611	15.04	<.0001	8.81760
Square of the soil water content at 30 cm [v/v]	1	-21.87583	2.68098	-8.16	<.0001	8.03896
Soil water content at 120 cm [v/v]	1	2.47406	0.39361	6.29	<.0001	4.23675
Daily maximum relative humidity [%]	1	-0.02688	0.00421	-6.38	<.0001	1.64991
Daily minimum relative humidity [%]	1	0.01014	0.00242	4.20	<.0001	1.74666
Daily minimum air temperature [°C]	1	-0.06331	0.00919	-6.89	<.0001	1.37980
Soil class A	1	-0.23040	0.04474	-5.15	<.0001	1.84979
Soil class C	1	-0.05790	0.01133	-5.11	<.0001	1.75820
Soil class D	1	-0.05328	0.01137	-4.69	<.0001	1.54395
Gravel class A	1	0.12437	0.04566	2.72	0.0069	2.11489
Gravel classD	1	0.12263	0.02501	4.90	<.0001	3.28861

Table 5.26. Parameter estimates of nonlinear regression model with soil texture and gravel in Butte (SLE, SLS = 0.05)

Butte: Parameter Estimates						
Variable	DF	Parameter Estimate	Standard Error	t Value	Pr > |t|	Variance Inflation
Intercept	1	-0.01900	0.51011	-0.04	0.9703	0
Soil water content at 30 cm [v/v]	1	7.21769	0.66336	10.88	<.0001	10.95033
Square of soil water content at 30 cm [v/v]	1	-17.00391	2.46332	-6.90	<.0001	7.16387
Soil water content at 60 cm	1	2.05947	0.50061	4.11	<.0001	7.63771
Soil water content at 120 cm	1	0.85548	0.35633	2.40	0.0171	3.49711
fPAR	1	0.02627	0.00379	6.93	<.0001	1.38085
Daily maximum relative humidity	1	-0.02149	0.00355	-6.06	<.0001	1.12189
Daily minimum air temperature	1	-0.05002	0.00858	-5.83	<.0001	1.07005
Soil class A	1	-0.22223	0.04200	-5.29	<.0001	1.47885
Soil class B	1	-0.06109	0.02390	-2.56	0.0111	2.60117
Soil class C	1	-0.08868	0.01769	-5.01	<.0001	2.85251

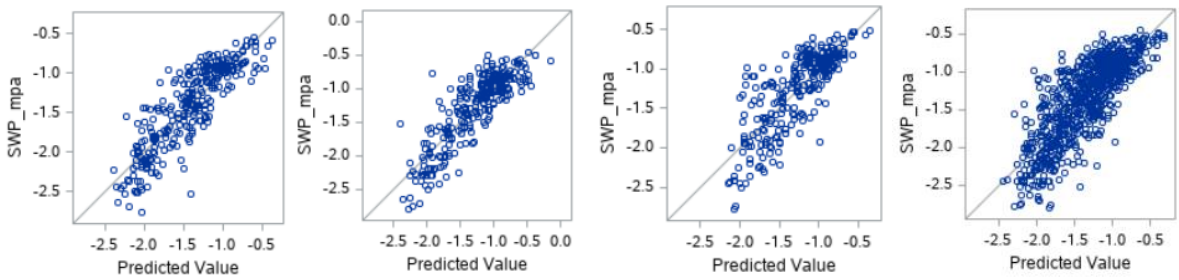

Figure 5.6. Predicted versus measured MSWP [MPa] in the Aldrich (far left), Butte (second from the left), Nonpareil (second from the right), and all varieties combined (far right).

Table 5.27. Parameter estimates of nonlinear regression model with soil texture and gravel in Nonpareil (SLE, SLS = 0.05)

Nonpareil: Parameter Estimates						
Variable	DF	Parameter Estimate	Standard Error	t Value	Pr > |t|	Variance Inflation
Intercept	1	-0.66479	0.51514	-1.29	0.1980	0
Soil water content at 30 cm [v/v]	1	7.58936	0.54994	13.80	<.0001	5.63808
Square of the soil water content at 30 cm [v/v]	1	-20.31812	3.01386	-6.74	<.0001	5.74425
fPAR	1	0.01310	0.00320	4.09	<.0001	1.17869
Daily maximum relative humidity [%]	1	-0.01295	0.00377	-3.43	0.0007	1.15899
Daily minimum air temperature [°C]	1	-0.06155	0.00931	-6.61	<.0001	1.08504
Gravel class B	1	0.08723	0.02885	3.02	0.0027	1.20579

5.3.6. Multiple linear regression model of MSWP using commercial sensor data

The previous data-driven modeling results involved using data from research-grade sensors, (i.e., the neutron probe for soil water content and the pressure chamber for stem water potential). This section investigates whether commercial grade sensors that a farmer might have at their orchard can be used instead of research grade sensors to achieve similar levels of predictive performance of MSWP. The commercial sensor data was only available from Nonpareil trees at six locations. Soil texture and gravel content were not included as potential explanatory variables in this section because soil texture and gravel content data were not available at all six locations.

The input variables for the regression model were the same as the previous stepwise selected inputs for Nonpareil: soil water content at 30 cm, the square of soil water content at 30 cm, daily minimum air temperature, daily maximum relative humidity, and fPAR. Soil water content was measured using Meter Group TEROS 10 sensors instead of with the neutron probe and MSWP was measured using the pressure chamber. The adjusted R^2 was 0.48 and the RMSE

was 0.32 when the TEROS 10 soil water content sensors (77 observations), which was worse than when soil water content derived from the neutron probe was used (adjusted $R^2 = 0.58$). This indicates that the correlation between soil water content and MSWP depends on the soil water content sensor, with the neutron probe yielding better correlations. Table 5.28 shows the parameter estimates of this model.

Table 5.28. Multiple linear regression model of MSWP using commercial soil water content sensors

Parameter Estimates						
Variable	Label	DF	Parameter Estimate	Standard Error	t Value	Pr > |t|
Intercept	Intercept	1	-3.95716	1.57640	-2.51	0.0143
Soil water content at 30 cm [v/v]	SWC1_m3/m3	1	26.98888	5.72157	4.72	<.0001
Square of the soil water content at 30 cm [v/v]	SWC1_sq	1	-55.20217	15.04103	-3.67	0.0005
Daily minimum air temperature [°C]	Min_Air_Temp_C	1	-0.04522	0.01668	-2.71	0.0084
Daily maximum relative humidity [%]	Max_Rel_Hum_perc	1	-0.02219	0.01014	-2.19	0.0320
fPAR	fPAR	1	0.03194	0.00837	3.82	0.0003

The same possible input variables were used but with MSWP measured with Saturas sensors instead of the pressure chamber and with soil water content measured with Meter Group TEROS 10 sensors instead of the neutron probe. The correlation was considerably worse using Saturas sensor data instead of MSWP from the pressure chamber with an adjusted R^2 of 0.24 and RMSE of 0.42 (number of observations = 523). Table 5.29 shows the parameter estimates of this model.

Table 5.29. Multiple linear regression model of MSWP using commercial soil water content and stem water potential sensors

Parameter Estimates						
Variable	Label	DF	Parameter Estimate	Standard Error	t Value	Pr > |t|
Intercept	Intercept	1	-1.75863	0.64208	-2.74	0.0064
Soil water content at 30 cm [v/v]	SWC1_m3/m3	1	17.24895	2.36223	7.30	<.0001
Square of the soil water content at 30 cm [v/v]	SWC1_sq	1	-38.16615	6.35141	-6.01	<.0001
Daily minimum air temperature [°C]	Min_Air_Temp_C	1	-0.00946	0.00748	-1.26	0.2067
Daily maximum relative humidity [%]	Max_Rel_Hum_perc	1	-0.01680	0.00297	-5.66	<.0001
fPAR	fPAR	1	0.00354	0.00616	0.57	0.5660

5.3.7. Prediction of MSWP using the nonlinear regression model

The best research-grade model of MSWP was used for prediction of MSWP in Nonpareil using the commercial sensor data. The model was developed using the research-grape neutron probe and pressure chamber data and then used for prediction with the commercial sensor data. The results in Figures show that the nonlinear regression model was good at predicted MSWP at high MSWP (less negative) but was unsatisfactory at low MSWP (more negative).

$$MSWP\ [MPa] = -2.15268\ [MPa] + 7.7683\ [MPa] \times \theta_{30cm} - 22.19709\ [MPa] \times \theta_{30\ cm}^{2}$$
$$+ 0.01849[MPa] \times fPAR - 0.05551[MPa\ \times {}^{\circ}\mathrm{C}^{-1}] \times T_{air,daily\ minimum}$$

Equation 5.2

where MSWP is the midday stem water potential, θ_{30cm} is the soil water content at 30 cm, $fPAR$ is the fraction of photosynthetically active radiation intercepted by the canopy, and $T_{air,daily\ minimum}$ is the daily minimum air temperature. Figures 5.7 through 5.12 show the results of the predictions of MSWP using the regression model for Nonpareil versus the measured MSWP using the pressure chamber and using the Saturas sensors.

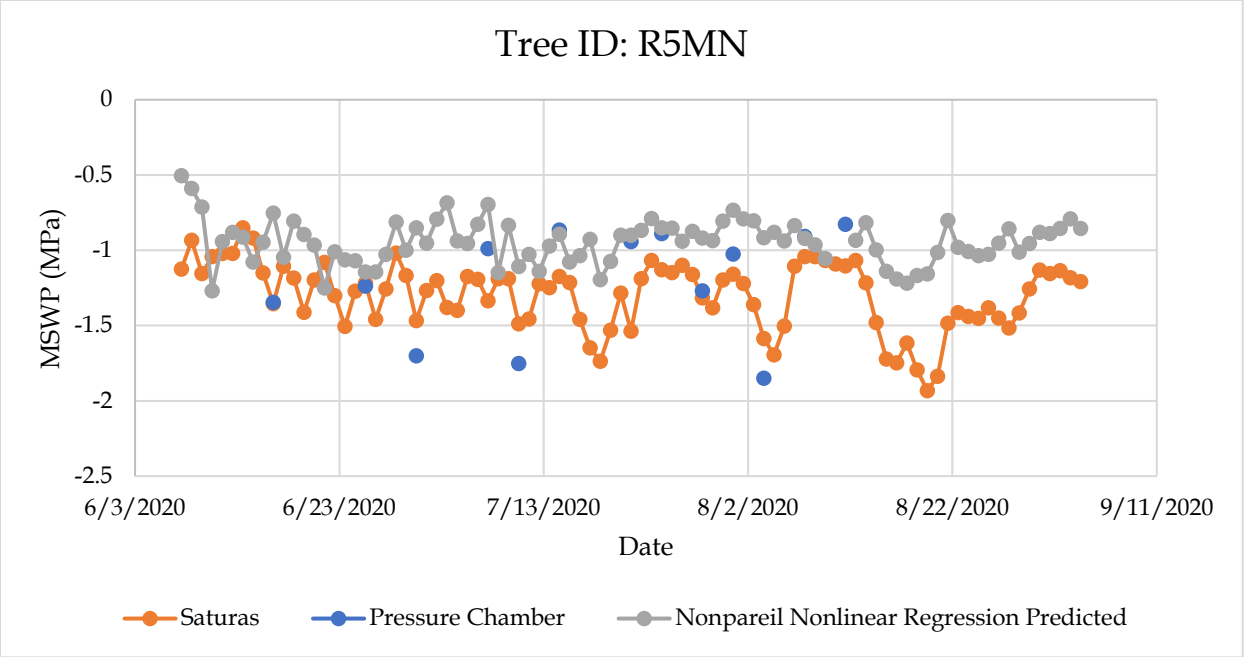

Figure 5.7. Nonlinear regression model prediction of MSWP compared to the pressure chamber and Saturas sensors in tree ID R5MN.

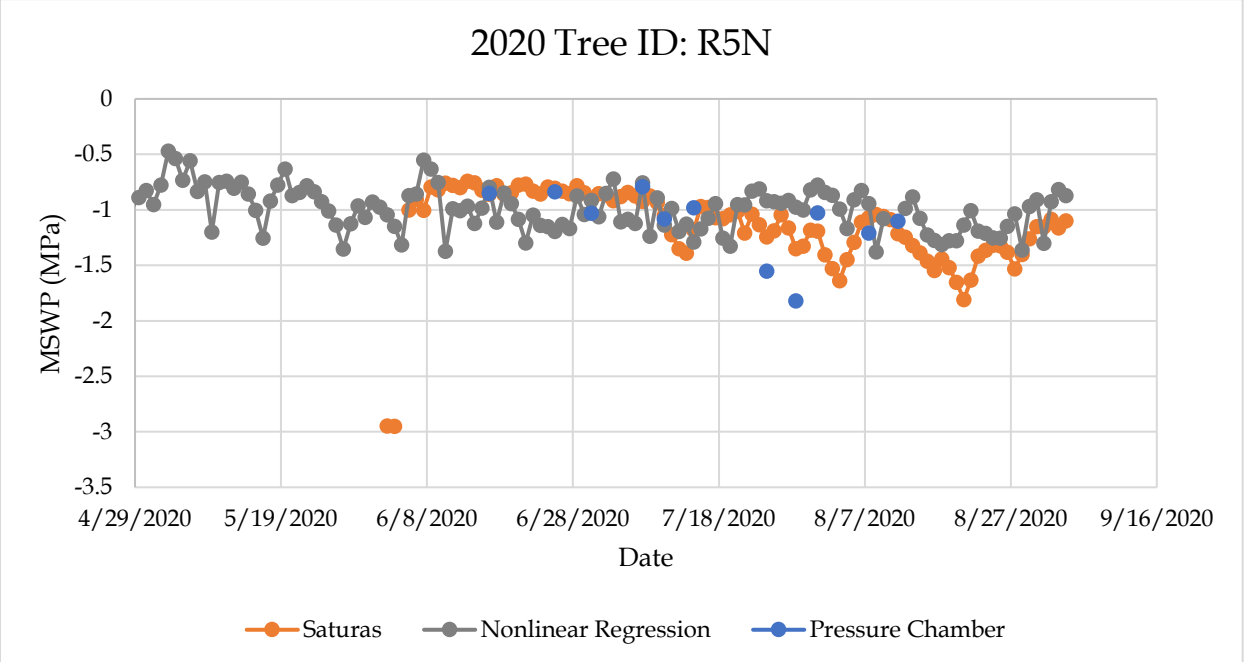

Figure 5.8. Nonlinear regression model prediction of MSWP compared to the pressure chamber and Saturas sensors in tree ID R5N.

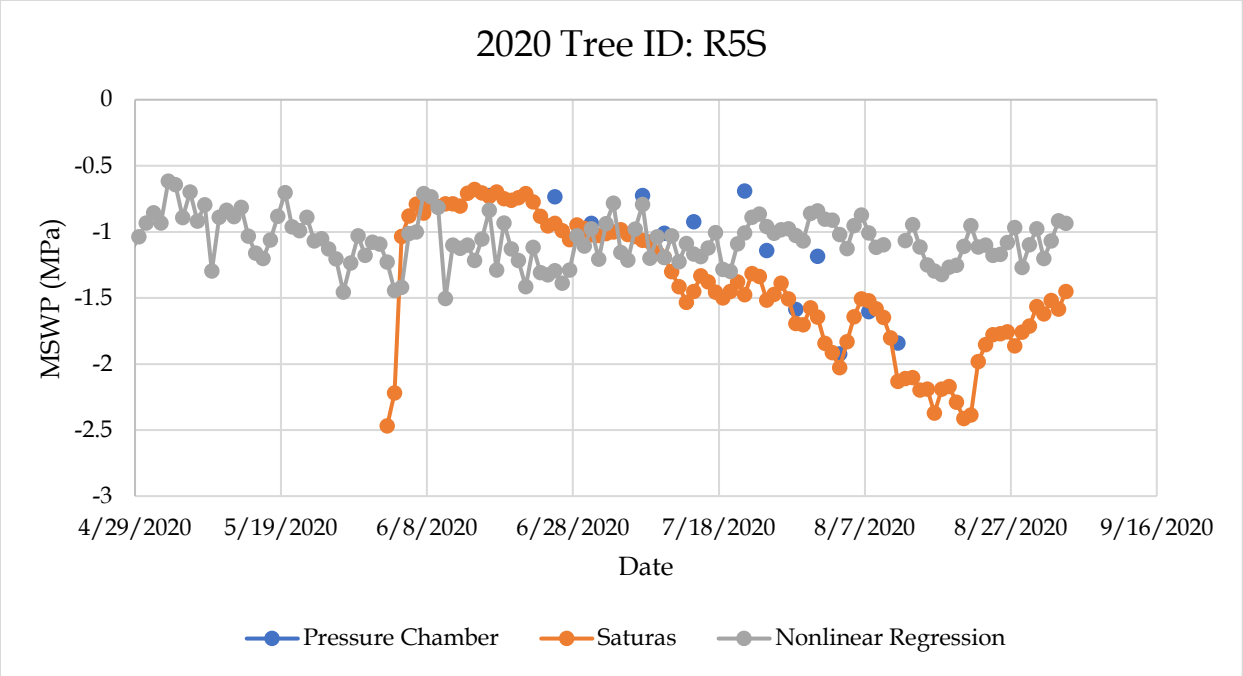

Figure 5.9. Nonlinear regression model prediction of MSWP compared to the pressure chamber and Saturas sensors in tree ID R5S.

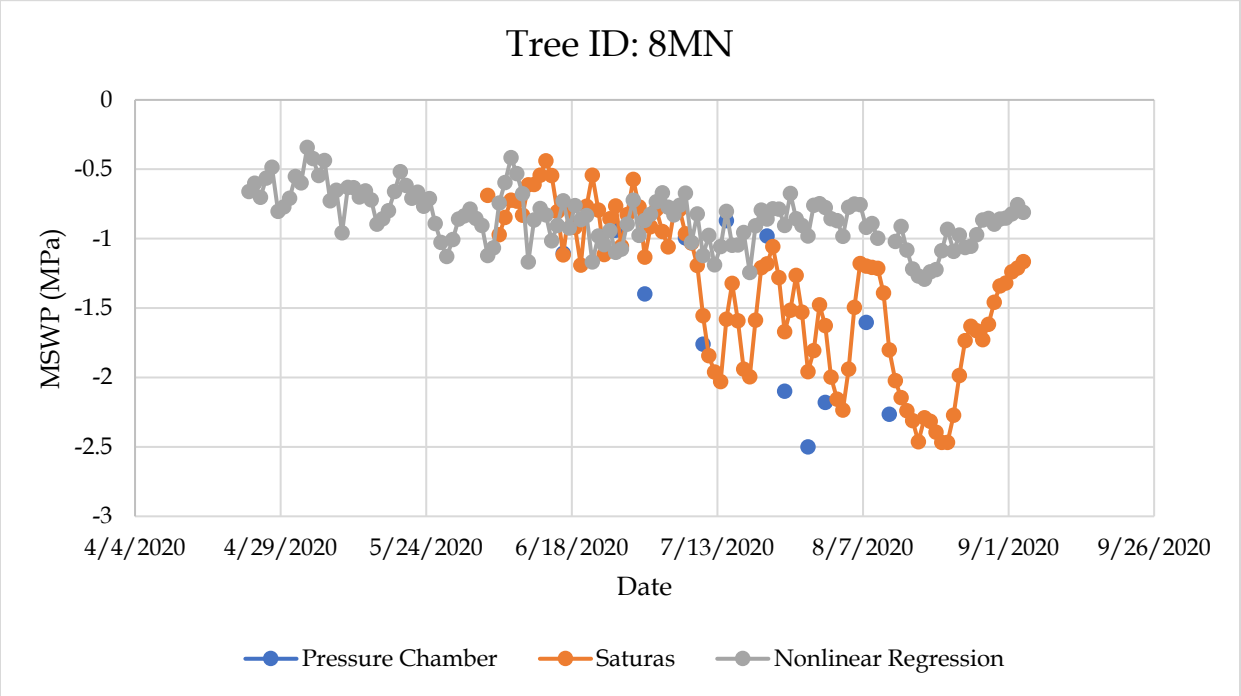

Figure 5.10. Nonlinear regression model prediction of MSWP compared to the pressure chamber and Saturas sensors in tree ID R8MN.

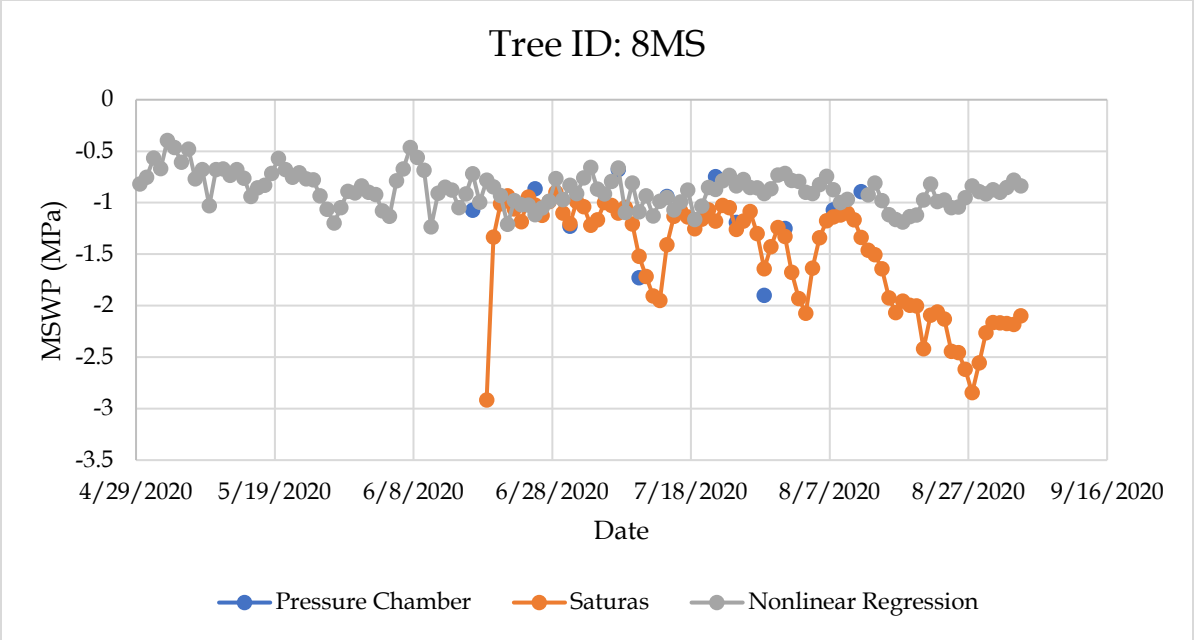

Figure 5.11. Nonlinear regression model prediction of MSWP compared to the pressure chamber and Saturas sensors in tree ID R8MS.

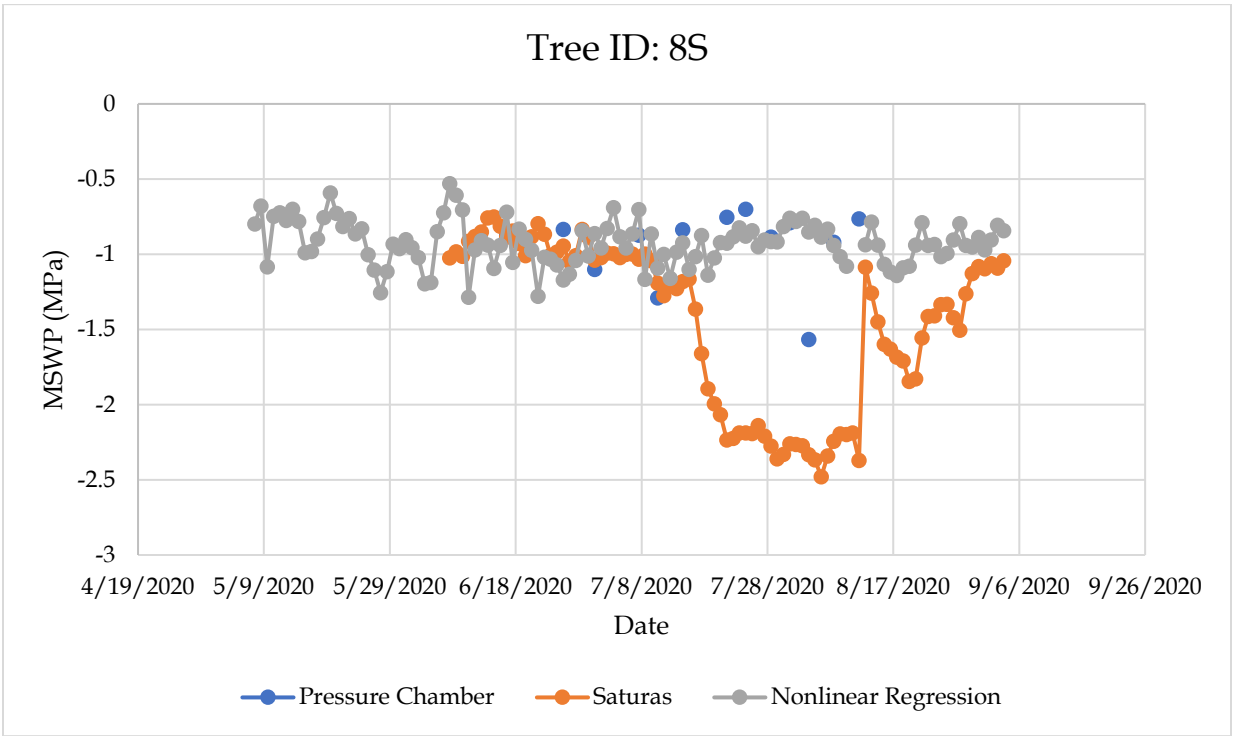

Figure 5.12. Nonlinear regression model prediction of MSWP compared to the pressure chamber and Saturas sensors in tree ID R8S.

5.4. Discussion

The most significant explanatory variable in all the candidate models of MSWP was the soil water content at 30 cm. This depth was observed to be where most of the root water uptake in almond trees occurred according to the neutron probe derived measurements of soil water content in relation to irrigation events. A simple explanation of the correlation between MSWP and soil water content at 30 cm is that the reduction in availability of water in the root zone led to a reduction in water potential of the entire plant, as suggested by other researchers (Shackel et al., 2000). Research has previously confirmed strong correlations between MSWP and soil water content in the root zone measured using a neutron probe (Sanden et al., 2010). A regression model of MSWP with soil water content at 30 cm as the sole linear explanatory variable did not provide a satisfactory correlation (adjusted R^2=0.44, RMSE=0.39), but a quadratic regression model of MSWP with linear and squared terms of soil water content at 30 cm substantially improved the correlation (adjusted R^2 =0.52, RMSE was 0.36) when all varieties were combined. The correlation further improved when meteorological explanatory variables were added, including fPAR, daily maximum relative humidity, daily minimum relative humidity, and daily minimum air temperature (adjusted R^2 =0.63, RMSE=0.32) when all varieties were combined. The correlation improved again when the soil texture at layer B was added as an explanatory variable (adjusted R^2 =0.66, RMSE=0.31) when all varieties were combined and SLE=0.001 and SLS=0.001. When the SLE and SLS was decreased to 0.05, additional variables of soil water content at 120 cm, daily maximum air temperature, daily average solar radiation, soil texture at layer C, and gravel content at layer B, entered the model and the correlation only slightly improved (adjusted R^2 =0.67, RMSE=0.30). Since the correlation only slightly improved with the addition of those variables, it may not be necessary to measure those extra variables for data-driven models of MSWP.

The regression models had better correlation in the Aldrich and Butte varieties than in the Nonpareil variety. The Nonpareil variety had greater diversity of irrigation treatments (50% ET_c, 75% ET_c, and 100% ET_c) than the Aldrich and Butte varieties during the July and August months. There were measurements of 100% ET_c in the Aldrich and Butte varieties in April through June and September, but measurements were done less frequently during those months (once every 1 or 2 weeks) compared to in July and August (twice a week). A greater range of MSWP and soil water content measurements in the Nonpareil variety complexified the model of MSWP to include a wider range of plant water stress conditions and may be a reason for weakening the correlation of the selected model. The data-driven models with the best correlations for the Aldrich and Butte varieties included irrigation treatments that were mostly 50% ET_c and 75% ET_c and had very good correlation coefficients (adjusted R^2 of 0.74 and 0.73, respectively).

Including the square of soil water content at 30 cm considerably improved the prediction of MSWP. There is a known nonlinear relationship between soil water content and soil water potential (Hillel, 2004). Since the soil water potential will affect the MSWP, it makes sense that soil water content is also nonlinear with MSWP. Other research confirms the nonlinear relationship between soil water content derived from neutron probe measurements and MSWP (Sanden et al., 2010). The graph shown in Figure 5.5 likely captures a region of various soil water retention curves due to various soil textures.

Daily minimum air temperature and daily maximum relative humidity were significant explanatory variables of MSWP. Interestingly, these data points occurred in the early morning and not in the afternoon when MSWP was measured. This means that the recovery period in the early morning affects the MSWP later in the day. This is the opposite of the findings of Brillante et al. (2016), who found that the maximum air temperature was very significant to

midday stem water potential in grapevine. The daily maximum air temperature and daily minimum relative humidity (which occurred in the afternoon when MSWP was measured), were only sometimes significant in this study.

The labeled outliers in Figure 5.13 were all in 2019 and many were from tree 1MN. There was no justifiable reason to remove the data points from the model.

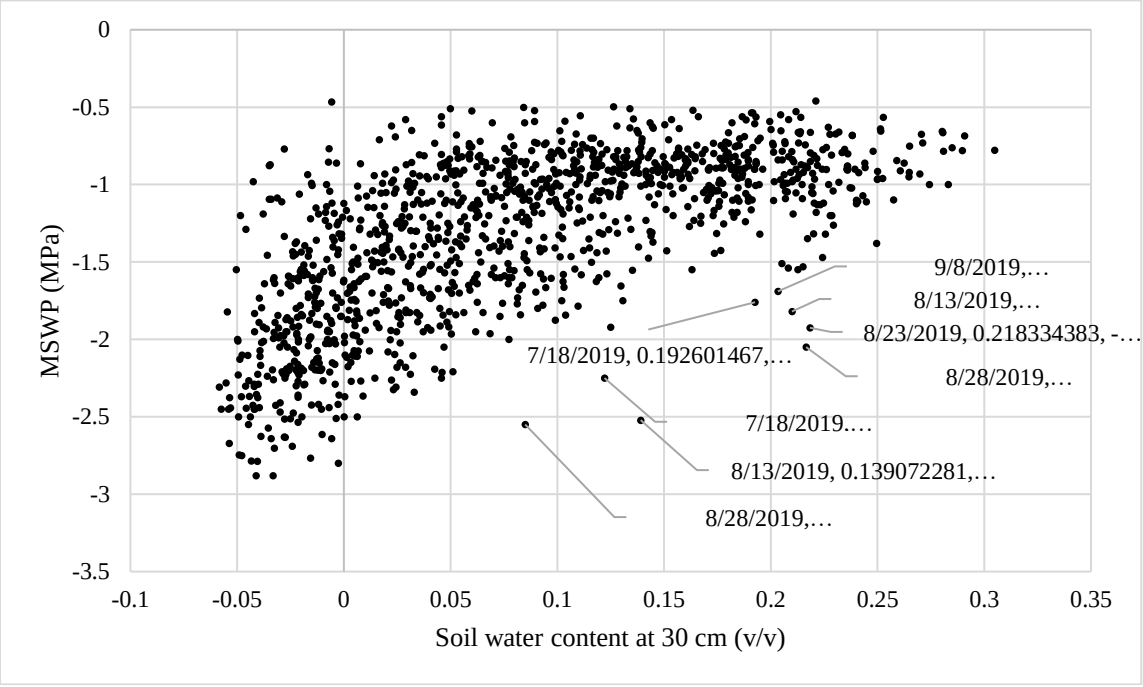

Figure 5.13. Potential outliers in the relationship between soil water content at 30 cm and midday stem water potential.

Uncertainty in the regression models could include excluded explanatory variables, measurement errors, inadequate range of data, incorrect model coefficients, and low density of measurements in certain regions (particularly, high and low MSWP). Further research should investigate how the model might improve if an onsite weather station was used instead of the CIMIS station. Future research should collect MSWP measurements and data from the explanatory variables discussed in this paper in other varieties, crops, soil textures, gravel

contents, and fPAR ranges. Further research should investigate whether there is hysteresis in the wetting and drying of soil, affecting the relationship between soil water content and MSWP in wetting versus drying scenarios.

Using neutron probe derived soil water content data considerably improved predictions of MSWP compared to using dielectric soil water content sensors (TEROS 10). Dielectric soil water content sensors have a smaller volume of influence (430 mL) compared to soil water content measurements derived from a calibrated neutron probe (approximately the size of a volleyball). Using in-tree MSWP sensors in conjunction with dielectric soil water content sensors to develop a data-driven model of MSWP yielded poor results. This questions whether affordable in-tree MSWP and dielectric soil water content sensors can be reliably used together in decision support tools since they appear to share poor correlation as opposed to their research-grade counterparts that showed good correlation. Further research developing data-driven models of MSWP with the use of dielectric soil water content sensors should involve multiple sensors at the same depth to increase the volume of influence with the hope of obtaining better correlations with MSWP. This study involved multiple dielectric sensors at different depths, but further research should investigate how multiple sensors at the same depth might improve predictions of MSWP.

5.5. Conclusions

This research developed data-driven models of midday stem water potential using soil water content at various depths, meteorological data, and canopy and soil characteristics. The best data-driven model offered a tradeoff between correlation and simplicity and included the following explanatory variables: soil water content at 30 cm, the square of soil water content at 30 cm, daily minimum air temperature, daily maximum relative humidity, daily minimum

relative humidity, fraction of photosynthetically active radiation, and soil texture class between 10 to 86 cm (adjusted R^2=0.66, RMSE=0.31). The advantage of this data-driven modeling approach is that it requires soil water content at only one depth of 30 cm, uses weather station data from the nearest California Irrigation Management Information System (CIMIS), fraction of photosynthetically active radiation (fPAR), and simple soil texture information at layer 10-86 cm. When separate data-driven models were developed for Butte and Aldrich almond varieties, the correlations improved (adjusted R^2=0.74, RMSE=0.27 and adjusted R^2=0.73, RMSE=0.28, respectively), but slightly worsened in the Nonpareil variety (R^2=0.64, RMSE=0.30). Attempts at using the data-driven model developed for Nonpareil, which were developed using soil water content derived from a calibrated neutron probe and MSWP measurements from a pressure chamber, using commercially available and affordable dielectric soil water content sensors and in-tree MSWP sensors yielded poor results. This data-driven model could be used as (1) a prediction tool for coarse estimates of midday stem water potential, (2) simulating the effect of soil water deficits on midday stem water potential in different almond varieties, and (3) as an educational tool for helping students and farmers understand midday stem water potential in the context of soil water content, meteorological data, and soil and canopy characteristics. The data-driven modeling approach presented in this paper decompresses midday stem water potential into explanatory variables that a farmer might have measurements of at or near their almond orchard.

Acknowledgments

Thanks to the Almond Board of California and the METER Group Grant A. Harris Fellowship for funding this research. Thanks to Franz Niederholzer, Stan Cutter, Ubaldo Salud, and the rest of the Nickels Soil Lab staff for providing and maintaining an almond orchard to conduct this research. Thanks to Jazmin Melendez, Aya Suzuki, and David Moyers for their critical roles in collecting pressure chamber and neutron probe measurements. Jazmin Melendez, Aya Suzuki, and Nitya Raisinghani analyzed the soil texture and gravel content. Thanks to Prudentia Gugulethu Zikalala, Jingyuan Xue, Iael Raij Hoffman, Omar Samara, Nitya Raisinghani, Usama Al-Dughaishi, Julie Meyers, Yangyang Li, Mackenzie Guilliams, Jae Sung Kim, Tibin Zhang, Carson Fogg, Kyle Johnson, Marcoluis Garcia, Fatemeh Mehrabi, and Matt Read for assistance with equipment and sensor installation.

Chapter 6
Conclusions

This research led to new insights for developing site-specific irrigation management strategies for almond orchards for optimizing water use while minimizing detriments to yield and nut quality. This research presented new information on the crop water use and crop coefficients (K_c) for young almond orchards and on the effects of imposing regulated deficit irrigation (RDI) in multiple almond varieties according to variety-specific hull-split schedules. A farmer could use the crop coefficients developed in this study in conjunction with reference evapotranspiration measurements from the nearest CIMIS station to guide irrigation scheduling for each age up until the 4th leaf and then use mature almond crop coefficients while implementing RDI according to variety-specific hull-split schedules. While imposing RDI, a farmer could use a site-specific, variety-specific data-driven model using the approach presented in this research to estimate the midday stem water potential (MSWP) to avoid excessive accumulation of water stress and to aim for target MSWP values. Based on the results of this study, the following conclusions can be made:

1. Crop water use increases as almond orchards increases in age up until the 4th year, indicating the need to adjust irrigation applied as orchards grow.
2. Almond farmers should use age and development-specific K_c values for irrigation scheduling until the 4th year, and then mature almond K_c could be used.
3. Fraction of photosynthetically active radiation intercepted by the canopy, MSWP, and soil water content at 46 and 76 cm are good predictors of the ratio of actual evapotranspiration and reference evapotranspiration and could be used for determining site-specific crop coefficients.
4. RDI during Butte hull-split in Butte reduced the fraction of sealed shells compared to RDI

during Nonpareil hull-split in Butte, increasing the vulnerability of the kernel to the environment and possible pests.

5. The kernel thickness increased in the Aldrich variety when RDI was implemented during Aldrich hull-split instead of Nonpareil hull-split period.
6. Water use efficiency decreased in the Butte variety when it was irrigated during Butte hull-split instead of Nonpareil hull-split due to fewer number of days in between the initiation of Butte hull-split and harvest compared to Nonpareil.
7. RDI during hull-split in Aldrich, Butte, and Nonpareil varieties did not significantly decrease marketable kernel yield, showing that RDI is a promising strategy for reducing water use in almond orchards with multiple varieties while minimizing yield losses.
8. No significant change in marketable kernel yield was achieved by implementing RDI according to variety-specific hull-split compared to scheduling RDI in all three varieties according to Nonpareil hull-split.
9. In terms of yield only, the best strategy for implementing RDI in almond orchards with multiple varieties would the least labor-intensive method of irrigating all varieties in the same orchard according to the Nonpareil variety hull-split schedule.
10. The best site-specific data-driven model of MSWP offered a tradeoff between correlation and simplicity and included the following explanatory variables: soil water content at 30 cm, the square of soil water content at 30 cm, daily minimum air temperature, daily maximum relative humidity, daily minimum relative humidity, fraction of photosynthetically active radiation, and soil texture class between 10 to 86 cm (adjusted R^2=0.66, RMSE=0.31).
11. When separate data-driven models of MSWP were developed for Butte and Aldrich almond varieties, the correlations improved (adjusted R^2=0.74, RMSE=0.27 and adjusted

R^2=0.73, RMSE=0.28, respectively), but slightly worsened in the Nonpareil variety (R^2=0.64, RMSE=0.30).

12. Attempts at using the data-driven model of MSWP developed for Nonpareil, which were developed using soil water content derived from a calibrated neutron probe and MSWP measurements from a pressure chamber, using commercially available and affordable dielectric soil water content sensors and in-tree MSWP sensors yielded poor results.

Chapter 7
Recommendations for Future Studies

The research presented in this paper generated new insights on site-specific irrigation management strategies for almond orchards with multiple varieties and different ages of trees. There are still gaps in the research on site-specific irrigation management of almond orchards.

7.1. Crop water use and crop coefficients of young almond orchards

New research should focus on estimating evapotranspiration of young almond trees under various irrigation systems (mister, flood, drip, etc.), varieties, soil characteristics, climates, management practices, and cover crops. This information would help a farmer who is starting a new almond orchard understand the site-specific water requirements. Research should be conducted on how much the evapotranspiration changes by planting cover crop in young almond orchards. Also, new research should conduct a surface renewal versus eddy covariance comparison for young almond orchards, which have sparse canopy, to determine if the inexpensive surface renewal method for estimating evapotranspiration is a good candidate for irrigation scheduling.

7.2. Regulated deficit irrigation in almond orchards with multiple varieties

Future work could develop and evaluate regulated deficit irrigation during variety-specific phenological stages other than hull-split (e.g., post-harvest period, etc.) in different varieties (e.g., Monterey, Padre, Fritz, etc.) and under various irrigation methods (e.g., mister, sprinkler, subsurface drip, etc.). Also, further research and development should refine the technology of remote irrigation control systems to achieve a high level of reliability for the application of irrigating by variety by row to reduce the labor and time for the farmer to implement RDI by

variety. Further research should investigate the tradeoff between irrigating according to variety needs and irrigating according to management zones based on soil characteristics, and whether those two approaches could be combined into one holistic irrigation strategy.

7.3. Site-specific data-driven modeling of midday stem water potential

Future research should expand the data-driven modeling of midday stem water potential to other almond varieties, soil textures, and climates. Artificial intelligence methods could be used instead of regression modeling to develop data-driven models of midday stem water potential. With more data than what was available in this paper, deep learning could be used. Further research should investigate if multiple nearby dielectric soil water content sensors at 30 cm could substitute for neutron probe derived measurements of soil water content in the data-driven modeling approach of MSWP. Dielectric sensors would be significantly more available to farmers and can be automated for irrigation scheduling, unlike the neutron probe. Further research could also develop and evaluate water retention curves between soil water content and midday stem water potential under various soil textures.

References

Adaskaveg, J.E., Gubler, W.D., Duncan, R.A., Stapleton, J.J., Holtz, B.A., Trouillas, F.P., 2017. Almond Kernel Shrivel [WWW Document]. UC IPM. URL https://www2.ipm.ucanr.edu/agriculture/almond/Almond-Kernel-Shrivel/

Allen, Richard G., Luis, S.P., RAES, D., Smith, M., 1998. FAO Irrigation and Drainage Paper No. 56. Crop Evapotranspiration (guidelines for computing crop water requirements). Irrig. Drain. 300, 300. https://doi.org/10.1016/j.eja.2010.12.001

Allen, R.G., Pereira, L.S., 2009. Estimating crop coefficients from fraction of ground cover and height. Irrig. Sci. 28, 17–34.

Allen, R.G., Pereira, L.S., Raes, D., Smith, M., 1998. Crop evapotranspiration: guidelines for computing crop water requirements. FAO Irrig. Drain. Pap. No. 56.

Allen, R.G., Pereira, L.S., Smith, M., Raes, D., Wright, J.L., 2005. *FAO-56* Dual Crop Coefficient Method for Estimating Evaporation from Soil and Application Extensions. J. Irrig. Drain. Eng. 131, 2–13. https://doi.org/10.1061/(ASCE)0733-9437(2005)131:1(2)

Allen, R.G., Pruitt, W.O., Jensen, M.E., 1991. Environmental requirements of lysimeters. ASCE 170–181.

Allen, R.G., Tasumi, M., Morse, A., Trezza, R., Wright, J.L., Bastiaanssen, W., Kramber, W., Lorite, I., Robison, C.W., 2007. Satellite-Based Energy Balance for Mapping Evapotranspiration with Internalized Calibration (METRIC)—Applications. J. Irrig. Drain. Eng. 133, 395–406. https://doi.org/10.1061/(ASCE)0733-9437(2007)133:4(395)

Almond Board of California, 2019. Almond Orchard 2025 Goals.

Almond Board of California, 2015. Varieties and Sizes.

Anderson, R.G., Alfieri, J.G., Tirado-Corbalá, R., Gartung, J., McKee, L.G., Prueger, J.H., Wang, D., Ayars, J.E., Kustas, W.P., 2017. Assessing FAO-56 dual crop coefficients using eddy covariance flux partitioning. Agric. Water Manag. 179, 92–102. https://doi.org/10.1016/j.agwat.2016.07.027

Ayars, J.E., Johnson, R.S., Phene, C.J., Trout, T.J., Clark, D.A., Mead, R.M., 2003. Water use by drip-irrigated late-season peaches. Irrig. Sci. 22, 187–194. https://doi.org/10.1007/s00271-003-0084-4

Bastiaanssen, W, et al., 2005. SEBAL model with remotely sensed data to improve water-resources management under actual field conditions. J. Irrig. Drain. Eng. 131.

Bastiaanssen, W.G.M., Menenti, M., Feddes, R.A., Holtslag, A.A.M., 1998. A Remote Sensing Surface Energy Balance Algorithm for Land (SEBAL) 1. Formulation 213, 90. https://doi.org/10.1016/S0022-1694(98)00254-6

Bowen, I.S., 1926. The ratio of heat losses by conduction and by evaporation from any water source. Phys. Rev. 27, 779–787.

Brillante, L., Mathieu, O., Lévêque, J., Bois, B., 2016. Ecophysiological modeling of grapevine

water stress in burgundy terroirs by a machine-learning approach. Front. Plant Sci. 7, 1–13. https://doi.org/10.3389/fpls.2016.00796

Bryla, D., Trout, T., Ayars, J., 2010. Weighing lysimeters for developing crop coefficients and efficient irrigation practices for vegetable crops. Hortic. Sci. 45, 1597–1604.

Buchner, R.P, et al., 2008. Effects of regulated deficit irrigation on walnut grafted on "Northern" California Black' or "Paradox" Rootstock. 5th Int. Symp. Irrig. Hortic. Crop.

Burchard-Levine, V., Nieto, H., Riaño, D., Migliavacca, M., El-Madany, T.S., Perez-Priego, O., Carrara, A., Martín, M.P., 2019. Adapting the thermal-based two-source energy balance model to estimate energy fluxes in a complex tree-grass ecosystem. Hydrol. Earth Syst. Sci. Discuss. 1–37. https://doi.org/10.5194/hess-2019-354

California Department of Food and Agriculture, 2020. 2019 California Almond Acreage Report 1–8.

California Department of Food and Agriculture, 2019. California Agricultural Statistics Review 2018-2019. Calif. Agric. Stat. Rev. 1–121.

California Department of Food and Agriculture, 2018a. California Agricultural Statistics Review 2017-2018.

California Department of Food and Agriculture, 2018b. 2018 California Almond Acreage Report 8.

California Irrigation Management Information System [WWW Document], 2018. URL https://cimis.water.ca.gov/

Campbell, G.S., Norman, J.M., 1998. An Introduction to Environmental Biophysics, 2nd ed. Springer Science.

Castellví, F., Snyder, R.L., 2009. Sensible heat flux estimates using surface renewal analysis. A study case over a peach orchard. Agric. For. Meteorol. 149, 1397–1402. https://doi.org/10.1016/j.agrformet.2009.03.011

Chalmers, D.J., Mitchell, P.D., Heek, L. van, 1981. Control of peach growth and productivity by regulated water supply, tree density, and summer pruning. J. Am. Soc. Hortic. Sci. 6.

Coates, R.W., Delwiche, M.J., Broad, A., Holler, M., 2013. Wireless sensor network with irrigation valve control. Comput. Electron. Agric. https://doi.org/10.1016/j.compag.2013.04.013

Connell, J.H., Gradziel, T.M., Lampinen, B.D., Micke, W.C., Floyd, J., 2010. Harvest maturity of almond cultivars in California's Sacramento Valley. XIV GREMPA Meet. Pist. Almonds 95965, 19–23.

Crop water use and yield, 2015.

Domingo, R., Ruiz-Sánchez, M.C., Sánchez-Blanco, M.J., Torrecillas, A., 1996. Water relations, growth and yield of Fino lemon trees under regulated deficit irrigation. Irrig. Sci. 16, 115–123. https://doi.org/10.1007/BF02215619

Doorenbos, J., Pruitt, W.O., 1977. Guidelines for predicting crop water requirements. FAO Irrig.

Drain. Pap. 24, 144.

Drechsler, K., Kisekka, I., Upadhyaya, S.K., 2019. A comprehensive stress indicator for evaluating plant water status in almond trees. Agric. Water Manag. 214–223.

Ebel, R.C., Proebsting, E.L., Patterson, M.E., 1993. Regulated Deficit Irrigation May Alter Apple Maturity, Quality, and Storage Life. HortScience 28, 141–143.

Eching, S., Frame, K., Snyder, R., 2013. Role of Technology in Irrigation Advisory Services: The CIMIS Experience.

Espadafor, M., Orgaz, F., Testi, L., Lorite, I.J., Villalobos, F.J., 2015. Transpiration of young almond trees in relation to intercepted radiation. Irrig. Sci. 33, 265–275. https://doi.org/10.1007/s00271-015-0464-6

Fereres, E., Aldrich, T.M., Schulbach, H., Martinich, D.A., 1981. Response of Young Almond Trees to Late-Season Drought. Calif. Agric. 35, 11–12.

Fereres, E., Goldhamer, D.A., 1990. Deciduous fruit and nut trees. Am. Soc. Agron. 30, 31.

Fetter, C.W., 2001. Applied Hydrogeology. Prentice Hall.

French, A.N., Alfieri, J.G., Kustas, W.P., Prueger, J.H., Hipps, L.E., Chávez, J.L., Evett, S.R., Howell, T.A., Gowda, P.H., Hunsaker, D.J., Thorp, K.R., 2012. Estimation of surface energy fluxes using surface renewal and flux variance techniques over an advective irrigated agricultural site. Adv. Water Resour. 50, 91–105. https://doi.org/10.1016/j.advwatres.2012.07.007

Fulton, A., Buchner, R., Grant, J., Prichard, T., Schwankl, L., Shackel, K., 2003. Tips for Using Pressure Chamber and Midday Stem Water Potential (SWP) Measurements in Orchard Crops.

Fulton, A., Grant, J., Buchner, R., Connell, J., 2017. Using the Pressure Chamber for Irrigation Management in Walnut, Almond and Prune. Using Press. Chamb. Irrig. Manag. Walnut, Almond Prune. https://doi.org/10.3733/ucanr.8503

Fulton, A., Grant, J., Buchner, R., Connell, J., 2014. 239178.

Fulton, A.E., Little, C.C., Snyder, R.L., Lampinen, B.D., Buchner, R.P., 2017. Evaluation of Crop Coefficients and Evapotranspiration in English Walnut, in: 2017 Spokane, Washington July 16 - July 19, 2017. pp. 1–12. https://doi.org/10.13031/aim.201701457

Girona, J., Mata, M., Arbonès, A., Alegre, S., Rufat, J., Marsal, J., 2003. Peach Tree Response to Single and Combined Regulated Defi cit Irrigation Regimes under Shallow Soils. J. Amer. Soc. Hort. Sci. 128, 432–440.

Glenn, E., et al, 2011. Vegetation index-based crop coefficients to estimate evapotranspiration by remote sensing in agricultural and natural ecosystems. Hydrol. Process. 25, 13.

Goldhamer, D.A. et al, 1988. Third year effects of deficit irrigation on walnut tree performance. Walnut Mark. Board 42–52.

Goldhamer, D.A., 2012. Almond in Crop Yield Response to Water. FAO Irrig. Drain. Pap. No. 66 246–296.

Goldhamer, D.A., Fereres, E., 2017. Establishing an almond water production function for California using long-term yield response to variable irrigation. Irrig. Sci. 35, 169–179. https://doi.org/10.1007/s00271-016-0528-2

Goldhamer, D.A., Viveros, M., 2000. Effects of preharvest irrigation cutoff durations and postharvest water deprivation on almond tree performance. Irrig. Sci. 19, 125–131. https://doi.org/10.1007/s002710000013

Goldhamer, D.A., Viveros, M., Salinas, M., 2006. Regulated deficit irrigation in almonds: Effects of variations in applied water and stress timing on yield and yield components. Irrig. Sci. 24, 101–114. https://doi.org/10.1007/s00271-005-0014-8

González-Altozano, P., Castel, J.R., 1999. Regulated deficit irrigation in "Clementina de Nules" citrus trees. I. Yield and fruit quality effects. J. Hortic. Sci. Biotechnol. 74, 706–713. https://doi.org/10.1080/14620316.1999.11511177

Gordon, P., 2019. Regulated deficit irrigation in almonds to manage hull rot [WWW Document]. UC ANR Publ. Stream.

Gutiérrez-Gordillo, S., Durán-Zuazo, V.H., García-Tejero, I., 2019. Response of three almond cultivars subjected to different irrigation regimes in Guadalquivir river basin. Agric. Water Manag. 222. https://doi.org/10.1016/j.agwat.2019.05.031

Hamby, K., Gao, L.W., Lampinen, B., Gradziel, T., Zalom, F., 2011. Hull split date and shell seal in relation to navel orangeworm (Lepidoptera: Pyralidae) infestation of almonds. J. Econ. Entomol. 104, 965–969. https://doi.org/10.1603/EC10396

Hamby, K.A., Zalom, F.G., 2013. Relationship of almond kernel damage occurrence to navel orangeworm (Lepidoptera: Pyralidae) success. J. Econ. Entomol. 106, 1365–1372. https://doi.org/10.1603/EC12473

Harter, T., 2015. California's agricultural regions gear up to actively manage groundwater use and protection. Calif. Agric. 69, 193–201. https://doi.org/10.3733/ca.E.v069n03p193

Hillel, D., 2004. Introduction to Environmental Soil Physics. Elsevier Academic Press, San Diego, CA.

Holtermann, J., 2016. How long is an almond orchard productive? [WWW Document]. Almond Living Mag. URL https://www.almonds.com/why-almonds/almond-living-magazine/how-long-almond-orchard-productive#:~:text=The main factor in an,years before it is removed.

Huband, N.D.S., Monteith, J.L., 1985. Radiative surface temperature and energy balance of a wheat canopy - II. Estimating fluxes of sensible and latent heat. Boundary-Layer Meteorol. 36, 107–116.

Jarvis-Shean, K., Fulton, A., Doll, D., Lampinen, B., Hanson, B., Baldwin, R., Lightle, D., Vinsonhaler, B., 2018. Young Orchard Handbook.

Jensen, M.E., Allen, R.G. (Eds.), 2016. Evaporation, Evapotranspiration, and Irrigation Water Requirements, Second. ed. American Society of Civil Engineers, Task Committee on Revision of Manual 70.

Jones, H.G., 2004. Irrigation scheduling: advantages and pitfalls of plant-based methods. J. Exp. Bot. 55, 2427–2436. https://doi.org/10.1093/jxb/erh213

Kizer, E.E., Upadhyaya, S.K., Ko-Madden, C.T., Drechsler, K.M., Meyers, J.N., Rojo, F.E., Schramm, A.E., Zhang, Q.S., 2017. Continuous, Proximal Leaf Monitoring System to Assist with Precision Irrigation Implementation Using a Wireless Mesh Network of Sensors and Controllers in Almond, in: An ASABE Meeting Presentation. American Society of Agricultural and Biological Engineers, Spokane, Washington, pp. 1–9. https://doi.org/10.13031/aim.201701094

Kustas, W.P., 1990. Estimates of evapotranspiration with a one- and two-layer model of heat transfer over partial canopy cover. J. Appl. Meteorol. https://doi.org/10.1175/1520-0450(1990)029<0704:EOEWAO>2.0.CO;2

Kustas, William P, Norman, J.M., 2000. A Two-Source Energy Balance Approach Using Directional Radiometric Temperature Observations for Sparse Canopy Covered Surfaces. Agron. J. 847–854.

Kustas, William P., Norman, J.M., 2000. A Two-Source Energy Balance Approach Using Directional Radiometric Temperature Observations for Sparse Canopy Covered Surfaces. Agron. J. 92, 847–854.

Lampinen, B.D., Udompetaikul, V., Browne, G.T., Metcalf, S., Stewart, W., Contador, L., Negron, C., Upadhyaya, S.K., 2012. A Mobile Platform for Measuring Canopy Photosynthetically Active Radiation Interception in Orchard Systems. Hortic. Technol. Prod. Reports 22, 237–244.

Lee, X., Massman, W.J., Law, B., 2005. Handbook of Micrometeorology, Handbook of Micrometeorology.

Little, C., 2006. The effect of deficit irrigation on yield and vegetative growth in English walnuts. University of California, Davis.

McCutchan, Harold, Shackel, K.A., 1992. Stem-water Potential as a Sensitive Indicator of Water Stress in Prune Trees (Prunus domestica L. cv. French). J. Am. Soc. Hortic. Sci. 117, 607–611. https://doi.org/10.1017/S1744137405000159

McCutchan, H, Shackel, K.A., 1992. Stem-Water Potential As a Sensitive Indicator of Water-Stress in Prune Trees (Prunus-Domestica L Cv French). J. Am. Soc. Hortic. Sci. 117, 607–611.

McElrone, A.J. et al., 2013. Surface Renewal: An Advanced Micrometeorological Method for Measuring and Processing Field-Scale Energy Flux Density Data. J. Vis. Exp.

Medellin-Azuara, J., et al., 2018. A Comparative Study for Estimating Crop Evapotranspiration in the Sacramento-San Joaquin Delta. UC Davis Cent. Watershed Sci.

Meyers, J.N., Kisekka, I., Upadhyaya, S.K., Michelon, G., 2019. Development of an artificial neural network approach for predicting plant water status in almonds. Trans. ASABE 62, 19–32.

Meyers, W.S., Green, G.C., 1980. Water use by wheat and plant indicators of average soil water.

Agron. Journal1 72, 253.

Mitchell, P.D., Jerie, P.H., Chalmers, D.J., 1984. The effects of regulated water deficits on pear tree growth, fruit growth, and yield. J. Am. Soc. Hortic. Sci. 109, 3.

Norman, J.M., Kustas, W.P., Humes, K.S., 1995. Source approach for estimating soil and vegetation energy fluxes in observations of directional radiometric surface temperature. Agric. For. Meteorol. 77, 263–293. https://doi.org/10.1016/0168-1923(95)02265-Y

Pathak, T.B., Maskey, M.L., Dahlberg, J.A., Kearns, F., Bali, K.M., Zaccaria, D., 2018. Climate change trends and impacts on California Agriculture: A detailed review. Agronomy 8, 1–27. https://doi.org/10.3390/agronomy8030025

Pavley, Dickinson, 2014. Sustainable Groundwater Management Act [And Related Statutory Provisions from SB1168 (Pavley), AB1739 (Dickinson), and SB1319 (Pavley) as Chaptered].

Ramos, D. et al., 1978. Water stress affects size and quality of walnuts. Calif. Agric. 10.

Ross, J., 1975. Radiative transfer in plant communities. Principles Academic Press, London, UK.

Sanden, B., 2007. Fall irrigation management in drought year for almonds, pistachios, and citrus. Kern Soil Water Newsl. 1–8.

Sanden, B., Brown, P., Snyder, R., 2012. New insights on water management in almonds, in: 2012 Conference Proceedings. American Society of Agronomy. California Chapter. pp. 88–91.

Sanden, B., Shackel, K., Brown, P., 2010. Correlation of soil water content determination by neutron backscatter and almond tree stem water potential for microirrigation scheduling in almonds. ASABE - 5th Natl. Decenn. Irrig. Conf. 2010, Held Conjunction with Irrig. Show 2010 2, 5–8.

Semmens, K.A., Anderson, M.C., Kustas, W.P., Gao, F., Alfieri, J.G., McKee, L., Prueger, J.H., Hain, C.R., Cammalleri, C., Yang, Y., Xia, T., Sanchez, L., Mar Alsina, M., Vélez, M., 2016. Monitoring daily evapotranspiration over two California vineyards using Landsat 8 in a multi-sensor data fusion approach. Remote Sens. Environ. 185, 155–170. https://doi.org/10.1016/j.rse.2015.10.025

Shackel, K., Buchner, R., Connell, J., Edstrom, J., Fulton, A., Holtz, B., Lampinen, B., Reil, W., Stewart, W., Viveros, M., 2010. Midday Stem Water Potential as a Basis for Irrigation Scheduling, in: An ASABE Meeting Presentation. American Society of Agricultural and Biological Engineers, Phoenix, Arizona, pp. 5–8. https://doi.org/10.1037/a0019906

Shackel, K., Lampinen, B., Sibbett, S., Olson, W., 2000. The relation of midday stem water potential to the growth and physiology of fruit trees under water limited conditions. Acta Hortic. https://doi.org/10.17660/ActaHortic.2000.537.50

Shapland, T.M., McElrone, A.J., Paw U, K.T., Snyder, R.L., 2013. A Turnkey data logger program for field-scale energy flux density measurements using eddy covariance and surface renewal. Ital. J. Agrometeorol. 5–16.

Snyder, R.L., Spano, D., Paw U, K.T., 1996. Surface renewal analysis for sensible and latent heat flux density. Boundary-Layer Meteorol. 77, 249–266. https://doi.org/10.1007/BF00123527

Soil Survey Laboratory Methods Manual, Soil Survey Investigations Report No. 42, 1992.

Stewart, W.L., Fulton, A.E., Krueger, W.H., Lampinen, B.D., Shackel, K.A., 2011. Regulated deficit irrigation reduces water use of almonds without affecting yield. Calif. Agric. 65, 90–95. https://doi.org/10.3733/ca.v065n02p90

Swinbank, W.C., 1951. The measurement of vertical transfer of heat and water vapour by eddies in the lower atmosphere. J. Meteorol. 8, 135–145.

Teviotdale, B.L., Goldhamer, D.A., Viveros, M., 2001. Effects of deficit irrigation on hull rot disease of almond trees caused by Monilinia fructicola and Rhizopus stolonifer. Plant Dis. 85.4, 399–403.

Twine, T.E., Kustas, W.P., Norman, J.M., Cook, D.R., Houser, P.R., Meyers, T.P., Prueger, J.H., Starks, P.J., Wesely, M.L., 2000. Correcting eddy-covariance flux underestimates over a grassland. Agric. For. Meteorol. 103, 279–300. https://doi.org/10.1016/S0168-1923(00)00123-4

United States Geological Survey, 2017. California Water Use 2010 [WWW Document]. United States Geol. Surv. URL https://ca.water.usgs.gov/water_use/2010-california-water-use.html (accessed 3.12.18).

Valdés-Vela, M., Abrisqueta, I., Conejero, W., Vera, J., Ruiz-Sánchez, M.C., 2015. Soft computing applied to stem water potential estimation: A fuzzy rule based approach. Comput. Electron. Agric. 115, 150–160. https://doi.org/10.1016/j.compag.2015.05.019

Wang, D., 2015. Water use dynamics of peach trees under postharvest deficit irrigation. J. Agric. Stud. 4.

Wilson, K.B., Hanson, P.J., Mulholland, P.J., Baldocchi, D.D., Wullschleger, S.D., 2001. A comparison of methods for determining forest evapotranspiration and its components: Sap-flow, soil water budget, eddy covariance and catchment water balance. Agric. For. Meteorol. 106, 153–168. https://doi.org/10.1016/S0168-1923(00)00199-4

Wright, J.L., 1991. Using weighing lysimeters to develop evapotranspiration crop coefficients. ASCE.

Zarate-Valdez, J.L., Whiting, M.L., Lampinen, B.D., Metcalf, S., Ustin, S.L., Brown, P.H., 2012. Prediction of leaf area index in almonds by vegetation indexes. Comput. Electron. Agric. 85, 24–32. https://doi.org/10.1016/j.compag.2012.03.009

Zhang, H., Theib, O., 1999. Water-yield relations and optimal irrigation scheduling of wheat in the Mediterranean region. Agric. Water Manag. 38, 17.

Zhang, H., Wang, D., Ayars, J.E., Phene, C.J., 2017. Biophysical response of young pomegranate trees to surface and sub-surface drip irrigation and deficit irrigation. Irrig. Sci. 35, 425–435. https://doi.org/10.1007/s00271-017-0551-y